Structural studies on mammalian septins –
New insights into filament formation

Inaugural-Dissertation zur

Erlangung des Doktorgrades des Fachbereiches Chemie

der Universität Dortmund

vorgelegt von

Minhajuddin Sirajuddin

aus Ranipet / Indien

Dortmund 2007

Die vorliegende Arbeit wurde im Zeitraum October 2003 bis August 2007 in der Abteilung I (Structurelle Biologie) des Max-Planck-Instituts für Molekulare Physiologie in Dortmund unter der Anleitung von Prof. Dr. Alfred Wittinghofer angefertigt.

1. Gutachter: Prof. Dr. Alfred Wittinghofer
2. Gutachter: Prof. Dr. Herbert Waldmann

Contents

Abbreviations

Å	Ångström (0.1 nm)
C-terminus	Carboxyterminus
DTE	1,4-Dithioerythritol
EDTA	Ehtylendiamintetraacetate
EM	Electron microscopy
E. coli	*Escherichia coli*
F_{calc}, F_{obs}	Structure-factor amplitudes (calc: calculated, obs: observed)
GAP	GTPase-activating Protein
GDP, GTP	Guanosine-5'-diphosphate, Guanosine-5'-triphosphate
GEF	guanine nucleotide exchange factor
GNBP	Guanine nucleotide binding Protein
GppNHp	Guanosine-5'-(β,γ-imido)-triphosphate
GSH	Reduced glutathione
GST	Glutathione-S-transferase
GTPase	GTP-hydrolysyzing Enzyme
HEPES	4-2-hydroxyethyl-1-piperazineethanesulfonic acid
HPLC	High performance liquid chromatography
IPTG	Isopropyl-β-D-1-thiogalactopyranosid
k Da	kilo-Dalton
λ	Wavelength
MAD	multiple wavelength anomalous disperssion
MES	2-Morpholinoethanesulfonic acid

MIRAS	multiple isomorphous heavy-atom replacement using anomalous scattering
nm	Nanometer
N-terminus	Aminoterminus
OD600	Optical density at 600 nm
PEG	Polyethylenglycol
PMSF	Phenylmethylsulfonylfluoride
SAD	single wavelenght anomalous disperssion
SDS-PAGE	Sodiumdodecylsulfate-Polyacrylamide gelelectrophoresis
SeMet	Seleno-L-Methionine
Tris	Tris-(hydroxymethyl)-aminomethan

For the amino acids, one and three letter code was used

A	Ala	alanine	I	Ile	isoleucine	R	Arg	arginine
C	Cys	cysteine	K	Lys	lysine	S	Ser	serine
D	Asp	aspartate	L	Leu	leucine	T	Thr	threonine
E	Glu	glutamate	M	Met	methionine	V	Val	valine
F	Phe	phenylalanine	N	Asn	asparagine	W	Trp	tryptophane
G	Gly	glycine	P	Pro	proline	Y	Tyr	tyrosine
H	His	histidine	Q	Gln	glutamine	x		any amino acid

1 Introduction

1.1 Cytoskeleton

1.1.1 Components of the cytoskeleton

Cytoplasm of the eukaryotic cells is spatially organized by a network of protein filaments known as the cytoskeleton. Cytoskeletons are involved in wide variety of cellular processes such as, cell division, trafficking of vesicles, maintaining shape and stability of the cell, muscle contraction and cell migration. Most eukaryotic cells contain three major types of cytoskeleton proteins which are actin, tubulin and intermediate filament proteins. These proteins assemble to form protein filaments namely; actin filaments (microfilaments), microtubules and intermediate filaments.

Actin filaments or microfilaments are composed of actin subunits. The actin subunit is a monomeric globular polypeptide chain. Each actin subunit has a binding site for ATP (or ADP). These actin subunits assemble head-to-tail to generate filaments with distinct structural polarity. The actin filament can be considered to consist of two parallel protofilaments that twist around each other in a right-handed helix (Figure 1.1 A). Actin filaments appear as flexible structures, with a diameter of 8-9 nm. They are organized into variety of linear bundles, and networks. Although actin filaments are dispersed throughout the cell, they are most highly concentrated in the cortex, just beneath the plasma membrane.

Microtubules are composed of tubulin subunits. The tubulin subunit is itself a heterodimer formed from two closely related globular proteins called α- and β-tubulin. These two tubulin proteins are tightly bound together and are found only in complex. Each α or β monomer has a binding site for one molecule of GTP. The GTP bound in the α-tubulin is trapped in the dimer interface and is never hydrolysed or exchanged. The nucleotide on the β-tubulin, in contrast may be in either GTP or GDP form, and is exchangeable. These tubulin heterodimers assemble head-to-tail to generate protofilaments with structural polarity. A microtubule is a stiff, hollow cylindrical structure built from 13 parallel protofilaments, with an outer diameter of 25 nm (Figure 1.1). Microtubules typically have one end attached to a single microtubule organizing centre (MTOC) called a centrosome.

Table 1.1 Components and composition of cytoskeletal systems

Cytoskeleton	Protein subunits	Function
Microfilaments	Actin monomers	Structural support, muscle contraction and motility.
Microtubules	α/β tubulin heterdimers	Structural support, cell polarity, and motility

Intermediate filaments
  Type I
  Type II
  Type III
  Type IV
  Type V
	
	Acidic keratins
	Basic keratins
	Vimentin, Desmin,
	Neurofilament proteins
	Lamins
		
		Structural support in different cell types

Intermediate filaments are made of different types of intermediate filament proteins, which constitute a large and heterogeneous family (Table 1.1). They are composed of individual polypeptides, which are elongated molecules with an extended central α-helical domain that forms a parallel coiled coil with another monomer. A pair of parallel dimers then associates in an anti-parallel fashion to form a staggered tetramer. This tetramer represents the basic subunit that is analogous to tubulin heterodimer or the actin monomer. Since the tetrameric subunit is made up of two dimers pointing in opposite directions, its two ends are the same. The assembled intermediate filament therefore lacks the overall structural polarity which is found in actin filaments and microtubules. The tetramers pack together laterally to form the filament, which includes eight parallel protofilaments. Each individual intermediate filament therefore has a cross section of 32 individual a-helical coils. This large number of polypeptides all lined up together, with the strong lateral hydrophobic interactions typical of coiled-coil proteins, gives intermediate filaments a rope-like character (Figure 1.1 C). These rope-like fibres have a diameter around 10 nm. Less is understood about the mechanism of assembly and disassembly of intermediate filaments than of actin filaments and microtubules.

Apart from these three major cytoskeleton proteins, several other proteins assemble into polymers and form cytoskeletal structures, for example septins. Septins are GTP binding proteins, which are involved in cytokinesis.
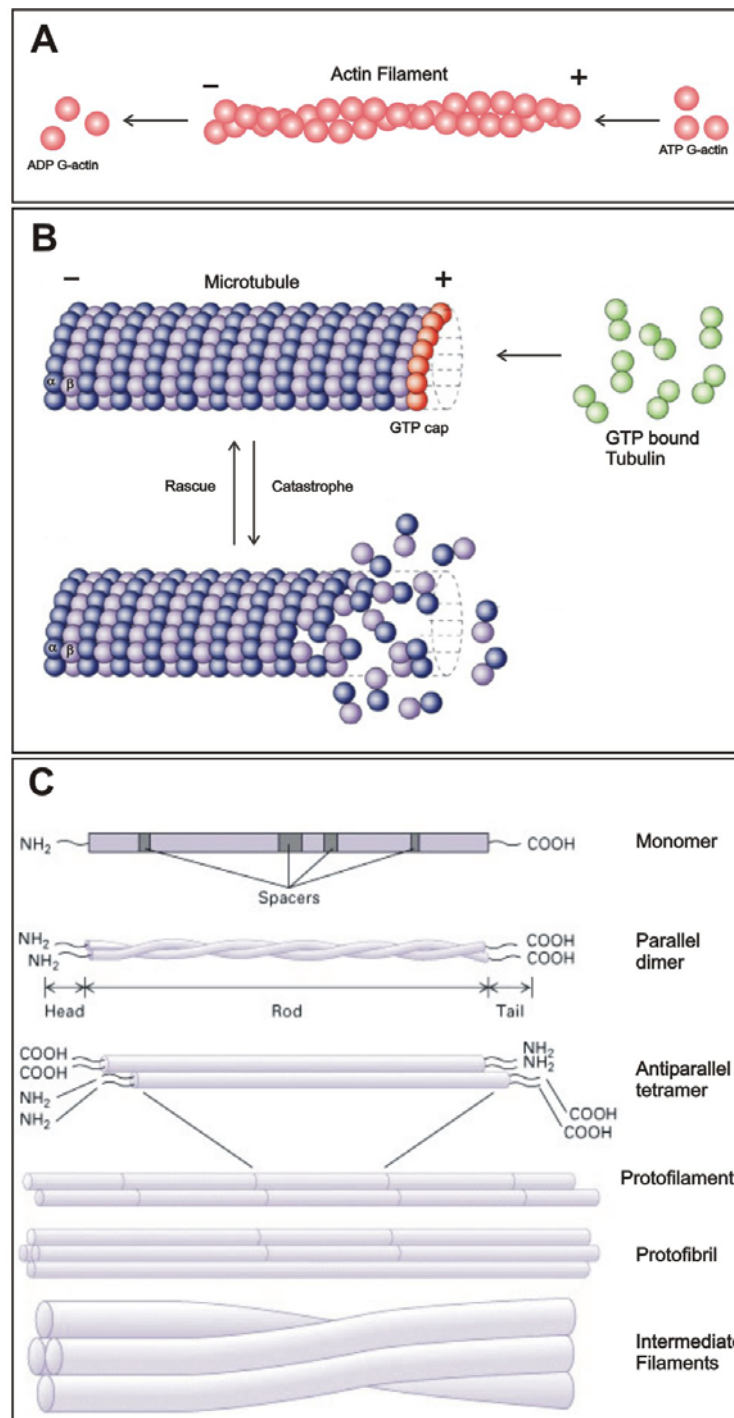
Figure 1.1   **A: Treadmilling actin filament. B: Microtubule cycles between rapid growth and shrinkage, called dynamic instability (Jordan and Wilson, 2004).**
C: A model of intermediate filament construction, image modified from
http://www.biology.iupui.edu/biocourses/Biol540H/images/grim_fil_struct_lab.jpg.

1.1.2 Polymerization and dynamics of cytoskeletal systems.

Cytoskeletal systems are dynamic in nature. Regulation of their dynamic behaviour and assembly allows eukaryotic cells to build an enormous range of structures from the three basic filaments. Polymerization of actin and tubulin is well characterized. For a new filament to form, subunits must assemble into an initial aggregate, or nucleus, that is stabilized by many subunit-subunit contacts and then can elongate rapidly by addition of more subunits. The initial process of nucleus assembly is called filament nucleation. The assembly of nucleus is relatively slow than the elongation. Therefore nucleation is the rate-limiting step in the formation of cytoskeletal polymers.

The structural polarity of actin filaments and microtubules is created by the regular, head-to-tail orientation of all their subunits. This orientation makes the two ends of each polymer different in ways that have a profound effect on filament growth rates. The fast-growing end is called the plus end, whereas the slow-growing end is called the minus end. In addition to their ability to form polymers, the actin and tubulin subunits are both enzymes that can catalyze the hydrolysis of ATP and GTP respectively. Hydrolysis proceeds very slow for the free subunits. However, it is accelerated when the subunits are incorporated into filaments. Shortly after incorporation of actin and tubulin subunits into the filament, nucleotide hydrolysis occurs. The free phosphate group is released from each subunit, but the nucleotide di-phosphate remains trapped in the filament structure. Hydrolysis of the bound nucleotide reduces the binding affinity within the subunits and makes it more likely to dissociate from the filament. Therefore, it is usually the tri-phosphate form (T-form) that adds to the filament and the di-phosphate form (D-form) that leaves the filament. The rate of addition of subunits to a growing filament can be faster than the rate at which their bound nucleotide is hydrolyzed. Under such conditions, the end has a cap of subunits containing the nucleoside tri-phosphate, an ATP cap on an actin filament or a GTP cap on a microtubule.

Filament treadmilling and dynamic instability are two behaviours observed in cytoskeletal polymers. Both are associated with nucleoside tri-phosphate hydrolysis. Dynamic instability is believed to predominate in microtubules, whereas treadmilling may predominate in actin filaments. During treadmilling, subunits are recruited at the plus end of the polymer in the T-form and shed from the minus end in the D-form (Figure 1.1 A).

Dynamic instability is characterized by the coexistence of polymerizing and depolymerising filaments. In the case of microtubules, presence of GTP cap stabilizes and aids rapid growth of the filament. Accidental loss of GTP cap would result in rapid shrinkage, and is called *catastrophe*. Reacquisition of the GTP cap would restore the growth, and is called *rescue* (Figure 1.1 B).

1.2 An overview of the cell cycle

A cell reproduces by performing an orderly sequence of events in which it duplicates its contents and then divides into two daughter cells. This cycle of duplication and division, known as the cell cycle, is the essential mechanism by which all living things reproduce. The most basic function of the cell cycle is to duplicate accurately the vast amount of DNA in the chromosomes and then segregate the copies precisely into two genetically identical daughter cells. These processes define the two major phases of the cell cycle, S and M phase. DNA duplication occurs during S phase (S for synthesis). After S phase, chromosome segregation and cell division occur in M phase (M for mitosis). Most cells require much more time to grow and double their mass of protein and organelles, than they require replicating their DNA and dividing. Partly to allow more time for growth, extra gap phases are inserted in most cell cycles, a G1 phase between M phase and S phase and a G2 phase between S phase and M phase. Thus, the eukaryotic cell cycle is traditionally divided into four sequential phases: G1, S, G2, and M (Figure 1.2). G1, S and G2 phase together are called interphase.

The M phase involves a series of dramatic events that begin with nuclear division, or mitosis and end with cell division or cytokinesis. M phase is divided into six stages; the first five stages constitute mitosis. Cytokinesis occurs in the sixth stage, which overlaps with the end of mitosis. The five stages of mitosis; prophase, prometaphase, metaphase, anaphase, and telophase occur in strict sequential order.

During prophase, the replicated chromosomes, each closely associated to the sister chromatids, condense together with the reorganization of the cytoskeleton, forming mitotic spindle pole. A mitotic spindle is made of radiating microtubules attached to the two centrosomes, which were duplicated during S phase. Prometaphase starts with the

breakdown of the nuclear envelope. Chromosomes get attached to the mitotic spindle (microtubules) via their kinetochores, a multiprotein complex. At metaphase, the chromosomes are aligned at the equatorial plate, midway between the spindle poles. The kinetochore-microtubules attach sister chromatids to opposite poles of the spindle. At anaphase, the sister chromatids synchronously pulled towards their respective spindle pole to form two set of chromosomes. This process of chromosome separation results because of shortening of kinetochore-microtubules. During telophase, the two sets of daughter chromosomes arrive at the poles and decondense. A new nuclear envelope reassembles around each set, completing the formation of two nuclei and marking the end of mitosis. Then cytokinesis begins with the assembly of the contractile ring. During cytokinesis, the cytoplasm is divided into two by a contractile ring of actin and myosin (actomyosin ring), which provides the mechanical force to pinch the cell into two daughter cells, each with one nucleus.
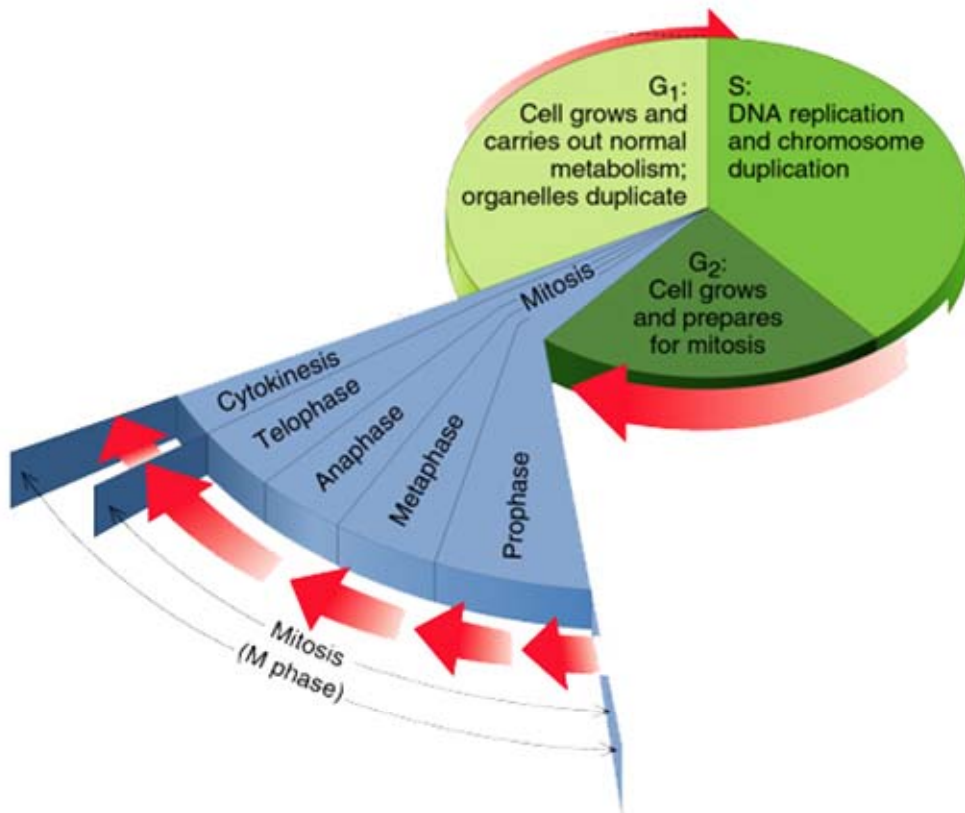
Figure 1.2   **Scheme of cell cycle, modified from http://fig.cox.miami.edu/~cmallery/255/255mitos/**

1.3 Guanine nucleotide binding proteins

Many fundamental cellular processes are regulated by GNBPs (guanine nucleotide binding proteins) with a common principle of GTP binding and hydrolysis (Bourne, 1991). GNBPs act as molecular switches and are present in two conformations, GTP bound (active form) and GDP bound (inactive form). The exchange of GDP to GTP turns on the switch and GTP hydrolysis turns it off. In GTP bound form, the GNBPs have high affinity for other macromolecules (effectors) mediating key cellular functions. The activation of GNBPs involves the exchange of GDP for GTP and is characterized as intrinsically slow process that is accelerated by guanine nucleotide exchange factors (GEFs). Similarly the hydrolysis of GTP to GDP which is also an intrinsically slow process is stimulated by the action of GTPase activating proteins (GAPs) (Figure 1.3).
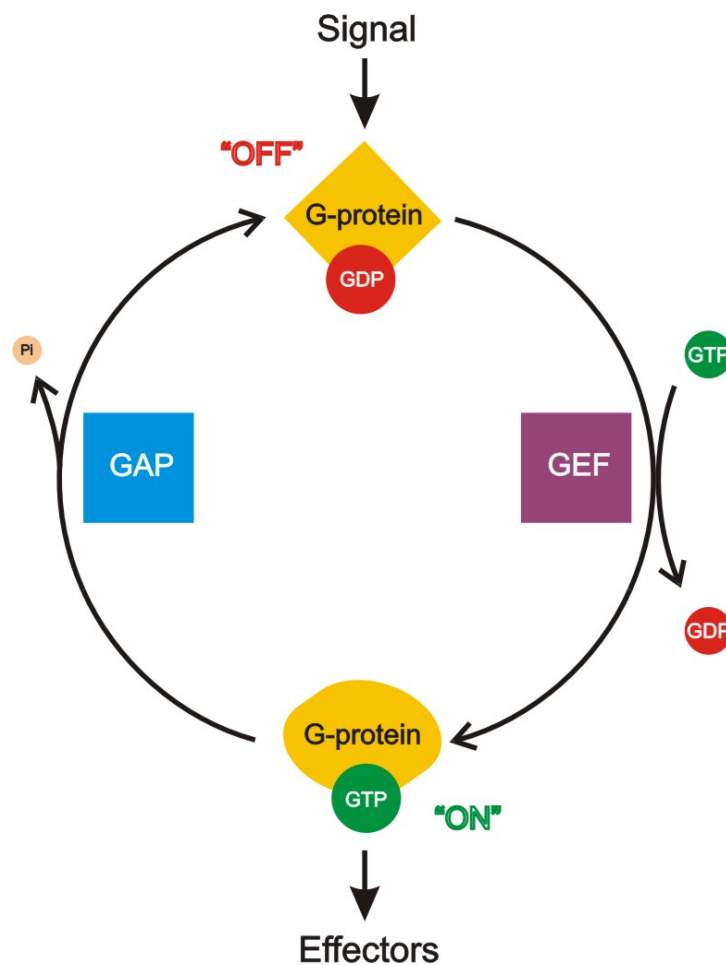
Figure 1.3   **Schematic representation of GTPase cycle**

1.3.1 Classification of GTPase superclass

The GTPase superclass was recently classified based on sequence and structural alignments of all available GNBPs. These are TRAFAC and SIMIBI class (Leipe et al., 2002).

The TRAFAC class (<u>tra</u>nslation <u>fac</u>tors) mostly contains regulatory proteins involved in signal transduction and translation such as, Ras-like superfamily, translation factor superfamily, Myosin-kinesin superfamily, TrmE-Era-EngA-Septin like superfamily.

The Ras-like superfamily contains more than 140 small GNBPs and can be subdivided into Ras, Rab, Rho, Ran, Arf, subfamilies (Garcia-Ranea and Valencia, 1998; Takai et al., 2001). These GNBPs in principle consist of only the G (GTPase) domain of 21 kDa, essential for the GTPase activity and regulatory processes, therefore also known as small GTPases. The Ras family members mainly regulate gene expression. The Rho family members control cytoskeletal reorganization. Members of the Ran family regulate nucleo-cytoplasmic transport. The Rab and Arf GNBPs control intracellular vesicular transport.

The translation factor superfamily proteins play important role at several stages of translation process such as initiation, elongation and release of nascent polypeptides. The translation factor proteins appear ubiquitously in bacteria and eukaryotes. Initiation factor IF2, elongation factors ET-Tu and EF-G, and releasing factors (RF-3) are a few important members of the translation factor superfamily.

The myosin-kinesin superfamily proteins contain motor proteins such as kinesin and myosin. These motor proteins are mechano-chemical enzymes which hydrolyze ATP and move along cytoskeleton. According to Leipe et al., these proteins evolved from a common GTPase ancestor and later on lost their specificity towards GTP (Leipe et al., 2002).

The dynamin-like superfamily contains dynamin, Mx, GBP (guanine-nucleotide binding protein) etc. Members of dynamin-like superfamily are multi domain GTPases, and their G domain usually contains insertions, which are often called large GTPases. Many of the family members are believed to be mechano-chemical enzymes. Dynamin proteins are involved in membrane fission of clathrin coated vesicles (Praefcke and McMahon, 2004). Mx proteins are involved in viral resistance by binding to specific viral components (Urrutia et al., 1997). GBP proteins are induced by interferons, which act against viral infection (Prakash et al., 2000).

TrmE-Era-EngA-Septin like superfamily contains proteins mainly of bacterial origin. Era family is characterized by a central GTPase domain and a C-terminal KH domain, a RNA-binding domain (Johnstone et al., 1999). Era proteins are likely to be translation factors, whose association with 16 S RNA via the KH domain stimulates the GTPase activity (Meier et al., 2000). EngA family is named after Essential Neisserial GTPase A (Mehr et al., 2000). EngA and its orthologs are composed of two similar GTPase domains. Both Era and EngA are ubiquitous in Bacteria and plants but are absent in Eukaryotes and Archea.

TrmE is ubiquitous in Bacteria and is a wide spread mitochondrial protein in Eukaryotes, but is absent in Archea. TrmE plays an important role in tRNA modifaction. The structure of TrmE shows an N-terminal domain, a central helical domain and C-terminal G domain (Scrima et al., 2005). Recently it has been shown that the G domains of TrmE can dimerize in a potassium dependent manner and induce GTP hydrolysis (Scrima and Wittinghofer, 2006). Septin is also a member of this superfamily and is the main subject of this study, which has been discussed in more detail in latter sections.

The SIMIBI class (signal recognition particle, MinD and BioD) contains proteins of signal recognition associated GTPase family, MIND/Mrp-Etk superfamily and BioD/FTHFS superfamily. All these proteins share structural and sequence similarities that clearly distinguish them from the TRAFAC class (Leipe et al., 2002). The best known examples are the SRP (signal recognition particle) and SR (SRP-receptor). Both are involved in targeting of nascent secretory and membrane proteins to the endoplasmic reticulum.

1.3.2 Characteristic features of the G domain

The G domain is highly conserved in all guanine nucleotide binding proteins. The conserved G domain has an approximate molecular mass of 21 kDa and has a typical fold consisting of a mixed six-stranded β sheet and five α helices (Figure 1.4). Crystal structures of all available GNBPs of TRAFAC class show that Ras shares a common structural core – the G domain fold (Vetter and Wittinghofer, 2001). Therefore, Ras is considered a paradigm for most of the GNBPs of the TRAFAC class.
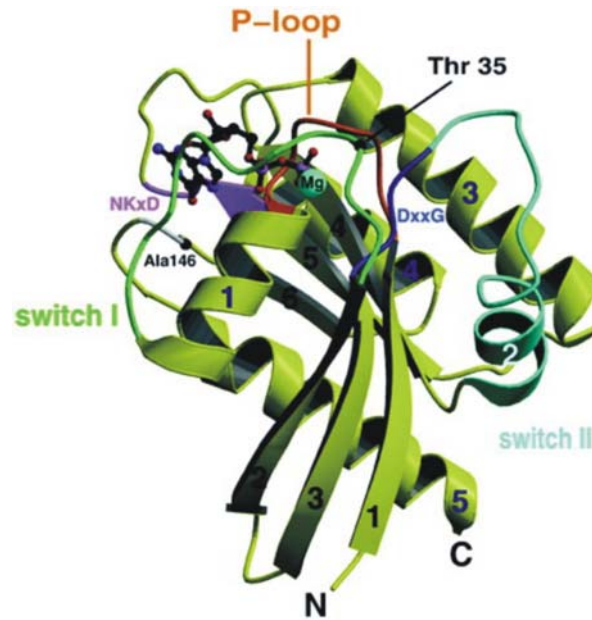
Figure 1.4   **Ribbon plot of the minimal G domain, with the conserved sequence elements and the switch regions in different colors as indicated. The nucleotide and Mg^{2+} ion are shown in ball-and-stick representation, after Vetter and Wittinghofer, 2001.**

The G domain contains five conserved sequence elements around the guanine nucleotide binding site, called G1 to G5 (Bourne et al., 1991; Saraste et al., 1990). The G1 motif (GxxxxGKS), also known as P-loop (phosphate binding loop) interacts with the α- and β-phosphates of the nucleotide. The G2 motif contains an invariant threonine (Thr35 in Ras) which is involved in Mg^{2+} coordination and direct binding to the γ-phosphate. The conserved aspartate (Asp57 in Ras) of G3motif (DxxG) binds to the magnesium ion via a water molecule and the glycine (Gly60 in Ras) makes a main chain contact to the γ-phosphate. Together these two motifs G2 and G3 trigger conformational changes when the γ-phosphate is hydrolyzed. Therefore the regions that include these motifs are termed switch regions. Switch I includes the G2 motif and switch II includes the G3 motif. The switches are the main determinants for binding of effector molecules. The G4 motif (NKxD) is important for guanine nucleotide specificity. The aspartate (Asp119 in Ras) makes a bi-furcated contact to the guanine base ensuring the specificity. The alanine (Ala146 in Ras) of G5 motif (SAL/K) makes a main chain interaction with the guanine base (Vetter and Wittinghofer, 2001).

1.4 Septins identification

Septins were first identified in budding yeast (*Saccharomyces cerevisiae*), during the analysis of temperature sensitive mutants defective in cytokinesis and were called *CDC* (cell division cycle) mutants (Hartwell, 1971). Sequencing of these *CDC* genes revealed that they were highly similar. This novel family of proteins was named septins to indicate their role in septation and cell division (Longtine et al., 1996). Mutations in any one of the four septin genes *CDC3, CDC10, CDC11,* and *CDC12* prevent cytokinesis leading to an accumulation of large multinucleated budded cells in conditional mutants at restrictive temperature (Adams and Pringle, 1984). All four septins were found to colocalize into a set of 10nm filaments at the bud-neck as observed by thin-section electron microscopy (Figure 1.5) (Byers and Goetsch, 1976a).

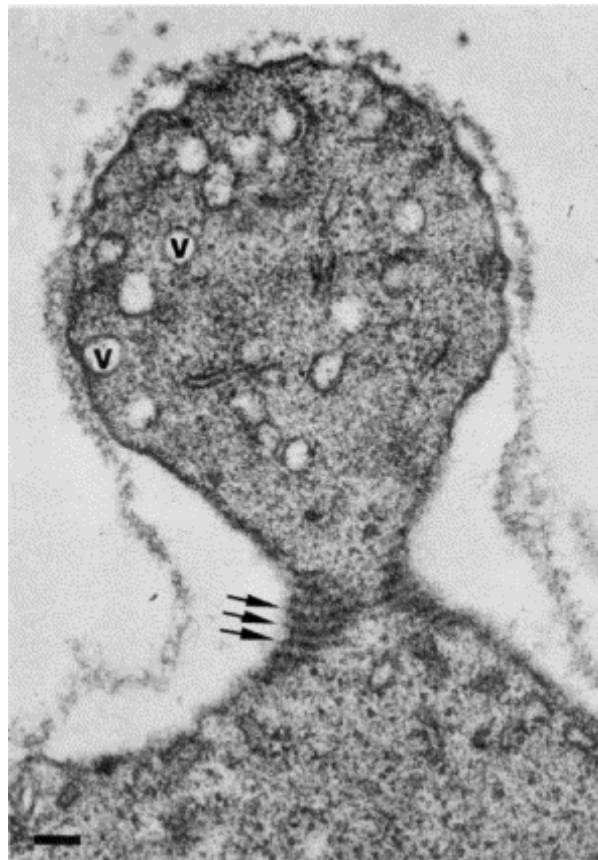**Figure 1.5** **Thin-section electron microscopy of an early bud of *S. cerevisiae* after Byers et al 1976**

Inactivation of any of the septins lead to loss of the neck filaments (Byers and Goetsch, 1976b). In addition, the loss of other septins from the bud neck was judged by immuno-fluorescence studies (Haarer and Pringle, 1987; Kim et al., 1991). These studies suggest that the septins are structural components of the bud neck filaments. Cytoplasmic septin complexes assemble into a ring at the presumptive bud site in late G1 phase, and then expand to demarcate an hourglass-shaped cortical zone at the mother-bud neck as the bud forms. At the end of cell cycle, the septin hourglass splits into two rings that are then inherited by daughter cells, and dissemble during the next cell cycle G1 phase.

The neck filaments were considered to be unique component of yeast until septin (product of *pnut* gene) was discovered in *Drosophila* (Neufeld and Rubin, 1994). Many septin genes were identified in humans (Longtine et al., 1996) and the Nedd5/Septin 2 has been shown to be required for cytokinesis in mammals (Kinoshita et al., 1997). Since then septins have been identified in most of the eukaryotic organisms with the exception of plants.

In mammals, septin identification dates back to the early 1990s where a series of genes Diff6 (Septin 1), H5 (Septin 4), Nedd5 (Septin 2), hCDC10 (Septin 7), KIAA05158 (Septin 6) were identified and found to belong to the septin family. The old names were replaced to new names (in brackets) according to the new guidelines proposed for mammalian septin nomenclature (Macara et al., 2002). To date, 13 septin genes and their products have been identified named SEPT1-SEPT13 in humans (Kinoshita, 2006; Hall et al., 2005). Mammalian septins can be co-purified as complexes from tissues and cells (Hsu et al., 1998; Kinoshita et al., 2002) similar to *Drosophila* septins (Field et al., 1996). However each preparation contains far more than three proteins (compared to septin complex purified from *Drosophila* embryos) with an obscure stochiometry, suggestive of mixed complexes of distinct composition (Kinoshita, 2003). A simple mammalian septin complex with a 1:1:1 stochiometry has been isolated from NIH3T3 cell lysate by affinity chromatography using GST-Borg3, a Cdc42 effector protein (Joberty et al., 2001). Thus a simple three component system comprising of SEPT2, SEPT6 and SEPT7 is regarded as the orthologs of the *Drosophila* Sep1, Sep2 and Pnut septin complex. Taken together the SEPT2-SEPT6-SEPT7 complex serves as a model for biochemical and structural analyses for the mammalian septin complex.

The complexity of the human septin gene family is further increased by the existence of alternate splicing in most of the septins. This dramatically increases the number of potential isoforms expressed. The most extreme case so far defined is *SEPT9*, where six 5' splice variants, and three 3' splice variants can combine a common core domain to give at least 18 transcripts encoding 15 polypeptides. In addition multiple splice variants encoding the same polypeptide have also been reported for *SEPT8* and *SEPT6* (Hall and Russell, 2004). The genomic, transcriptional and isoform complexity, coupled with sheer number of human septins, has hindered progress in understanding this family.

1.5 Domains and motifs
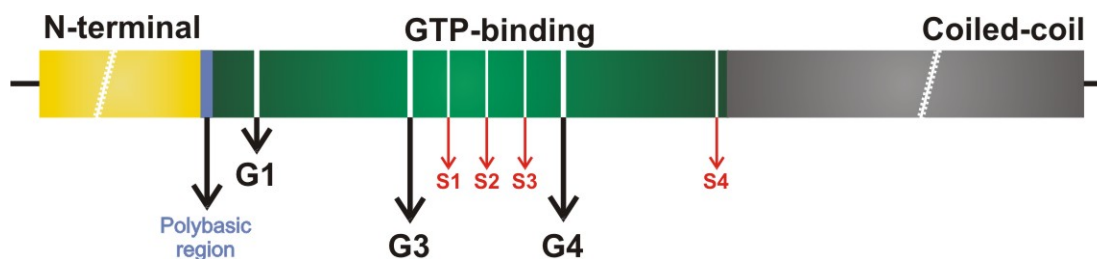
Figure 1.6   **Primary structure of septin, modified from Pan et al., 2007**

A typical septin primary structure contains a central core GTP-binding domain (G domain), flanked by a variable N-terminus and C-terminus. The N-terminus has no similarity among the septins except for the poly-basic region just before the GTP-binding domain. The C-terminal is predicted to form coiled-coils. The length of the coiled coil regions varies between 50 -100 amino acids, and some septins even lack the coiled-coil region (SEPT3, SEPT9 and SEPT12). The G-domain is more Ras-like where the septins clearly contain G1, G3, and G4 signature motifs (Figure 1.6). G2 motif is either missing or difficult to locate from the sequence.

In addition to the GTP-binding signature motifs, G1, G3 and G4, a new set of septin unique motifs have been identified (Pan et al., 2007). The authors identified four new septin motifs namely Sep1-4 (S1-4) and six new conserved single amino acid positions (Pan et al., 2007). The Sep1 motif, ExxxxR, the Sep2 motif, DxR[VI]Hxxx[YF]F[IL]xP, the Sep3 motif, GxxLxxxD. All these three new motifs were located in between the well known G3 and G4 motifs. The Sep4 motif, WG is at the end of the GTP-binding domain (Figure 1.6).

1.6 Redundancy of the mammalian septin system
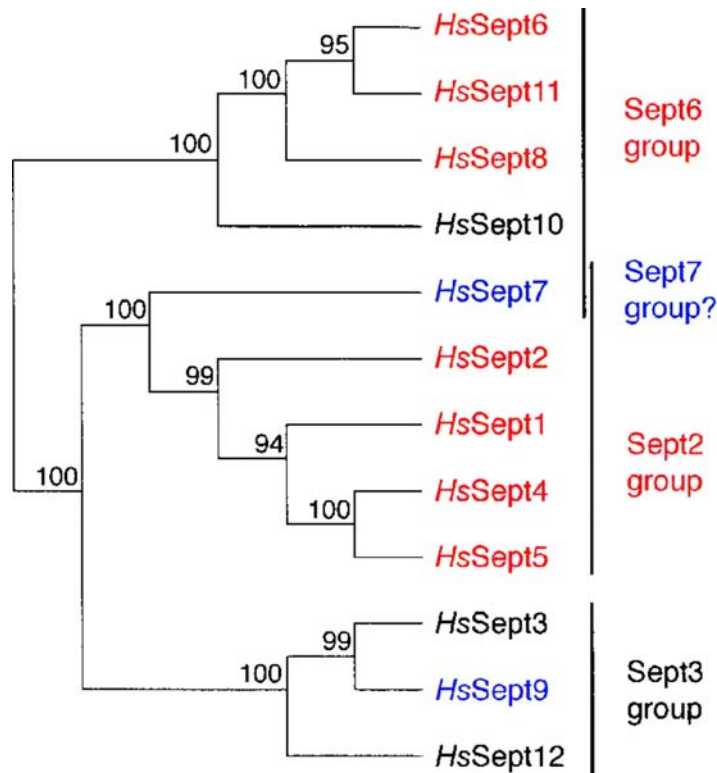
Figure 1.7   **Phylogenetic tree of the human septins, after Kinoshita, 2003**

The mammalian septin family members can be classified into four groups based on the amino acid sequence homology. The homology based classification so far agrees with the compatibility in the recombinant complex formation tested in insect cells (Kinoshita et al unpublished observation (Kinoshita, 2003)). SEPT1, SEPT2, SEPT4 and SEPT5 can each form an equimolar complex with the SEPT6-SEPT7 partial complex giving rise to SEPT**X**-SEPT6-SEPT7 complexes of ~1:1:1 stochiometry, where **X**=1, 2, 4, 5. SEPT6 in the SEPT2-SEPT6-SEPT7 complex is replaceable with SEPT11, and probably the other components of SEPT6 group (Figure 1.7). SEPT3, SEPT9, and SEPT12 are predicted to lack a coiled-coil region, unlike the other septins, form another group. SEPT7 is unique and may not be replaceable. Each septin polypeptide seems to have temporally and spatially distinct expression patterns *in vivo* (Kinoshita et al., 2000; Beites et al., 1999; Hall et al., 2005). The redundancy and inter-changeability among the septin subunits may contribute to diversify the repertoire of the septin complexes in a combinatorial fashion. The redundancy and flexibility obviously contribute to secure the mammalian septin system. It is still not

clear whether the complexes with distinct composition have distinct biochemical and functional properties. Apart from SEPT2-SEPT6-SEPT7 a complex comprising SEPT7-SEPT9b-SEPT11 was isolated and charaterized (Nagata et al., 2004) supporting the argument that septins from each group could in principle form complexes.

1.7 Septins and disease

There is an increasing body of evidence that septins are involved in the pathogenesis of various diseases like neoplasia and neurodegenerative diseases (Hall and Russell, 2004). Missense *SEPT9* mutations were recently found to be responsible for HNA (hereditary neuralgic amyotrophy) (Kuhlenbaumer et al., 2005).

Few septins have been found to accumulate into pathological cytoplasmic structures in common neurodegenerative disorders in humans, such as Alzheimer's disease (Kinoshita et al., 1998), Parkinson's disease and other synucleinopathies (Ihara et al., 2003). SEPT5_v2, a splice variant has been reported to be a parkin-binding protein and parkin can function as an E2-dependent ubiquitin ligase capable of promoting the degradation of SEPT5. SEPT5 accumulates in the brains of individuals with autosomal recessive juvenile parkinsonism (Ihara et al., 2003). Although *SEPT5* is expressed in the brain, involved in exocytosis and has been associated with parkinsonism, it is dispensable for normal development and function as shown by the viability and normal development of *SEPT5* null mice (Peng et al., 2002). The first clue about the role of septins in neoplasia came from the observation where the MLL (Mixed Lineage Leukaemia) protein was fused in frame to almost the entire open reading frame of *SEPT9* in leukaemia. Subsequently, it has been found that three other septins SEPT5, SEPT6 and SEPT11 can form very similar fusion proteins with MLL again with the N-terminal moiety of MLL fused in frame to almost the entire open reading frame of the respective partner septin (Russell and Hall, 2005). SEPT9 overexpression has been observed in diverse tumor types. It is observed that neoplasia is associated not just with altered expression of SEPT9 but also by alterations in the expression of specific *SEPT9* transcripts. *SEPT9_v4* and *SEPT9_v4** are distinct mRNAs but encode identical polypeptides. While the *SEPT9_v4* is the predominant transcript in normal tissues, it is replaced by *SEPT9_v4** in tumors (Scott et al., 2006; Scott et al., 2005). The *SEPT9_v4**

transcript appears to be translated more efficiently than the *SEPT9_v4* transcript (Mcdade et al., 2007) and thus this change in transcript profile has a profound effect on the level of this SEPT9_v4 protein isoform. Based on this, a model was proposed where the *SEPT9_v4** transcript is non-regulated and the *SEPT9_v4* transcript is highly regulatable. Therefore the translational control is a general mechanism for the regulation of septin polypeptide expression and it is lost during neoplasia.

1.8 Septin orthologs between different organisms

With the increased availability of genome sequences, it is now clear that septins are found in fungi, animal and microsporidia. The number of septin proteins in a single organism ranges from two in *Caenorhabditis elegans* (nematode) to 13 in humans, 7 in *Saccharomyces cerevisiae* (budding yeast) & *Saccharomyces pombe* (fission yeast) and 5 in *Drosophila* (fly). Recently phylogenetic analysis were carried out for all available septin sequences and classified into five major clades, Group1 - Group5 (Pan et al., 2007). Group1 and Group2 contain fungal and animal septins, Group3 and Group4 contain fungal and microsporidial septins and Group5 contain only fungal septins. From these five major groups the authors propose a model for septin evolution. However, functional orthologs among different organisms cannot be readily classified based on primary structure alone.

Table 1.2 Functional orthologs across different organisms.

Budding yeast	Nematode	Fly	Human
Cdc3	Unc-61	Sep2, Sep5	SEPT6, SEPT8, SEPT10, SEPT11
Cdc10	-	-	SEPT3, SEPT9, SEPT12
Cdc11	-	Sep1, Sep4	SEPT1, SEPT2, SEPT4, SEPT5
Cdc12, Spr3	Unc-59	Pnut	SEPT7, SEPT13

Phylogenetic analysis also reveals that some mammalian septins belonging to SEPT3 group are the counterparts of Cdc10 (and Spn2), as they all lack C-terminal coiled-coil domains (Table 1.2). Since all mammalian septin complexes characterized so far contain both SEPT6 (or another septin from SEPT6 group) and SEPT7 (Nagata et al., 2004; Sheffield et al., 2003). Therefore, it was proposed that mammalian SEPT6-SEPT7 and fly Sep2-Pnut are the counterparts of the yeast Cdc3-Cdc12 complex (Versele and Thorner, 2005).

Septin complexes isolated from tissues and cells also contain either one or two additional septins, one from the SEPT2 group and/or one from the SEPT3 group, which lacks the coiled-coil region. All the isolated complexes, containing 3-4 septin subunits were shown to form filaments in vitro (Kinoshita et al., 2002; Field et al., 1996; Joberty et al., 2001; Farkasovsky et al., 2005). Based on this, it is widely believed that a ternary complex comprising three different septins Cdc3-Cdc11-Cdc12 or Cdc3-Cdc10-Cdc12 (Farkasovsky et al., 2005; Versele et al., 2004) and SEPT2-SEPT6-SEPT7 in case of mammals is the minimal complex required to form a functional septin filament. In *Caenorhabditis elegans* only two septin genes have been found. Both the proteins UNC-59 and UNC-61 have similar properties like that of septins from other organisms. Based on the sequence similarities, it seems likely that UNC-59 and UNC-61 function as an obligate complex that is the counterpart of the yeast Cdc3-Cdc12 complex (Table 1.2). These findings also support the assumption that a Cdc3-Cdc12-like heterodimer is the non-reducible core that is essential for septin function in vivo. But the recombinatly purified heterodimers of yeast (Cdc3-Cdc12) and mammals (SEPT6-SEPT7) does not form filaments (Farkasovsky et al., 2005; Sheffield et al., 2003). However, UNC-59 and UNC-61 are the only septins in *Caenorhabditis elegans* and when purified form filaments *in vitro*, they represent an exception to the above mentioned rules based on other organisms.

1.9 Septin filaments
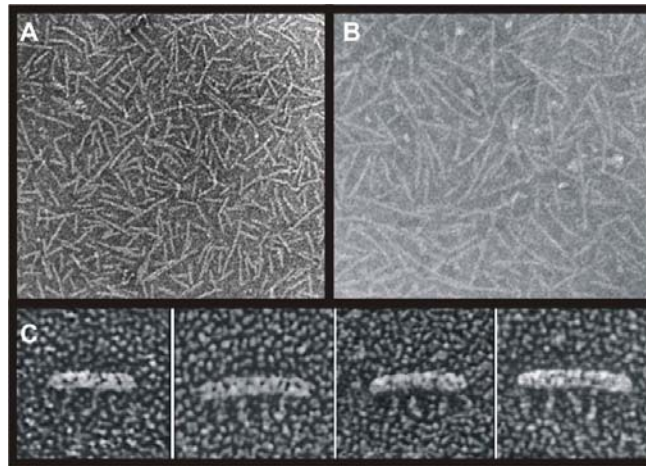
Figure 1.8   **A and B: negative stain electron micrographs of *Drosophilla* and yeast septin complexes, modified from Field et al., 1996 and Frazier et al., 1998. C: Rat septin complex analysed by quick-freeze/deep-etch electron microscopy modified from Hsu et al., 1998.**

Filamentous structures similar to those of *Saccharomyces cerevisiae* have been seen at the mother-bud neck and near the bases of hyphae in the dimorphic yeast *Candida albicans* (Didomenico et al., 1994). The possibility that neck filaments comprise a new class of cytoskeletal polymers prompted biochemical investigation of septin polymerization. A septin complex consisting of multiple septin polypeptides was first isolated using the immunoaffinity chromatography from the *Drosophila* embryos. The purified complex comprised of gene products of *pnut*, *Sep1,* and *Sep2* isolated via the gel filtration and density gradient centrifugation and a native molecular mass of ~340 kDa was estimated. Negative stain electron microscopy revealed that the septin complex has the ability to self assemble into polymers. For these filaments a diameter of 7-9 nm was consistently observed with varying lengths of 26 nm periodicity (Field et al., 1996). Septin complexes from various organisms like *Saccharomyces cerevisiae* (Frazier et al., 1998), rat (Hsu et al., 1998), and mammalian (Kinoshita et al., 2002) were purified endogenously and found to have varying number of polypeptides. All the purified complexes are found to form filaments *in vitro* and a similar 7-9 nm diameter was consistently reported (Figure 1.8). The periodicity of the filaments varies with number of polypeptides (32 nm for yeast septin

complex and 25 nm for rat oligomeric septin complex). The length of the filaments was greatly increased by reducing the salt concentration.
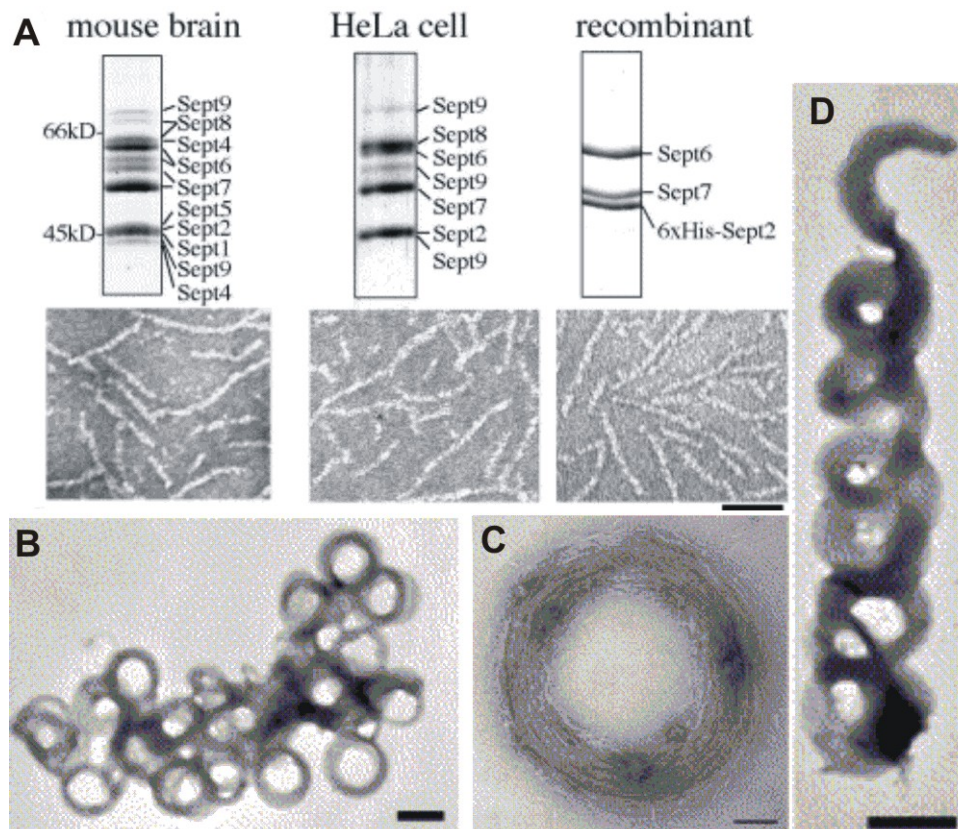
Figure 1.9 **A: Purified septin complexes from different sources. B-D: Electron micrographs of the septin complex forming higher order structures under low salt conditions. Modified from Kinoshita et al 2002.**

The striking feature of septins is its ability to form filaments *in vitro* without adding any cellular factors. Mammalian septin complexes from mouse brain and HeLa cells were purified using peptide antibody ubiquitous to SEPT2 and shown to contain far number of septin polypeptides (Figure 1.9 A). Co-expression of SEPT2, SEPT6 and SEPT7 and purification resulted in a complex with 1:1:1 stochiometry of the three polypeptides (Figure 1.9 A). This was the first reported recombinant co-expression and co-purification of mammalian septins from insect cells (Kinoshita et al., 2002). The endogenous and recombinant septin complexes showed no difference in filament formation (Figure 1.9 A). The latter was found to have similar properties as described for the endogenous fly and yeast septin complexes (Field et al., 1996; Frazier et al., 1998; Farkasovsky et al., 2005). The diameter of the filaments was again reported to be ~7nm. Higher order structures like

rings (Figure 1.9 B and C), and uniformly curved coils (Figure 1.9 E) were observed *in vitro* when the recombinant mammalian septin complex was dialysed in 50mM KCl (low salt concentration).

During interphase, septins are found to form filamentous structures and partially colocalize with actin structures. The septin-actin colocalization can be perturbed by drugs like Cytochalasin D which disrupts actin structures (Kinoshita et al., 1997). Recombinant septin complexes alone showed no detectable affinity for F-actin in co-sedimentation assays. Therefore an adaptor protein was proposed to mediate the interaction between F-actin and septin filaments. A series of actin binding proteins were tested and it was found that only anillin efficiently recruits septins to F-actin *in vitro* and shown to colocalize with F-actin and septin *in vivo* (Kinoshita et al., 2002; Oegema et al., 2000).

Several studies were carried out to elucidate the interaction of septins among each other. Two hybrid analyses of yeast septin proteins showed selective interaction patterns. Based on this study a preliminary model for the topology of the yeast septin complex was provided (Figure 1.10 A) (Farkasovsky et al., 2005). Similarly, models were proposed for septin complexes based on different observations and assumptions (Figure 1.10 B) (Versele and Thorner, 2005). Recently, *in vitro* FRET (Fluorescence-Resonance Energy Transfer) assays was carried out for mammalian septins and proposed that septins interact each other mainly via their coiled-coil regions (Figure 1.10 C) (Low and Macara, 2006).
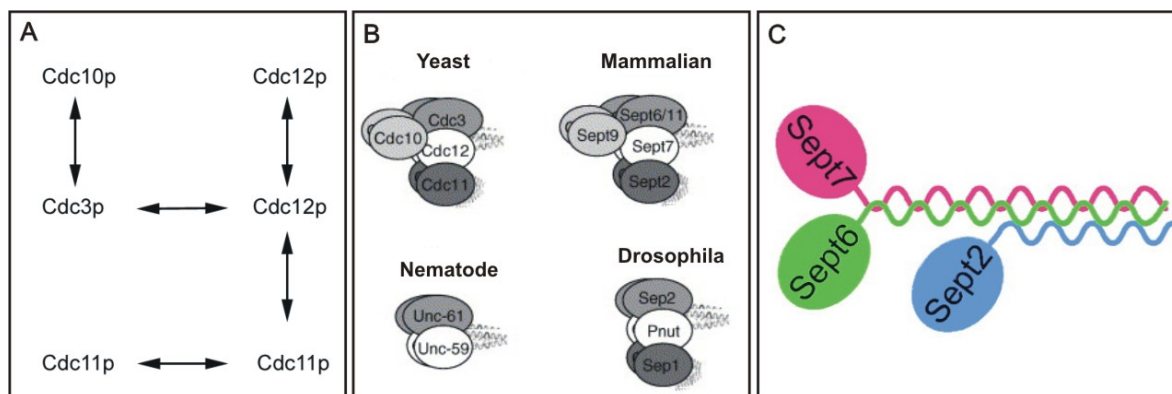

Figure 1.10　　**A: Topology of yeast complex modified from Farkasovsky et al., 2005 B: Proposed model for septin assembly from different organisms modified from Versele and Thorner, 2005 C: Model for mammalian septin complex based on FRET experiments, modified from Low and Macara, 2006.**

1.10 Regulation of septin polymerization

The regulation of septin assembly/disassembly might depend on the conformational changes induced by direct binding of the partner proteins, covalent modifications such as phosphorylation and SUMOylation or GTPase activity.

1.10.1 Regulation by interacting partners

Macara and co-workers identified one such protein partner, a downstream effector of Cdc42 called Borg (Binder of Rho GTPases) which contains a CRIB (Cdc42/Rac-interaction binding) motif, poly proline stretches and the Borg homology domains (BD1-3) (Joberty et al., 1999). The authors demonstrated that ectopic overexpression of Borg3 disrupts assembly of septins into fibrillar structures and the effect is inhibited by expression of a constitutively active mutant of Cdc42 (Rho family GTPase), which inhibits the Borg3-septin interaction (Joberty et al., 2001). The authors also show direct binding of the mammalian SEPT2-SEPT6-SEPT7 complex to Borg3 and mapped the regions of interaction and found that the BD3 (Borg homology domain 3) of Borg3 and coiled-coil regions of SEPT6-SEPT7 are involved. Neither of the septin monomers nor the other dimeric combinatorial complexes SEPT2-SEPT7 and SEPT2-SEPT6 were able to interact with Borg3 (Sheffield et al., 2003). However, not much work has been done to show the direct inhibition of septin assembly by Borg proteins. So far no clear Borg orthologs have been reported for yeast. Recent studies show Cdc42 GTPase-associated proteins Gic1 and Gic2 control cell polarity in yeast (Brown et al., 1997; Chen et al., 1997). Gic1 and 2 contain a CRIB motif, poly proline strtches and the C-terminal region homologous to BD3. Therefore, these Gic proteins could in principle act like Borgs in yeast (Wittinghofer et al., Unpublished work). New studies link Rho signalling to the regulation of septin assembly. Expression of a constitutively active mutant of Rho disrupts filamentous organization of Sept9b. Rhotekin was identified as the downstream effector that controls septin assembly into filaments which colocalize with actin stress fibres (Ito et al., 2005). In contrast to Rhotekin, which does not bind directly to SEPT9b, a septin associated RhoGEF has been shown as a direct binding partner whose overexpression leads to disruption of SEPT9b polymers (Nagata and Inagaki, 2005; Spiliotis and Nelson, 2006).

1.10.2 Regulation by covalent modifications
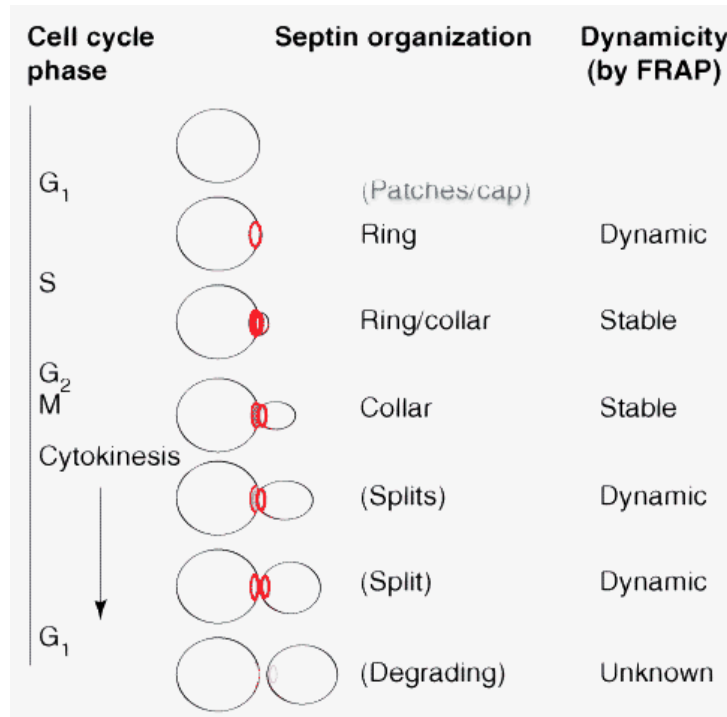
Figure 1.11   **Scheme showing transition of morphology and dynamicity of the yeast septin assembly, after Kinoshita, 2006.**

Much of the studies on septin post translational and covalent modifications have been done in yeast. Septins form collar-like structures for the majority of the yeast cell cycle (Figure 1.11). At the onset of cytokinesis the septin collar splits into a pair of rings on mother and bud sides. Using FRAP (fluorescence recovery after photobleaching) it was shown that septin collar exists in a dynamic or 'fluid' state (during the late G1 and M phase) and in a stable or 'frozen' state (during rest of the cell cycle) (Dobbelaere et al., 2003). Barral and colleagues show that activation of septin dynamics at the beginning of cytokinesis depends on de-phosphorylation of Shs1 septin by protein phosphatase2A (PP2A) and Rts1p, a kinetochore-associated regulatory subunit of PP2A phosphatase (Dobbelaere et al., 2003). Phoshorylation by two protein kinases, Cla4 and Gin4, also plays an important role in initiating and/or stabilizing the filament assembly during the collar formation and during emergence of the bud (Versele and Thorner, 2004; Versele and Thorner, 2005; Dobbelaere et al., 2003). Cla4 is an orthologs of mammalian p21-activated protein kinases (PAKs). Studies have shown that both kinases are recruited to the bud site early in the cell cycle by

direct binding to septins. Gin4 phosphorylates Shs1 exclusively, whereas Cla4 phosphorylates Cdc10, Cdc3, and Cdc11. Mutations in any of the Cla4 phosphorylation sites in Cdc10 (Ser256 and Ser312) shows distinct effects on cell morphology and septin architecture (Versele and Thorner, 2004).

After completion of cytokinesis and separation of mother and daughter cells, the septin rings disassemble for a short period in G1 phase (Figure 1.11). Whether disassembly involves degradation or recycling has not been determined. A role for SUMOylation by SUMO (small ubiquitin-like modifier) has been proposed (Johnson and Blobel, 1999). In fact septins have been extensively used as substrates for SUMOylation studies. Preventing SUMO attachment to the septins Cdc3 and Cdc11 by mutagenesis causes old septin rings to persist, which indicates that the disassembly is affected. In contrast, inactivation of the major SUMO ligase by *siz1D* mutation does not cause the same phenotype (Johnson and Gupta, 2001). These findings cast doubt on the suggestion that SUMOylation is required for disassembly of septin rings after cytokinesis (Versele and Thorner, 2005). Clearly how covalent modifications of septins influences the septin organization, dynamics and function is still in infancy and an active field of research.

1.10.3 Role of nucleotide

Perhaps the most controversial factor concerning the regulation of septin polymerization is the role of nucleotide. Field et al first demonstrated that purified *Drosophila* septin complex (Pnut-Sep1-Sep2) co-purifies with one molecule of guanine nucleotide per polypeptide, with an average GDP/GTP ratio of 2.6. The ratio is virtually unchanged when the complex was incubated for longer periods at 37$^\mathrm{o}$C. The authors also showed by exchange with radio-labelled GTP and a photo-cross-linking assay that Sep2 is most likely to be bound to GTP. When GTP was added extraneously, the complex exhibits GTPase activity (Field et al., 1996). Similar properties have been observed for recombinant mammalian and yeast septin complexes (Farkasovsky et al., 2005; Sheffield et al., 2003). In particular the nucleotide:septin ratio (1:1) and the bound GDP:GTP (2-3:1) are highly conserved between theses organisms (Kinoshita et al., 2002; Sheffield et al., 2003; Farkasovsky and Wittinghofer, 2003). In contrast the *Caenorhabditis elegans* septin complex comprising UNC-59 and UNC-61 are substochiometric with polypeptide (<0.1)

and found to have no GTP. This difference may be due the species-specific difference between nematode and other organism's septins (John et al., 2007). Intriguingly a single septin (Sept2) from *Xenpus laevis* was recombinatly expressed in *Escherichia coli* cells found to have no nucleotide bound to it. Further more the authors show that filament assembly does not require GTP hydrolysis, but the extent of filament assembly is greater in the presence of GTP-γ-S, a slowly hydrolysing GTP analog and also suggested that septin filaments assemble as a nucleated polymer (Mendoza et al., 2002). But soon this idea was rejected by Mitchison and colleagues that GTP-driven polymerization is not valid for heteromeric septin complexes (Mitchison and Field, 2002).

There is no evidence to support the hypothesis that the higher-order assembly of septin complexes depends on hydrolysis of guanine nucleotides. Using an *in vivo* ^{15}N-dilution assay it was shown that the majority of the yeast septin complexes do not turn over GTP during one cell cycle. Similar observation was seen for yeast complex *in vitro* during GTP binding/exchange assay (Farkasovsky et al., 2005). Since the GTP:GDP ratio is fixed, and the GTP bound to particular septin might add to the stability of the complex by binding tightly to its neighbouring septin(s). Vrabiou et al propose a structural role for the nucleotides bound to the septins which is important for stabilising the septin polypeptides (Vrabioiu et al., 2004).

Although septins are polymerizing proteins, so far no chemical molecule has been reported which can disrupt or inhibit septin polymerization. Unlike other cytoskeletal proteins which can be targeted by chemical inhibitors. For example, lantraculin, phallodin and cytochalasin which perturb actin polymerization reaction. Similarly, colchicines, vinblastine, nocodazole, and taxol acts on tubulin/microtubule. Recently, Iwase et al reported Forcholorfenuron, a synthetic plant cytokinin which was found to disrupt yeast septin organization in a specific and reversible manner. However, this drug has yet to be tested in mammalian cells (Iwase and Toh-e, 2004).

1.11 Septin function

1.11.1 Septins and cytokinesis

Although several aspects of how septins might function in cytokinesis were identified in yeast, the role of septins in cytokinesis is still not completely clear. In yeast, cytokinesis is the result of two redundant processes: the actomyosin ring contraction and the formation of the septum by vesicle fusion with the plasma membrane. Disruption of either one of the process leads to delay in cytokinesis, but not complete failure in cell separation (Mahamadou et al., 2002). In contrast disruption of septin function fully impairs cytokinesis (Adams and Pringle, 1984; Frazier et al., 1998). The septin complexes comprising Cdc3, Cdc10, Cdc11, Cdc12 and Shs1 of budding yeast assemble into tubular collar of highly ordered filaments at the cortex of the mother-bud neck throughout the cell cycle, except for disassembly and reassembly during G1 (Figure 1.11).

At the molecular level, two roles of septins have been proposed in yeast. First, the filaments formed by septin complexes serve as a scaffold that recruits other proteins and, perhaps activates them (Field and Kellogg, 1999). The second function of septin filaments is to establish discrete cellular compartments (Barral et al., 2000).

In the scaffold model, septins are postulated to form a scaffold at discrete cortical regions, such as the mother-bud neck in the budding yeast. The localization of at least 21 proteins at the bud neck requires proper assembly of septin filaments. These proteins include several protein kinases and other enzymes like chitin synthases and components of the bud-site selection machinery (Gladfelter et al., 2001). In mammalian cells septin bundles integrated with actin-based structures at the basal cortex of the interphase cells may also act as scaffolds, interacting directly or indirectly with two molecules of RhoGEF and rhotekin (Ito et al., 2005; Nagata and Inagaki, 2005). Although the functional details are still elusive, it was proposed that the septin bundles might thus help coordinate Rho-mediated control of the actomyosin bundles (Kinoshita, 2006).

Some observations on septin function are not easily reconciled with the scaffold model. For example the integral membrane protein Ist2p, a regulator of the mitotic exit network (MEN), Lte1p and cortical actin patches are exclusively localized to the daughter cell

before G2-M transition of the cell cycle (Takizawa et al., 2000; Barral et al., 2000; Jensen et al., 2002). The asymmetric localization of these proteins depends on bud-neck localized septins, suggesting that septins can function as a diffusion barrier. During cytokinesis in budding yeast, the tubular collar of septin filaments is split into two separate rings, rotate in the membrane plane and assemble into ring structures (Vrabioiu and Mitchison, 2006). This compartmentalization function appears to be conserved in fission yeast, where a double ring of septin filaments encompasses the contractile apparatus and provides for efficient dissolution of the primary septum (Wu et al., 2003). It appears that septins might have similar role in mammalian cells because septins are the prominent components of the cleavage furrow and a diffusion barrier within the cleavage furrow has been demonstrated (Schmidt and Nichols, 2004).

It remains unclear how the septins are anchored to the plasma membrane; consequently, it is not clear how the septin mediated diffusion barrier is generated at the bud neck. Septins also function in other processes associated with cell division, such as spindle positioning, cell-cycle checkpoints and have a role in maintaining cell polarity in the yeast (Longtine and Bi, 2003; Mahamadou et al., 2002).

1.11.2 Membrane organization and vesicle trafficking

Yeast and mammalian septins associate with biological membranes through a highly conserved polybasic region at the N-terminus of the GTP-binding domain. Through this region recombinant yeast septins associate preferentially with phosphotidylinositol (4)-phosphate [PtdIns(4)P] and phosphotidylinositol (5)-phosphate [PtdIns(5)P], whereas SEPT4 specifically binds phosphotidylinositol (4,5)-bisphosphate [PtdIns(4,5)P_2] and phosphotidylinositol (3,4,5)-trisphosphate [PtdIns(3,4,5)P_3]. In yeast cells defective in PtdIns(4)P synthesis, septins fail to assemble properly at the mother-bud neck. In mammalian cells, reduction of overall level of PtdIns(4,5)P_2 leads to loss of SEPT4 filaments (Casamayor and Snyder, 2003; Zhang et al., 1999). Association of septins with phospholipids is crucial to the formation and maintenance of membrane domains as demonstrated by Barral and colleagues for the compartmentalization of yeast cell membranes during interphase and mitosis (Barral et al., 2000; Spiliotis and Nelson, 2006).

The role of septins in secretion has been implicated by studies in mammalian cells. Among the few interactions reported for mammalian septins is their physical association with components of secretory apparatus, such as the exocyst complex and the SNARE complex. Septins were co-purified or co-immunoprecipitated with the secretory sec6/8 complex from rat brain cells and soluble N-ethylmaleimide-sensitive fusion (NSF) protein and receptors, which mediate vesicle docking and fusion respectively (Beites et al., 1999; Hsu et al., 1998). Beites and colleagues suggest that SNARE complexes associate with SEPT5, which competes for binding with the NSF protein and its attachement receptor SNAP. SNAPs are known to mediate dissociation of SNARE complexes following membrane fusion. Hence septin might regulate the availability of SNAREs for membrane fusion. This is consistent with data showing inhibition of exocytosis upon over-expression of SEPT5 in insulin-secreting cells and upregulated release of serotonin in platelets from *Sept5*-knockout mice (Beites et al., 1999; Ware et al., 2001). Thus, current evidence exists for a dual role of septins in exocytosis: as potential regulators of SNARE protein interactions and membrane fusion events, and as additional tethering or targeting proteins that interact with the exocyst complex during the transport of vesicle to sites if membrane fusion at the plasma membrane. The question of whether these functions are carried out by different septin members and what roles the state of bound guanine nucleotide or phospholipids play, are still largely unknown (Kartmann and Roth, 2001).

1.12 Objective of this work

Septins were identified over three decades ago. Since then, many cell-biological and biochemical studies revealed septins as guanine nucleotide binding proteins and multi-protein complex which forms higher order structures. These higher order structures act as a scaffold for many cellular processes. Electron microscopic studies show septins can self assemble in to filaments *in vitro*. Despite that, septins still remains a final frontier in terms of structural biology. Since no high resolution structure is available for either septin monomers or for the septin complexes until now. The assembly of the septins in hetero-oligomers and/or filamentous structures is poorly defined (Low and Macara, 2006; Versele and Thorner, 2005). Moreover, studies from budding yeast show differential localization of proteins to the mother and daughter side septin rings during the process of budding (Kozubowski et al., 2005; Barral et al., 2000). However, it is not clear whether this asymmetric localization across the bud is due to structural polarity of the septin filaments or some other independent mechanism. The structural studies should reveal the structural polarity of septin filaments.

The main objective of this work is structure determination of any of the septin monomers and also the septin complex to show the assembly of septins in to filamentous structure. Since, SEPT2-SEPT6-SEPT7 is a minimal functional complex isolated from NIH3T3 cells which can form filaments (Joberty et al., 2001). Mammalian septin complex comprising SEPT2-SEPT6-SEPT7 was chosen for this study.

It was widely believed in the field, that the purification of stable septin monomers was not possible except for couple of cases (Sheffield et al., 2003; Mendoza et al., 2002). Moreover, studies carried out on septin monomers was considered not to represent the heteromeric septin complex (Mitchison and Field, 2002). Nevertheless in this work, a septin monomer (SEPT2) was chosen for further structural studies, due to the fact that there is no structural data available for any of the septins. Furthermore, due to high sequence homology between septins the monomeric model can be used in generating model for larger multimeric complexes.

2 Materials and Methods

2.1 Materials

2.1.1 Chemicals

All chemicals were purchased from Aldrich (Steinheim), Amersham-Pharmacia (Freiburg), Boehringer Mannheim (Mannheim), Fluka (Neu-Ulm), Merck (Darmstadt), Roche (Mannheim), GERBU (Gaiberg), Serva (Heidelberg), Invitrogen (Karlsruhe), Qiagen (Hilden), Roth (Karlsruhe), Serva (Heidelberg), Sigma-Aldrich (Deisenhofen), and Jena Bioscience (Jena).

2.1.2 Molecular biology enzymes, Proteins, Primers and Markers

All molecular biology enzymes were purchased from New England Biololabs, DNase I from Roche, Thrombin from Serva, PreScission protease was made in-house according to the Invitrogen protocol, Complete EDTA free Protease Inhibitor cocktail from Roche, all primers were obtained from MWG Biotech, and SDS-7 marker from Sigma-Aldrich.

2.1.3 Bacterial Strains

XL1BLUE: recA1, end A1, gyrA96, thi-1, hsdR17, supE44, relA1, lac, [F', pro AB, lacIqZΔM15, Tn10 (Tetr)] from Stratagene.

TG1:   supE, hsdΔ5thi, Δlac-proAB), F'[traΔ36, proAB+, lacI, lacZΔM15] from Promega.

BL-21(DE3): E. coli B, F-, omp T, hsd S (rB- mB-), gal, dcm from Novagen

Rosetta: E. coli B, F-, omp T, hsd S (rB- mB-), gal, dcm lacY1 (DE3) pRARE (Cm^R) recognizes AGG, AGA, AUA, CUA, CCC, GGA

2.1.4 Media and Antibiotics

Bacterial cells were grown in Luria Bertini (LB) medium: 5g/L yeast extract; 10g/L NaCl. Expression was done in Terrific Broth (TB) medium: 12g/L bacto tryptone; 24g/L yeast extract; 0.4% (v/v) glycerol; 0.17mM KH_2PO_4; 0.072mM K_2HPO_4.

SeMet-Medium was prepared as described (Doublie, 1997). It is a minimal medium which contains 50 mg/l Seleno-L-methionine (Calbiochem-Novabiochem, Schwalbach), no

methionine, a high concentration (250 mg/l) of the amino acids Val, Leu, Ile, Lys, Thr, Phe to suppress bacterial methionine biosynthesis and 50 mg/ml of the other amino acids.

Selection of colonies over a LB-Agar plate: 10g/L bacto tryptone; 5g/L yeast extract; 10g/L NaCl; 15g/L bacto agar.

Ampicillin (Amp) from GERBU was prepared as a stock solution of 50g/L in water.

Kanamycin (Kan) from GERBU stock solution was made as 50g/L in water.

Chloramphenicol (Cm) from Sigma stock solution was made 25g/L in Ethanol.

2.1.5 Protein purification columns and Materials

Ni-NTA fast flow agarose beads from Qiagen, GSH-Sepharose superflow from Amersham Pharmacia, and Amylose beads from New England Biolabs, were all packed in column and maintained according to manufacturer's specifications.

Size exclusion chromatography was performed using Sephacryl-400 (16/60), Superdex-75 and -200 (16/60) were all purchased as pre-packed columns and calibrated with marker proteins.

2.1.6 Crystallization screens, Reagents, and Heavy atom compounds

Crystallization screens were from Hampton Research and Nextal screens, Qiagen. All crystallization reagents, buffers and salts were from Fluka, PEGs were purchased from Hampton Research. Heavy atom compounds were from Johnson Matthey (Karlsruhe). Ta_6Br_{12} cluster was a gift from Dennis Fiegen.

2.2 Constructs

pFM 454 SEPT6:S-tag-6xHis-SEPT7

Provided by Marian Farkasovsky, constructed using three fragment ligation from plasmid obtained from Ian Macara (see Figure. 2 for more details).

pFM 454 SEPT6 (310):S-tag-6xHis-SEPT7 (305)

Stop codons were introduced using Stratagene Quick change protocol, after amino acids positions 310 and 305 in SEPT6 and SEPT7 respectively.

pFM 457 MBP-SEPT2

Provided by Marian Farkasovsky, constructed from plasmid obtained from Ian Macara (see Figure. 2.1 for more details).

pFM 457 MBP-SEPT2 (308)

Stop codon were introduced using Stratagene Quick change protocol, after amino acids positions 308.
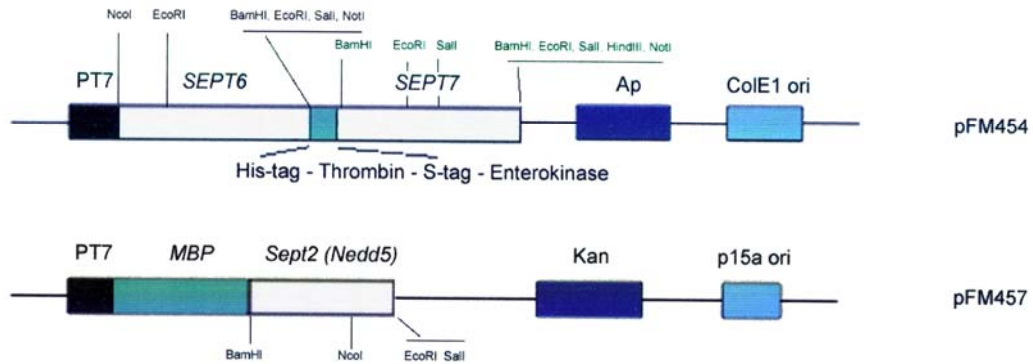
Figure 2.1 pFM454; pT7::hSEPT6 (NT)::HIS-SEPT7 x Nco I + Not I and x Not I + Hind III (three fragment ligation). pFM457; SEPT2 x BamH I + Sal I

pFM 454 SEPT6:6xHis-SEPT7(361)

Derived from above **pFM 454 SEPT6:S-tag-6xHis-SEPT7** where S-tag was removed and SEPT7 was shortened by 57 amino acids C-terminally using the following strategy. The above mentioned vector was cut using Hind III and Xho I, 90 base primers having the same restriction sticky ends was ordered from MWG Biotech (see below) which was used as an insert and ligated in to the digested vector. Then the restriction sites Not I and Xho I was used to insert a PCR amplified shorter version of SEPT7.

```
5`-AGCTTAAGAAGGAGATATACATATGCACCATCATCACCACCATTCTTCTGGTCTGGTGCCACGCGGTTCTGGTGCGGCCGCTTAATTAAC
        ATTCTTCCTCTATATGTATACGTGGTAGTAGTGGTGGTAAGAAGACCAGACCACGGTGCGCCAAGACCACGCCGGCGAATTAATTGAGCT- 5`


   HindIII     SD       M    6x His            thrombin site          NotI     PacI     XhoI
```

Hsep7_Not1_sens [5` primer for hsept7 (1→361)]
5`- CAG A GCGGCCGC T ATG GTA GCT CAA CAG AAG AAC CTT GAA GGC
Hsep7_361xho1_anti [3` primer for hsept7 (1→361)]

5`- C AGA GAA CTC GAG TTA CTG GAG CTC AGC TTC AGA GTC CTT CAG

pFM 454 SEPT6:GST-SEPT7(361)

GST was introduced in front of SEPT7, where first the PCR amplified SEPT7 was cloned into a pGEX 6P1 vector using BamH I and Xho I and then the SEPT7 along with GST was amplified using PCR and cloned back into the original vector using the same Not I and Xho I sites.

Hsep7_BamHI_S [5` primer for hsep7 with BamHI]
5`- CAG A GGATCC ATG GTA GCT CAA CAG AAG AAC CTT GAA GG
GST_NotI_S1 [5` primer for GST with NotI]
5` - CAG A GCGGCCGC T ATG GGG TCC CCT ATA CTA GGT TAT TGG

pGEX6P1 SEPT2 - 315

SEPT2 full length and SEPT2 – 315 were cloned into the vector using BamH I and EcorR I restriction sites.

S2_1S_Bam
5´ - CAG A GGA TCC ATG TCT AAG CAA CAA CCA AC
S2_361A_EcoISal
5´ - CAG A GTC GAC GAA TTC TCA CAC ATG CTG GCC GAG AGC CCC
S2_315A_EcoISal
5´ - CAG A GTC GAC GAA TTC TCA GTC CTC ATT CTC TAC TTT CC

pGEX4T3I Cdc42Q69L: Borg-6xHis

Provided by Dorothee Kühlmann (Doro 88.13)

pGEX6P1 Cdc42Q69L (177): Borg-6xHis

Cdc42 and Borg gene were digested using BamH I and Not I from the above mentioned vector in to pGEX6P1 vector, and then a stop codon was introduced after amino acid position 177 in Cdc42.

pGEX6P1 Borg3 (1 – 110)

Borg3 (1 – 110) was PCR amplified and cloned into pGEX6P1 using BamH I and Xho I sites. *Borg1A_Bam*

CAG A GGA TCC ATG CCC GTG ATG AAG CAG C

Borg110S_Xho

C GAA CTC GAG GTC CAT GAC GCC TAA CAC C

pGEX6P1 BD3

BD3 fragment amino acids 83 – 110 from Borg3 was PCR amplified and cloned into pGEX6P1 using BamH I and Xho I sites.

Borg83A_Bam

CAG A GGA TCC GTG GCT GTG CCT TCA CC

2.3 Expression and purifcation of Septin 2

2.3.1 Growth and Harvest of bacteria

pGEX6P1 SEPT2 was transformed into Escherichia coli *BL21 (DE3),* and a single colony was inoculated in 100ml of LB-Amp media were grown in a 37^oC shaker at 160 rpm overnight. The overnight pre-culture was used to inoculate 5L TB-Amp media and grown in a 37^oC shaker at 160 rpm till A_{600} of 0.8. The culture was induced with 200μM Isopropyl-β-D-thiogalactoside and shaken at 28^oC overnight. The induced cells were harvested using centrifuge at 1500 g at 4^oC, the cells were suspended in 50mM TRIS-HCl pH 7.8, 150mM NaCl, 5mM MgCl2, 5mM β-mercaptoethanol, 100μM PMSF, and cocktail inhibitor tablets. Cells were either used for purification or frozen and stored at -80^oC.

2.3.2 GSH-Sepharose affinity chromatography

The cells were thawed (if necessary), and were lysed using a microfluidizer at a pressure of 600kPa. The protein was extracted from the soluble fraction after centrifugation at 90000 g, 4^oC, and 30 min. The N-terminal GST-fusion protein was purified using a GSH-Sepharose superflow affinity column which has a volume of 30ml with a flow rate of 1ml/min after equilibration with three column volumes of 50mM TRIS-HCl pH 7.8, 150mM NaCl, 5mM MgCl$_2$, 5mM β-mercaptoethanol. After loading the supernatant the column was washed with five column volumes of equilibration buffer. The GST fusion was cleaved using 0.5ml of 15mg/ml PreScission protease on the resin, overnight at 4^oC. The cleaved protein was eluted with the same wash buffer. The cut GST protein was eluted with 20mM Glutathione,

and the column was regenerated using one column volume of 6M Guanidinium hydrochloride and finally with five column volumes of water.

2.3.3 Concentrating proteins by ultra-filtration

After analysis of the cleaved protein by SDS-PAGE, the protein was concentrated using Amicon ultrafiltration tubes with a cut off filter of 30kDa by continuous centrifugation at 4000g, 4°C, to 30mg/ml. The concentrated protein was either used for size exclusion chromatography immediately or flash frozen and stored at -80°C till further use.

2.3.4 Size Exclusion Chromatography

The protein was subjected to size exclusion chromatography as further purification procedure, in order to remove all higher oligomers and aggregates. Superdex-200 16/60 was equilibrated with 50mM TRIS-HCl pH 7.8, 150mM NaCl, 5mM MgCl$_2$, and 5mM DTE. 2ml of protein was loaded and eluted with a flow rate of 1ml/min, all the fraction were collected and analyzed by SDS-PAGE.

The desired fractions pooled and concentrated up to 20mg/ml using Amicon ultrafiltration. The concentrated protein aliquots were flash frozen using liquid nitrogen and stored in -80°C till further use.

2.4 Purification of Human Septin Complex (HSC 2, 6, 7)

2.4.1 Co-expression of SEPT2, SEPT6, and SEPT7

Co-expression of SEPT2, SEPT6, and SEPT7 was achieved by co-transforming the two plasmids pFM 454 SEPT6:S-tag-6xHis-SEPT7 and pFM 457 MBP-SEPT2 in to *Rosetta* cells and selection of colonies bearing both the plasmids was achieved using three antibiotics Ampicillin, Kanamycin, and Chloramphenicol. A single colony was inoculated in 4ml of LB-Amp-Kan-Cm media and grown in a 37°C shaker at 160 rpm till A$_{600}$ of 0.8. 2ml of the culture was transferred to a fresh tube and induced with 200µM Isopropyl-β-D-thiogalactoside (IPTG) and shaken at 28°C overnight, same procedure was followed with the rest of 2ml culture without adding IPTG. 1ml of induced and un-induced cells were harvested in a 1.5ml reaction tubes, resuspended in to 250µl of 1x SDS gel loading buffer

(Sambrook, 1989), and heated at 95°C for 5minutes. 20µl of this sample was loaded in to 12% SDS-PAGE, and checked for expression. A glycerol stock was made for the expression checked colonies flash frozen using liquid nitrogen and stored at -80°C

2.4.2   Large scale co-expression of SEPT2, SEPT6, and SEPT7

200ml of TB-Amp-Kan-Cm media was inoculated with the glycerol stock made from the expression checked colonies were grown in a 37°C shaker at 160 rpm overnight. The overnight pre-culture was used to inoculate 10L TB-Amp-Kan-Cm media and grown in a 37°C shaker at 160 rpm till A$_{600}$ of 0.8. The culture was induced with 200µM Isopropyl-β-D-thiogalactoside (IPTG) and shaken at 28°C overnight. The induced cells were harvested using centrifuge at 1500 g at 4°C, the cells were suspended in 100ml of 25mM Sodium-phosphate buffer pH7.8, 8% glycerol, 300mM NaCl, 5mM MgCl$_2$, 5mM β-mercaptoethanol, 200µMPMSF and cocktail inhibitors tablets. Cells were either used for purification or frozen and stored at -80°C.

2.4.3   Purification using Ni-NTA affinity chromatography

The cells were thawed (if necessary), and were lysed using a microfluidizer at a pressure of 600kPa. To the lysate DNase (10mg/ml) and 0.1% Triton X 100 was added and mixed for 10 minutes at 4°C. The protein was extracted from the soluble fraction after centrifugation at 90000 g, 4°C, and 30 min. The fusion complex (SEPT6 – His-SEPT7 – MBP-SEPT2) was purified in a Ni-NTA fast flow agarose beads affinity column which has a volume of 50ml with a flow rate of 1ml/min after equilibration with five column volumes of 25mM Sodium-phosphate buffer pH7.8, 8% glycerol, 300mM NaCl, 5mM MgCl$_2$, 5mM β-mercaptoethanol and 0.1% Triton X-100. After loading the supernatant of fusion complex the column was washed with four column volumes of equilibration buffer, and one more column volume with the same equilibration buffer but without Triton X-100. The fusion complex was eluted with the buffer containing 300mM Imidazole. The column was regenerated according to Qiagen protocol.

2.4.4   Purification using amylose resin

The Ni-NTA eluted fusion complex was further purified using Amylose resin with a bed volume of 50ml. Prior to loading the amylose resin was equilibrated with buffer containing

25mM Sodium-phosphate buffer pH7.8, 8% glycerol, 300mM NaCl, 5mM MgCl$_2$ and 5mM β-mercaptoethanol. The column was washed with five column volumes of the same equilibrated buffer after loading the fusion complex. 750U of Thrombin was loaded in to the column and the fusion tags were cleaved on the resin overnight at 4°C. The fusion complex without the tags were eluted using the same wash buffer used, and concentrated up to 2ml using Amicon ultrafiltration tubes. The amylose column was regenerated by washing with one column volume of 0.1% SDS and the five column volumes of water.

2.4.5   Size Exclusion Chromatography

The protein was subjected to size exclusion chromatography as further purification procedure, in order to remove all higher oligomers and aggregates. Sephacryl-400 16/60 was equilibrated with 20mM HEPES pH 8, 500mM NaCl, 5mM MgCl2, and 5mM DTE. 2ml of protein was loaded and eluted with a flow rate of 1ml/min, all the fraction were collected and analysed by SDS-PAGE.

Only the fractions which were desirable pooled and concentrated up to 10mg/ml using Amicon ultrafiltration. The concentrated protein aliquots were flash frozen and stored in -80°C till further use.

2.5   Crystallization and Crystallography

2.5.1   Crystallization screens

Protein crystals are formed by slowly precipitating protein from its solution, the classical procedure for inducing proteins to separate from solution and produce a solid phase is to gradually increase the level of saturation by addition of a precipitant. The precipitating agent may be a salt such as ammonium sulphate, organic solvent such as ethanol or methyl-pentanediol (MPD) or a highly soluble synthetic polymer such as polyethylene glycol (PEG).

Protein crystallization is a trial-and-error procedure, to improve the success rate of hitting a right condition where the given protein crystallizes. Commercial screens are available, which are based on the previous successful conditions and rational matrices of different precipitant concentration with buffers varying pH values. Initial crystallization screens were performed in 96 well Corning crystallography plate using semi-automatic nano-litre

sitting drop screening with commercial Qiagen/Nextal screening kits or Hampton screens and Mosquito pipetting station.

2.5.2 Optimizing Crystals

Once initial crystallization hit was obtained, the conditions were optimized to get better crystals, as often the initial screens do not provide best crystals and leave more room for optimization. All crystallization trials were carried out at 20^oC, using hanging drop vapour diffusion method. 1ml of reservoir solution containing buffer, salt and precipitant was temperature equilibrated and put in 24-well cell culture linbro plate (Linbro, Flow Laboratories Inc., USA). The hanging drop consisted of 1 - 2 µl protein solution and 1 - 2 µl reservoir solution. The 24-well linbro plate provides the opportunity to test many conditions by varying precipitant concentration in rows and different buffers in columns.

2.5.3 Seeding

Seeding is an extremely useful technique to obtain optimized crystals or sometimes initial crystals also. A seed provides a nucleation for the assembly of molecules to form a crystal with the same characteristics as the crystal from which it originated. Here in this study seeding was successfully employed to obtain HSC selenomethionine protein crystals from native crystals, as selenomethionine protein didn't crystallize under the same native crystallization condition.

2.5.4 Crystal Soaking with Heavy atom compounds

Crystal soaking is done by adding desired compounds like inhibitors, substrates, products, or heavy atoms to the crystal bathing solution. The crystal should have sufficient freedom to undergo conformational changes in response to these effectors. Here in this study HSC crystals were soaked with many compounds in order to get heavy atom derivatized crystals, a detailed description has been given under Results section 3.5.3.

2.5.5 Cryo-Crystallography

Protein crystals are prone to physical and radiation damage over the time. Cryo-crystallography is a powerful means to overcome such hurdles, which also helps to measure a complete data from a single crystal. In some cases it provides high resolution compared to room temperature measurement, it is suggested that cooling may also increase the internal

order of the parts of the protein which are mobile at room temperatures (Petsko, 1975). The most common method is to transfer the crystal in to a suitable cryo-protectant and flash freeze in liquid nitrogen or liquid propane where the crystals can be stored at 100K indefinitely. The commonly used cryo-protectants are glycerol, ethylene glycol, MPD, low molecular weight PEGs (200-600), and sugars.

2.5.6   Data Collection

All frozen crystals were first tested at 100 K on an in-house source a copper rotating X-ray anode with an osmic mirror (λ = 1,5419 Å, 50 kV, 100 mA, 0,1 mm collimator). The final datasets were collected at beamline PXII at the Swiss Light Source, Villigen, Switzerland at different wavelengths for each crystal depending on the requirement. Data were processed, integrated, and scaled using XDS/XSCALE package (Kabsch, 1993). The quality of the datasets were validated based on the I / σ (signal to noise ratio) where generally a cut-off of 2-3 is widely accepted, and also by calculating R_{symm} which compares symmetry related reflections according to Equation 1

$$R_{symm} = \frac{\sum\limits_{hkl}\sum\limits_{i}\left|I_i - \langle I \rangle\right|}{\sum\limits_{hkl}\sum\limits_{i}\left|I_i\right|}$$ Equation 1

h, k, l – indices of independent reflections with the average intensity <I>

I_i – intensities of independent reflections.

2.5.7   Matthews Coefficient and Solvent content analysis

Based on the volume of the asymmetric unit and the molecular weight of the protein, the number of molecules in the asymmetric unit can be estimated (Matthews, 1968). The Matthew coefficient V_M is derived by Equation 2.

$$V_M = \frac{V}{M \cdot W \cdot Z}$$ Equation 2

M.W – Molecular weight of the monomer in Dalton

V – Volume the asymmetric unit in Å^3

Z – Number of molecules in the asymmetric unit

The average Matthew coefficient of a protein crystal is 2,5 Å^3/Da corresponding to a solvent content of 50% (Matthews, 1968). The solvent content X_s of a crystal can be estimated by Equation 3.

$$ x_s = 1 - \frac{1}{V_M \cdot N_A \cdot \rho_P} \sim 1 - \frac{1.23 \, A^3/Da}{V_M} \qquad \text{Equation 3} $$

V_M – Matthew coefficient

N_A – Avogadro constant

ρ_P – Protein density ~ 1.35 g/cm^3

2.5.8 Phase Determination – Importance of phases

During the data collection, the intensities of waves scattered from planes (*hkl*) in the crystal are measured. The amplitude of the wave $|F_{hkl}|$ is proportional to the square root of the intensity measured on the detector. To calculate the electron density at a position (*xyz*) in the unit cell of a crystal requires us to perform the following summation over all the *hkl* planes, which mathematically expressed in Equation 4.

$$ \rho(x,y,z) = \frac{1}{V} \sum_h \sum_k \sum_l |F_{hkl}| \cdot e^{-2\pi i(hx + ky + lz - \alpha'_{hkl})} $$

Equation 4

V – Volume of the unit cell

α_{hkl} – Phase associated with the structure factor amplitude $|F_{hkl}|$

During the data collection the amplitudes are measured, but the phases are lost during measurement, as there is no formal relationship between the amplitudes and phases. The only relationship is *via* the molecular structure or electron density. Therefore if there is some prior knowledge of the structure or electron density, this can lead to values of phases. This is the basis for all phasing methods which is tabulated in table below. A detailed description of phase problem is described elsewhere (Taylor, 2003).

Table: 2.1. Different phasing methods, modified from Garry Taylor *Acta Cryst*. (2003)

Method	Prior Knowledge
Direct methods	$\rho \geq 0$, discrete atoms
Isomorphous replacement	Heavy-atom substructure
Anomalous scattering	Anomalous atom substructure
Molecular replacement	Homology model
Density Modification (Phase Improvement)	Solvent content, Phase extension, Non-crystallographic symmetry etc.,

2.5.9 Phase Determination using Heavy atoms derivatization

The use of heavy atom substitution was invented very early by small molecule crystallographers to solve the phase problem, but it was Max Perutz and John Kendrew who first applied this method to proteins (Perutz, 1956)**.** Soaking protein crystals in heavy atom solutions creates isomorphous heavy-atom derivatives, which should give rise to measurable intensity changes which could be used to deduce the positions of the heavy atoms. In isomorphous replacement method, the amplitudes of a reflection are measured for the native crystal $|F_P|$, and for the derivative crystal $|F_{PH}|$. The isomorphous difference, $|F_H| \cong |F_{PH}| - |F_P|$ can be used as an estimate of the heavy-atom structure factor amplitude to determine the heavy atom position by Patterson or direct methods (Drenth, 1999). The phase angle of structure factor F_P can then be determined geometrically or numerically (Rhodes, 2000).

An alternative means of obtaining phases from heavy-atom derivatives takes advantage of the heavy atom's capacity to absorb X-rays of specified wavelength. The pairs of structure factors F_{hkl} and F_{-h-k-l} are called Friedel pairs, and it can be shown that $|F_{hk}| = |F_{-h-k-l}|$ and $\alpha_{hkl} = -\alpha_{-h-k-l}$ (Friedel's law (Drenth, 1999)). However, as a result of X-ray absorption by heavy atoms, Friedel pairs are not equal in intensity and do not have the same absolute value of α. This phenomenon is called anomalous scattering or anomalous dispersion. $FHP\lambda_1$ represents a structure factor for the heavy atom derivative which is measured at a

wavelength λ_1 where anomalous scattering does not occur. It can be expressed by FHPλ_2 which represents the equivalent structure factor at a wavelength λ_2 where anomalous scattering does occur according to Equation 5.

$$\mathrm{F}_{hkl}^{HP\lambda 2} = \mathrm{F}_{hkl}^{HP\lambda 1} + \Delta \mathrm{F}_r + \Delta \mathrm{F}_i \qquad \text{Equation 5}$$

Where, the vectors representing anomalous scattering contributions are $\Delta \mathrm{F}_r$ (real) and $\Delta \mathrm{F}_i$ (imaginary). The magnitude of anomalous scattering contributions $\Delta \mathrm{F}_r$ and $\Delta \mathrm{F}_i$ for a given element at a given wavelength is constant and can be found in crystallographic tables. The phases of $\Delta \mathrm{F}_r$ and $\Delta \mathrm{F}_i$ can be computed when the locations of the anomalous scatterers are determined by Patterson methods (Drenth, 1999). The phase angle of structure factor F_{HP} can then be determined from the difference in F_{hkl} and F_{-h-k-l} by geometrical or numerical means (Rhodes, 2000).

2.5.10 Phase Determination using Molecular replacement (MR)

If a homology model available, molecular replacement can be successfully employed to get phase information, which was first described by Rossmann & Blow (Rossmann and Blow, 1962). In this method, the phases for the model are obtained from the coordinates and the structure factor amplitudes (F_{Calc}) of the known structure. In general the space group and the orientation differ between the known and the unknown structure, therefore the known search model needs to be reoriented in the new unit cell properly. This is achieved by comparing the Patterson functions, obtained from the structure factor amplitude (F_{Obs}) of the measured diffraction intensities and from the search model (F_{Calc}) (Drenth, 1999; Rhodes, 2000).

2.5.11 Phase improvement using density modification

It is rare that experimentally determined phases are sufficiently accurate to give a completely interpretable electron density map. Experimental phases are often only the starting point for phase improvement using a variety of methods of density modification, which are also based on some prior knowledge of structure. Solvent flattening, histogram matching and non-crystallographic averaging are the main techniques used to modify electron density and improve phases. Solvent flattening is a powerful technique that removes negative electron density and sets the value of electron density in the solvent

regions to a typical value of 0.33 e $Å^{-3}$ in contrast to a typical protein electron density of 0.43 e $Å^{-3}$. Automatic methods are used to define the protein solvent boundary, first developed by Wang (Wang, 1985) and then extended into reciprocal space. Histogram matching alters the values of electron-density points to concur with an expected distribution of electron-density values. Non-crystallographic symmetry averaging imposes equivalence on electron density values when more than one copy of a molecule is present in the asymmetric unit. These methods are encoded into programs such as DM (Cowtan and Zhang, 1999), RESOLVE (Terwilliger, 2003) and CNS (Brunger et al., 1998). Density-modification techniques will not turn a bad map into a good one, but they will certainly improve promising maps that show some interpretable features. It is also used in extending the phases beyond the resolution for which the experimental phases information is available, assuming higher resolution data have been collected. In such cases, the modified map is back-transformed to a slightly higher resolution on each cycle to provide new phases for higher resolution reflections.

2.5.12 Model building and Refinement

The models were built manually using the software COOT (Emsley and Cowtan, 2004). Helix and strand templates were generated using Moleman (Kleywegt, 2004). Chain tracing was guided by selenomethionine positions.

Refinement is necessary as a manually built protein model is afflicted with errors. An initial model is improved by minimizing the energy of the geometrical and a crystallographic term. The geometrical term of a model contains bond length, bond angles, non-bonded interactions, hydrogen bonds, van-der-Waals interaction, planar restraints and chiral centre restraints of the input model. The crystallographic term appreciates the amplitudes of the measured reflections $|F_{Obs}|$, with the refined model, new structure factor (F_{Calc}) are calculated. A measure of the quality of a model can be derived from R_{cryst} which compares measured and calculated structure factors according to Equation 6

$$R_{cryst} = \frac{\sum \left| |F_{obs}| - |F_{calc}| \right|}{\sum |F_{obs}|} \qquad \text{Equation 6}$$

Using the calculated phases and the measured reflection intensities, an improved electron density map can be calculated. Since the calculated phases are biased towards the

potentially wrong model, a test set of reflections is excluded from the refinement (typically 5–10% of the reflections). These reflections are used to calculate R_{free} similar to Equation 6 (Brunger, 1992; Brunger, 1997). R_{free} is a rather non-biased measure of the quality of the protein model.

The program Refmac5 (Murshudov et al., 1997) was used for refinement here. Typically, it refines the temperature factors of every atom and then the position. 5% of the reflections were used as test set. A typical refinement cycle started with 10 cycles of TLS (translation, libration, screw-rotation displacement) refinement using independent protein bodies. The model was validated by the program Procheck (Laskowski et al., 1993).

Figure preparation

Buried surface area between two monomers was determined sing the CNS program suite (Brunger et al., 1998). All figures were generated using Pymol (www.pymol.org), and the final figures were prepared using CorelDraw11 (Corel Corporation).

2.6 Electron Microscopy (EM) and Single particle analysis

EM studies were done in collaboration with Electron microscopy lab, Max-PlanckInstitut für Biophysikalische Chemie, Göttingen. The analysis of the sample and images were kindly provided by Holger Stark and Florian Hauer.

3 Results

3.1 Characterization of Septin 2

3.1.1 Purification

Expression of Septin2 was chosen here in this study for the characterization of single septins since it was shown that it can be purified in the absence of other septins from *Escherichia coli* (Sheffield et al., 2003). Furthermore, the construct pFM 457 MBP-SEPT2 (used in co-expression of septin complex) was readily available for expression and solubility analysis.

SEPT2-Wt and -315 (amino acids 1→315) were cloned into a pGEX6P1 vector as mentioned in section 2.2 and purified as described in methods section 2.3. The yield of proteins was ~20mg/L of culture. A typical protein product eluted from GSH column after the cleavage of the GST tag is shown in Figure 3.1. SEPT2-315 was used hereafter for further characterization.
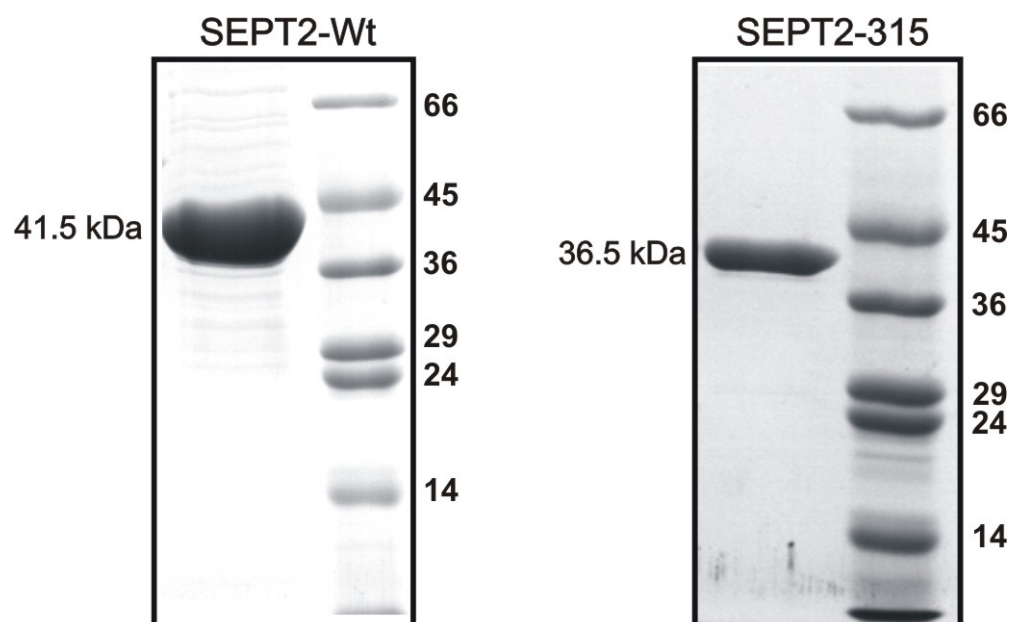
Figure 3.1   **12% SDS-PAGE of the protein after GSH column**

3.1.2 Nucleotide content

The protein was analysed for its nucleotide content using a reversed-phase C-18 HPLC column. Known quantites of denatured proteins were loaded onto the column. The running buffer contained 10mM tetrabutylammoniumbromide, 100mM potassium phosphate (pH 6.5) with 7.5% acetonitrile. Nucleotide peaks were detected by measuring absorption at 254 nm and quantified by integration. ~50% of protein was saturated with GDP which varies with different preparations. When GTP was added to the protein extraneously, the protein exhibits multi-turnover GTPase activity with similar to other proteins of TRAFAC (Leipe et al., 2002) family such as TrmE and other large GTPases, but on a much slower rate.

3.1.3 Monomer, dimer and oligomer equilibrium

During purification using size exclusion chromatography the protein elutes as monomer and dimer according to the mass calibration of Superdex-200 16/60, a preparative gel filtration column. Apart from these two states, majority of the protein eluted at the void volume of the column, indicating oligomerization or aggregation of protein. The same was observed during the purification of SEPT2-Wt. The dimeric and monomeric fractions were pooled separately and concentrated, and subjected to another round of gel filtration separately. The protein exhibited a dynamic equilibrium between monomer and dimer state, as both the fractions again eluted as monomer and dimer, but no further oligomers were observed. Nucleotide content analysis showed no difference between monomer and dimer.

To check whether the presence of nucleotide has any influence on the dimerization of SEPT2-315, analytical gel filtration was performed over Superdex-200 10/30 under different conditions. 50mM TRIS-HCl pH 7.8, 150mM NaCl, 5mM $MgCl_2$, and 5mM DTE was used as buffer. The GDP protein was prepared by incubating the protein with 3x excess of GDP for 30minutes at 4°C. The GppNHp protein was prepared by treating with 5-units of alkaline phosphatase and 3x excess of GppNHp, a slowly hydrolysing analogue of GTP, for 4hours at 4°C. The same procedure was followed for alkaline phosphatase treated protein, where no extra nucleotide was added. The chromatograms were obtained by plotting the data from analytical gel filtration. They showed nucleotide dependent dimerization of SEPT2-315 (Figure 3.2).
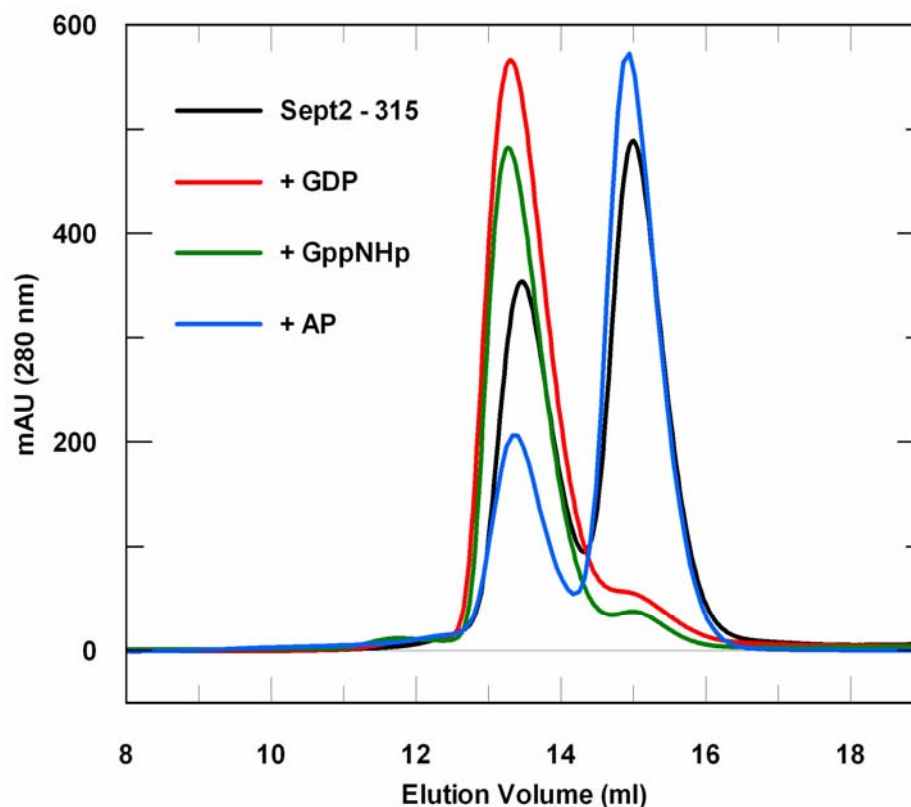
Figure 3.2 **Gel filtration chromatogram of SEPT2-315 under different nucleotide states, the chromatogram was plotted using program Grafit-5.0**

When the protein was incubated for longer period with alkaline phosphatase the protein precipitates, indicating that the nucleotide is necessary for stabilization. Further more, attempts to make nucleotide free protein using EDTA, a standard procedure used in making nucleotide free small GNBPs, were unsuccessful, questioning the role of Mg^{2+} ions. During this study, Huang and co-workers (Huang et al., 2006) independent work also suggest that Mg^{2+} ions are dispensable for GDP binding.

3.2 Structure of Septin 2

3.2.1 Crystallization of SEPT2-315

Dimeric SEPT2-315 was used for crystallization (20 mg/ml with 1mM GDP final concentration). For high throughput crystallization screens a semi-automatic nano-litre sitting drop was setup in 96-well Corning crystallography plates. Using a Mosquito pipetting station, 100nl protein were mixed with equal amounts of precipitant (Hampton

and Qiagen/Nextal screens) and left undisturbed at 20ºC and checked for crystals after one day. Initial crystals were obtained from Hampton's PEG/Ion screen under conditions, where the main components of precipitant are 5-10% polyethylene glycol 6000 and Tris-HCl or Bicine buffer from pH 7.5-8.0 (Figure 3.3 A). Optimization of the conditions was done using the hanging drop vapour diffusion method in a 24-well Linbro plate. It led to tiny crystals in 10 - 15 minutes after the setup (Figure 3.3 B) the crystals grew to a maximum size in 2 days (Figure 3.3 C). The optimized crystallization conditions are 5% polyethylene glycol 6000, 0.1M bicine pH9.0, and 0.1M glycine. Selenomethionine substituted protein was prepared and crystallized (Figure 3.3 D) under the optimized conditions.
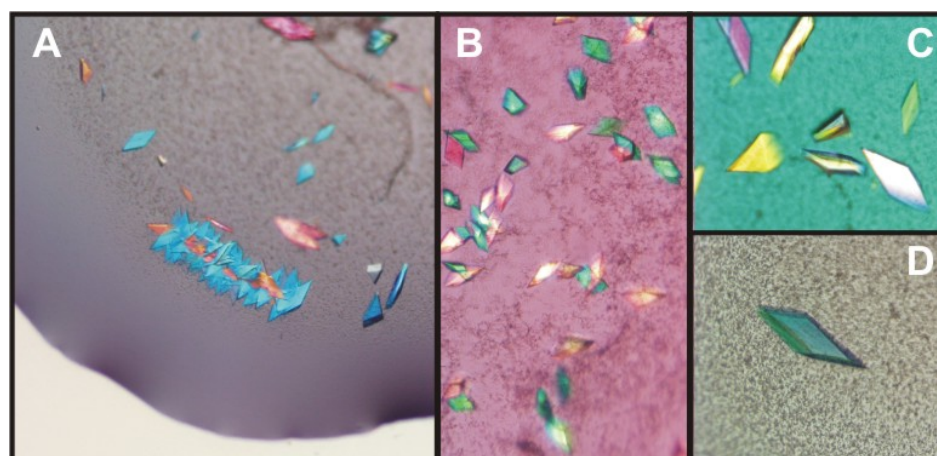

Figure 3.3   **Crystals of SEPT2-315 with GDP.**

3.2.2   Data collection and Data processing

Crystals were transferred to a cryoprotectant solution containing 25% ethylene glycol along with mother liquor, and immediately flash frozen in liquid nitrogen. The frozen crystals were then always maintained at 100K and tested in-house using a rotating anode beam. A complete SAD (Single Anomalous Dispersion) dataset for SEPT2-315 selenomethionine crystal was collected at synchrotron beamline X10SA, Swiss Light Source, Villigen, Switzerland. Data processing was done using XDS software package (Kabsch, 1993). The crystals belonged to space group C2 with unit cell dimensions a=163 Å, b=54 Å, c=110 Å, β=128º. Data collection statistics are summarized in Table 3.1

3.2.3 Structure determination

SAD data from the selenomethionine protein crystals were used to obtain phases. Eight selenomethionine sites were found using SHELXD (Schneider and Sheldrick, 2002) and these sites were fed into SOLVE (Terwilliger, 2003) for phase calculation and subsequently RESOLVE (Terwilliger, 2003) for solvent flattening. After a cycle of further density modification using program DM of CCP4 package (Bailey, 1994), the electron density was used for manual building. The electron density indicated one dimer per asymmetric unit, Matthews co-efficient of 2.6 $Å^3/Da^{-1}$ was calculated indicating approximately ~53% solvent content. By utilizing the non-crystallographic symmetry obtained from the selenomethionine sites, the monomer model could be extended to the remaining molecule of asymmetric unit. After several cycles of model building and improvement, the final model was refined to 3.4 Å using REFMAC (Murshudov et al., 1997). The model has R_{work} and R_{free} of 28% and 31.4% respectively. Refinement statistics are summarized in Table 3.2. The final model includes 469 amino acids out of 630 (for dimer), which includes residues 20-62, 78-101, 116-139, 141-214, 224-246, 253-268, and 270-304 and two GDP molecules. The model exhibits excellent geometry with 89.4% in favourable, 10.4% in allowed, and no residues in disallowed regions of the Ramachandran plot (Figure 3.4). In the asymmetric unit of the crystal, SEPT2-315 is dimerized in two ways one of which we consider to represent the dimer in solution, as analysed and discussed in detail latter under section 3.4.

Table 3.1 Data statistics of SEPT2-315 Se-Met	
Wavelength (Å)	0.9792
Space group	C2
R_{work}/R_{free}	0.279 / 0.313
Cell dimensions	
a,b,c (Å)	162.96, 53.92, 110.27
α,β,γ (°)	90, 128.37, 90
Resolution (Å)[*]	20 – 3.4 (3.5 – 3.4)
Rsym (%) [†*]	8.0 (33.9)
I / σ (I)[*]	14.79 (5.52)
Completeness (%)[*]	98.2 (98.3)
Redundancy	5.4
Phasing Statistics	
No. of Sites	8
FOM	0.33
FOM (solvent flattened)	0.52

Table 3.2 Refinement statistics of SEPT2-315	
Resolution (Å)	20 – 3.4
Number of reflections (working / test)	9927 / 502
R_{work}[a] /R_{free}[b] (%)	27.9 / 31.3
Number of atoms	
Protein	3650
Ligand	56
B-factors	
Protein	80.27
Ligand/ion	65.43
R.m.s deviations	
Bond lengths (Å)	0.012
Bond angles (°)	1.589

[*] Values in parentheses indicate outermost resolution shells

[†] $R_{sym} = \Sigma|Ih – <Ih>| / \Sigma Ih$ where $<Ih>$ is the intensity of the symmetry-equivalent measurements.

[a] $R_{work} = \Sigma|F_O – F_C| / \Sigma F_O$, where F_O and F_C are the observed and calculated structure factor amplitudes.

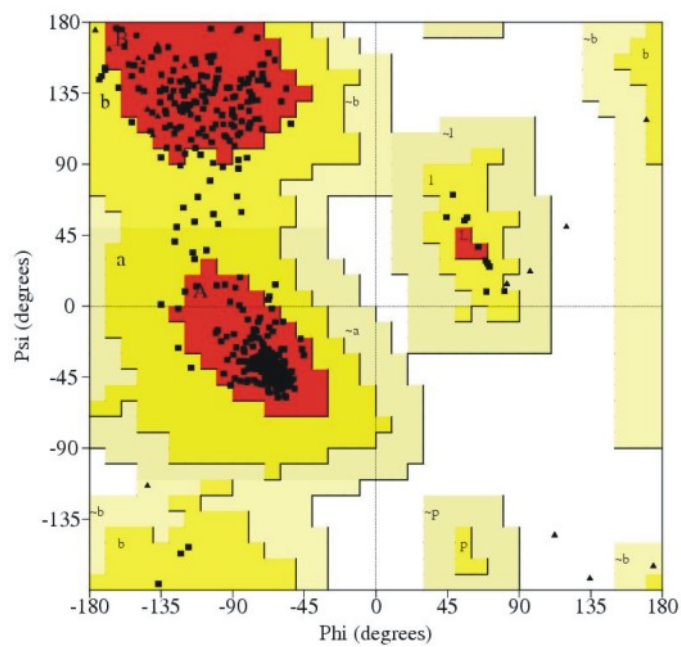[b] R_{free} is calculated similarly to R_{work} using 5% of the test set reflections.

Figure 3.4   **Ramachandran plot showing torsion angles of the peptide bonds of the SEPT2-315 dimer model, triangles represents glycines and prolines, squares represent all other amino acids. The plot was generated using PROCHECK (Laskowski et al., 1993)**
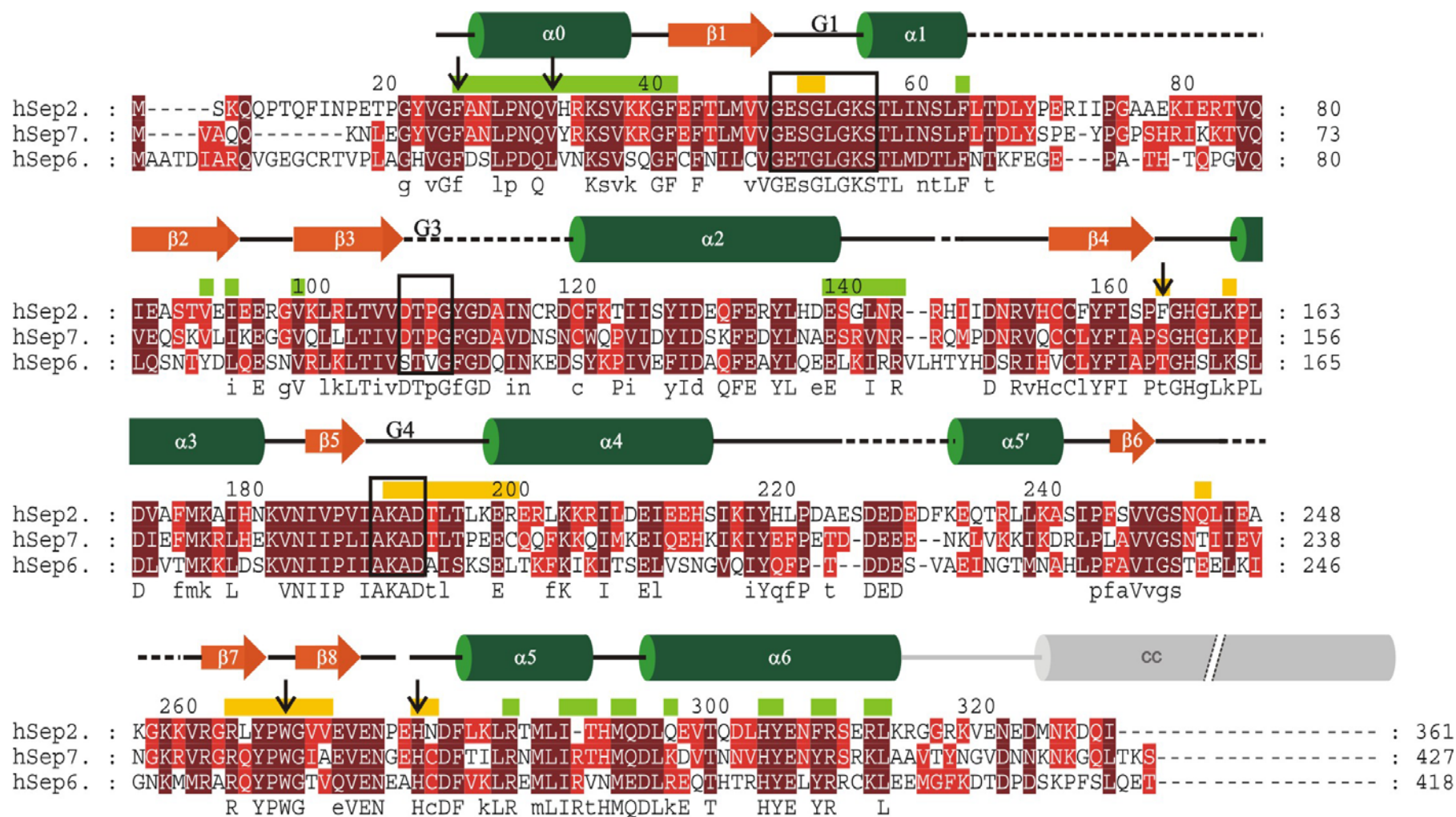
Figure 3.5   **Sequence alignment of SEPT 2, 6, and 7 along with the secondary structural elements on top, residues invariant or highly conserved in 12 human septins are marked underneath. Vertical arrows indicate mutated residues, yellow and green lines indicate residues buried in the G- and NC-dimer interface respectively. The predicated coiled-coil symbolized in grey.**

3.3 Overview of Septin structure and topology

The basic structure of monomeric SEPT2 closely resembles the canonical G domain such as that of Ras, with six β-strands and five α-helices (Figure 3.6). The unique feature of SEPT2 is the presence of four additional secondary structural elements as compared to Ras. To preserve the canonical G domain nomenclature, the secondary structural elements were numbered according to Ras structure. The additional secondary structural elements are the N-terminal helix α0 before canonical β1, α5′ since it is in between the canonical α4 and β6, the two antiparallel strands β7 and β8 between the canonical β6 and α5, and the α6 C-terminal helix which points away from the G domain at a 90° angle relative to the axis of interaction between subunits (Figure 3.6 and Figure 3.7).
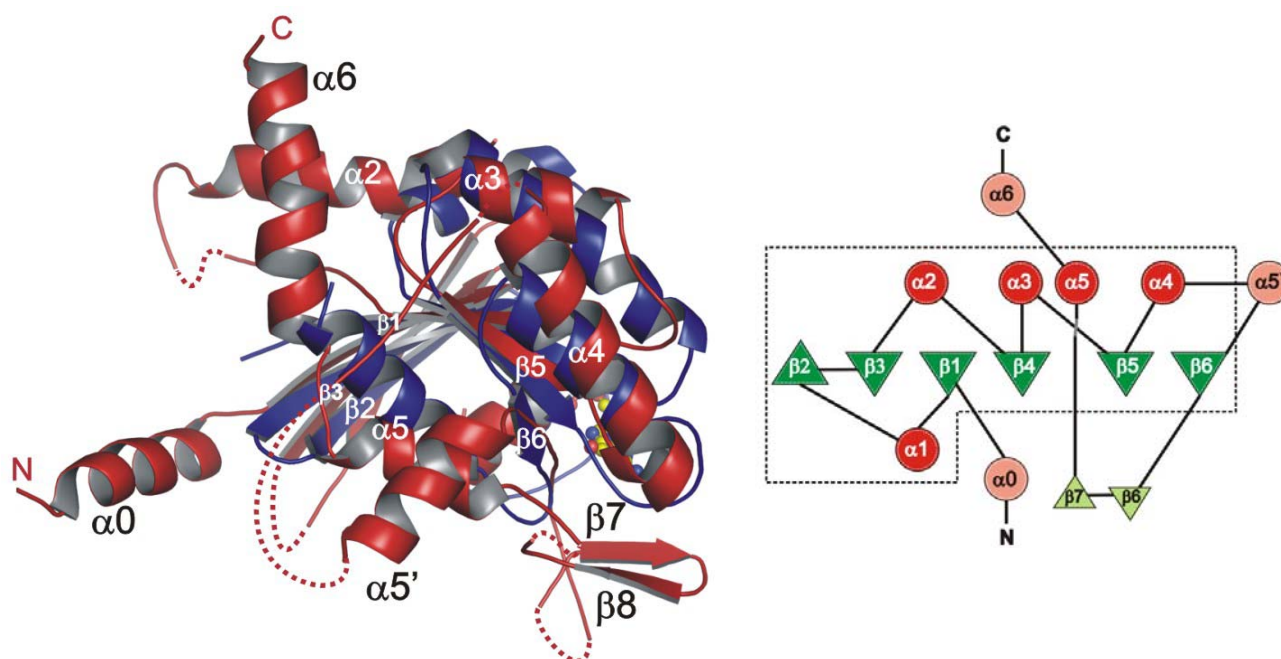

Figure 3.6   **Left: Overlay of SEPT2-315 structure in red with Ras-GppCp in blue (PDB: 121P).**
Right: Topology cartoon of SEPT2-315, the secondary structural elements align with
Ras are inside the dotted box.

The sequences of the additional elements are highly conserved. They contain residues that are invariant between SEPT2, SEPT6, SEPT7 and most other septins (Figure 3.5). The structure contains GDP in the nucleotide binding pocket. GDP is bound in a conventional way, with the phosphates occupying the P-loop or G1 motif. The conserved aspartic acid of the G4 motif (AKAD in septins) makes a standard bifurcated interaction to the guanine

base. The switch regions are disordered due to the absence of γ-phosphate, and not visible in the structure. Therefore, the DxxG or G3 motif is missing in the structure. Surprisingly SEPT2-315-GDP structure lacks the Mg^{2+} ion which coordinates the phosphate groups of the nucleotide. The Thr35 of Ras equivalent residue of the G2 motif is either missing or difficult to locate from the sequence is also not visible in the SEPT2-315-GDP structure.

3.4 Dimerization of Septin2

3.4.1 G and NC - dimer

In the asymmetric unit of the crystal, SEPT2 is dimerized in two different ways. Due to the linear continuous arrangement of subunits it was difficult to assign the actual dimer present in solution, so both the interfaces were analysed. Interface 1 and 2 were named G-dimer and NC-dimer respectively.
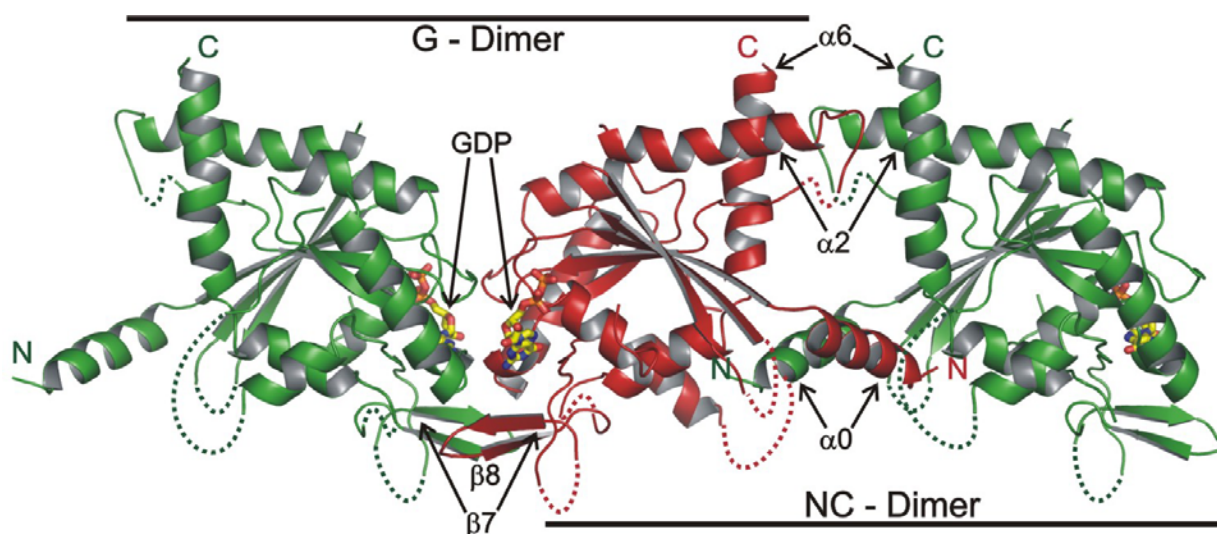

Figure 3.7   **Possible dimers found in the crystals of SEPT2-315.**

Interface 1 of the septin dimer is along the nucleotide binding site and thus called G-dimer. The G-dimer interface is formed by the loop regions between β1 and α1, β4 and α3 and β5 and α4 (Figure 3.5). The residues involved are Leu48, Phe156, Lys183 and Thr186. Apart from these regions a significant contribution to the G-dimer is from β7 and β8 elements (Figure 3.5 and Figure 3.7), involving Trp260, His270 and V263 (Figure 3.8).

Interface 2 is mediated by the extra N-and C-terminal helices and hence called NC-dimer (Figure 3.7). The NC-dimer interface is contributed by α0, α6 and α2 elements. α0 interacts with the α0 from the other subunit. α2 is somewhat longer when compared to Ras α2 (Figure 3.6) and this region interacts with the helix α6 of the other subunit (Figure 3.7). The NC-dimer interface can be divided into upper half and lower half (Figure 3.9). The upper half is formed by the C-terminal helix α6 and C-terminal end of α2, which involves mostly hydrophilic contacts between Glu133, Asn137, Arg138 and Arg300. The lower half is mediated by the N-terminal α0 helices, where Phe20, Val27, Val86, Ile88 Val93 and Ile281 are involved (Figure 3.8).

Open book surface representation shows both the interfaces are mostly mediated by conserved residues (Figure 3.9). Buried surface areas were calculated for both the interfaces with CNS (Brunger et al., 1998) using a default probe radius of 1.4 Å. The sizes of the interfaces are $1851Å^2$ and $2995Å^2$ for the G-dimer and the NC-dimer, respectively. The buried surface areas show that NC-dimer interface is larger (Figure 3.9), but based on the buried surface alone the biological dimer cannot be confirmed. In order to delineate which of the dimers represents the solution structure, residues that are likely to contribute to the binding energy and are highly conserved were mutated.
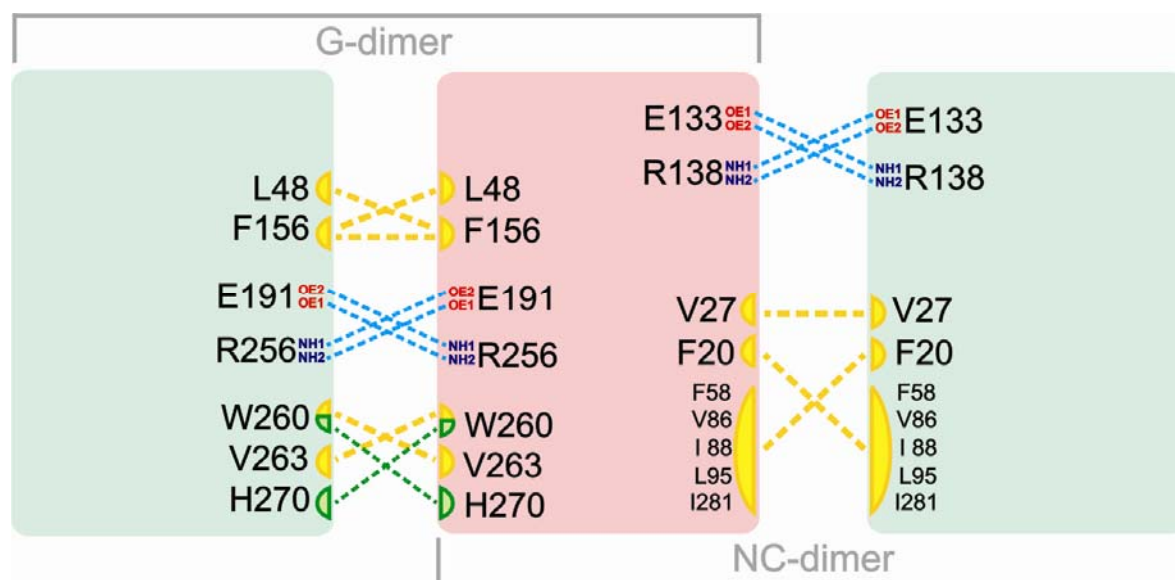

Figure 3.8 **Schematic representation of the G- and NC-dimer interface. Polar interactions are indicated by a blue line, hydrophobic interactions by a yellow line.**
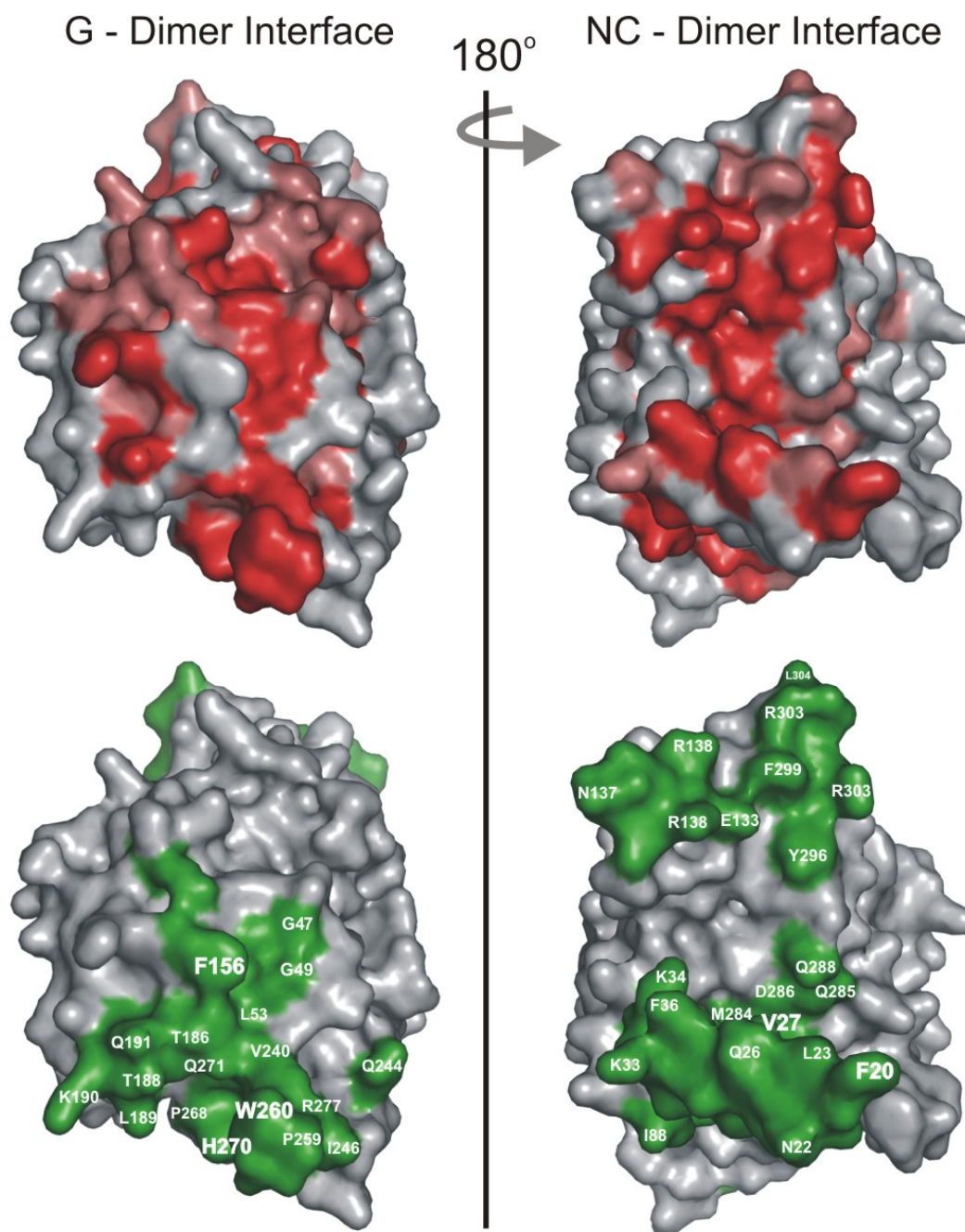
Figure 3.9   **Open book surface representation of both G- and NC-dimer interfaces. Residues conserved are shown in red (invariant in 12 septins) or pink (conserved in 8 of 12 septins) and those buried in the interface in green, with labels as indicated.**
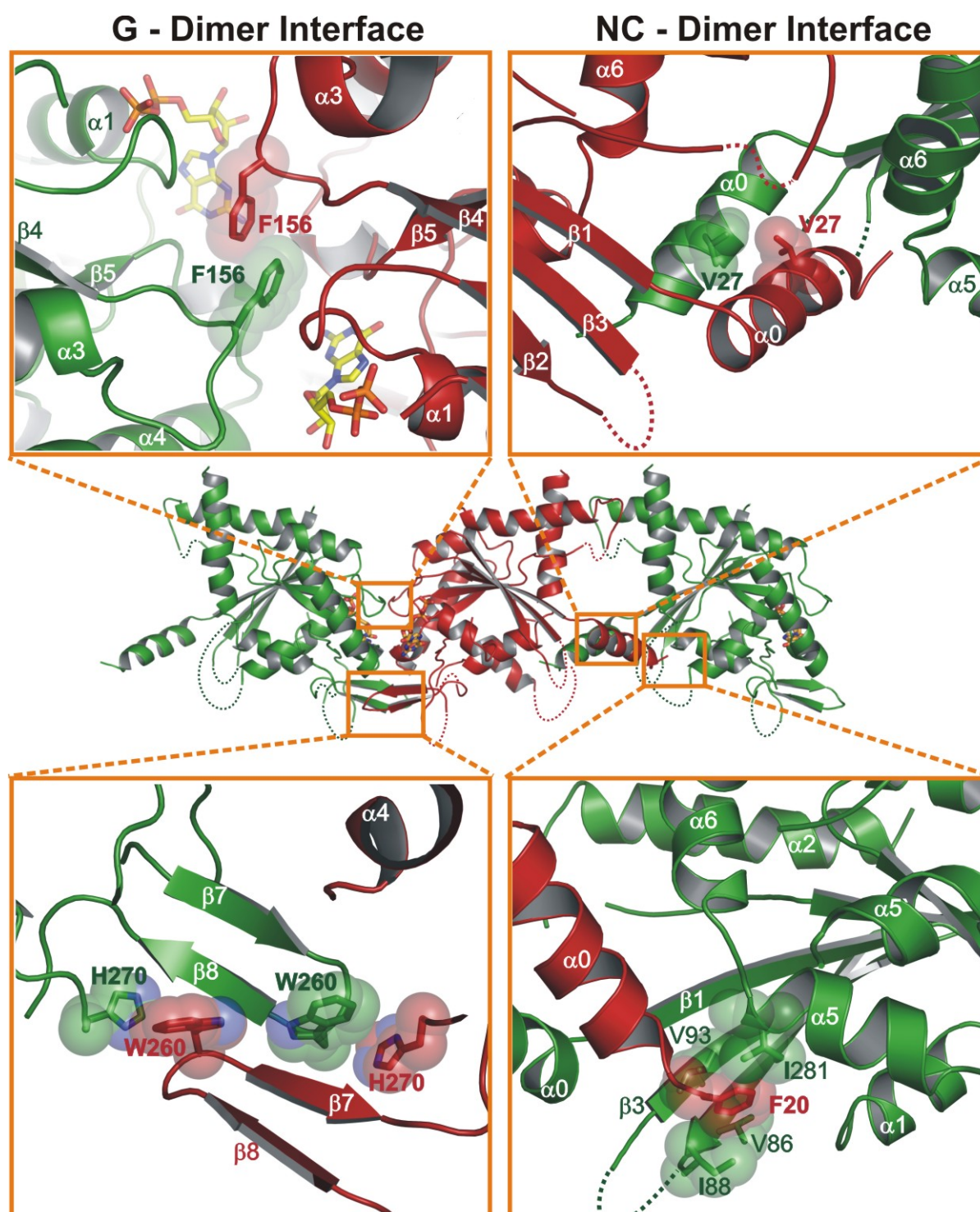
Figure 3.10   Details of the interfaces featuring residues, which were mutated and analyzed biochemically.

3.4.2 Mutational analysis of the dimer interface

In the G-dimer interface three residues were chosen, Phe156 which makes π-π interaction with Phe156 from the other subunit and was mutated to Asp, while Trp260, which makes a reciprocal cation-π interaction with His270 was mutated to Ala and Asp respectively. In the NC-dimer interface, Val27 makes a hydrophobic interaction with the same residue in α0, and Phe20 forms a hydrophobic pocket together with Val86, Ile88, Val93, Leu95 and Ile281 (Figure 3.10). Both Val27 and Phe20 were mutated to Asp. Mutant proteins were purified as described for wt and the dimer formation was analysed by analytical gel filtration in the presence of GDP (Figure 3.11). While mutants of the NC-dimer interface showed the same equilibrium between monomer and dimer as SEPT2, the G interface mutants eluted as monomers. These results demonstrate, that SEPT2-315 dimerizes across the nucleotide binding site, with a face to face orientation of nucleotide binding sites, similar to other GTP-binding proteins of the TRAFAC class (Leipe et al., 2002).
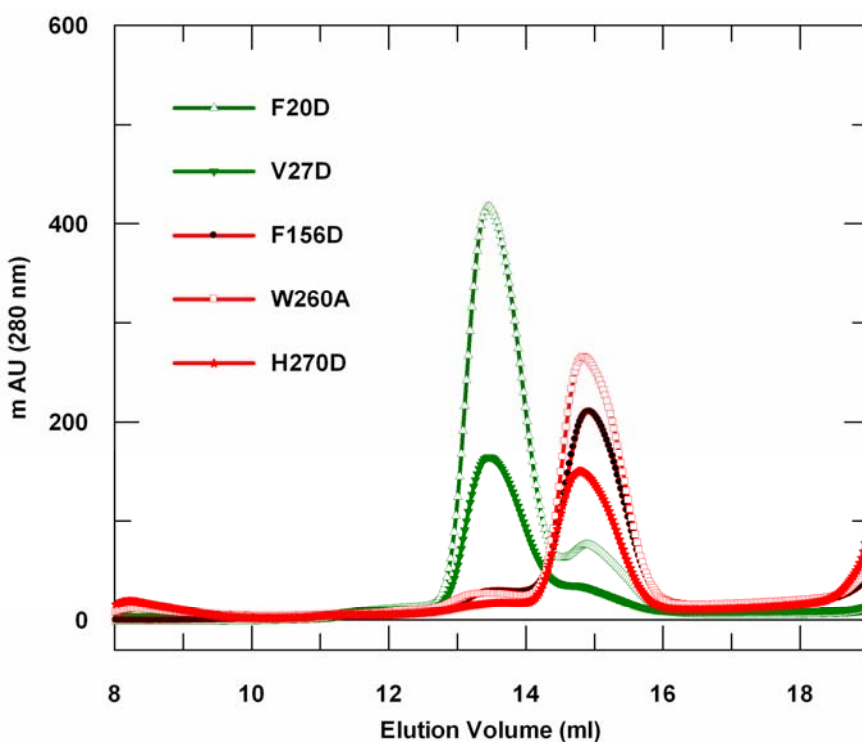

Figure 3.11   **Gel filtration chromatogram of SEPT2-315 mutants in the presence of excess of GDP, the chromatogram was plotted using program Grafit-5.0**

3.5 Crystallization of HSC

3.5.1 Purification and initial characterization

The purification of the human septin complex 2/6/7 (HSC) was achieved by co-expressing all three septins in a single *E.coli Rosetta (DE3)* cell. Constructs pFM454-SEPT6:S-tag-6xHis-SEPT7 and pFM457-MBP-SEPT2 were used and purified as described in Methods section 2.4. During gel filtration using a Sephacryl-400 16/60 the complex elutes as a hexamer according to the mass calibration of the column. The elution profile showed an overlapping peak for excess of uncomplexed Septin2. By using Superdex-200 16/60 the complex elutes at the exclusion volume but was well separated from small uncomplexed proteins. The hexameric fractions were pooled, concentrated using ultra-filtration up to 10 mg ml^{-1} and stored at -80°C until further use. A typical complex after the final purification step is shown in Figure 3.12
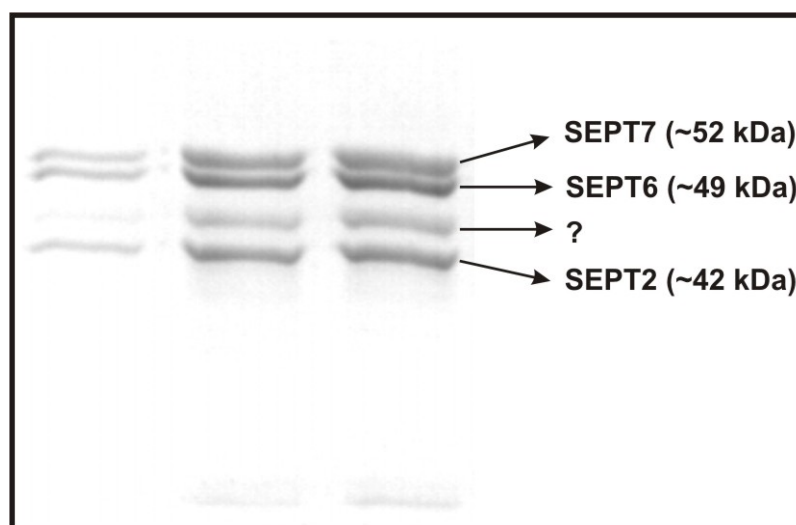

Figure 3.12 **12% SDS-PAGE of HSC after gel filtration applied increasing concentrations from left to right.**

From the SDS-gel (when applied at lower concentrations) it can be seen the three proteins have a 1:1:1 stochiometry and from the gel filtration the complex elutes as a hexamer. Therefore, the hexamer accounts for two copies of three proteins and the molecular weight of the complex was estimated to be ~285 kDa. When the complex was applied at increasing concentrations in the SDS-gel, and extra band appears. This might be the degradation product of either SEPT6 or SEPT7. Western blot analysis using anti-His antibodies revealed the extra band as C-terminally degraded SEPT7. Attempts to identify the actual

boundaries of the cleavage product were unsucessful, so a construct was made where N-terminal S-tag and C-terminal 57 amino acids were removed for more detail see methods section 2.2.

The truncated complex (HSC-361) was purified as described for HSC-wt, and has similar properties like HSC-wt. SDS-gel of HSC-361 is shown in Figure 3.13. SEPT7-361 now has approximately the same size as of SEPT2 and runs together with SEPT7-361 in SDS-gel. The complex was analysed by mass spectrometry and long SDS-gels to confirm that the complex has all the three septins (Figure 3.13 B).
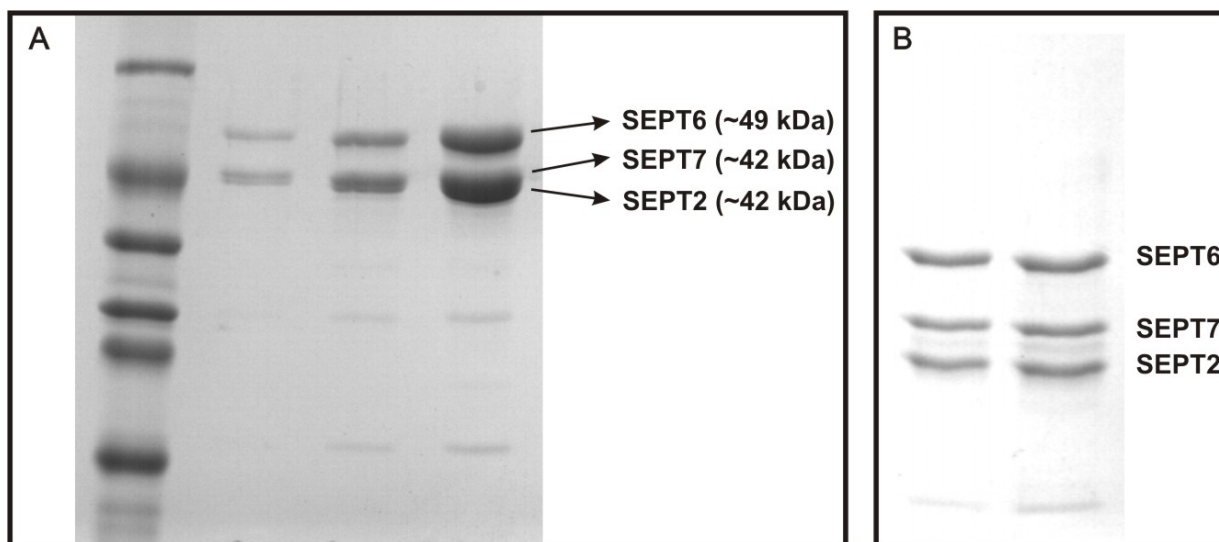

Figure 3.13 **A and B: 12% SDS-PAGE of HSC-361 after gel filtration applied increasing from left to right.**

Both complexes, HSC-wt and HSC-361, showed no difference when analysed for their nucleotide content using reversed-phase C-18 HPLC column as described for SEPT2-315. ~70% of the complex was saturated with nucleotide, meaning two of the six nucleotide binding remains empty. The nucleotide content of the complex varies with different preparation. The GDP:GTP ratio is >2:1, and the residual GTP is not hydrolyzed even after incubating the complex at 37°C for more than one day. When GTP was added to the complex extraneously, the protein exhibited multi-turnover GTPase activity, similar to SEPT-315. Similar properties have been observed with fly, yeast and mammalian septins (Field et al., 1996; Vrabioiu et al., 2004; Kinoshita, 2003; Farkasovsky et al., 2005). Both the complexes HSC-wt and -361 were able to form filaments (data not shown) as shown for

other recombinant septin complexes (Field et al., 1996; Frazier et al., 1998; Sheffield et al., 2003; Farkasovsky et al., 2005).

3.5.2 Crystallization

10 mg/ml protein concentration was used during crystallization trials. Initial crystallization trials were carried using high salt, such as 3-4M NaCl and HEPES buffer pH 7-8. These crystallization conditions had already been optimized for HSC-wt in Ian G. Macara's lab which diffracted anisotropically to 4.5Å and isotropically to about 6Å (Macara et al unpublished work). The crystals were reproduced (Figure 3.14 A), and the crystals large enough (Figure 3.14 A-D) were harvested for testing. However these crystals did not diffract X-rays, even after extensive adjustments in crystallizations conditions and freezing procedures.
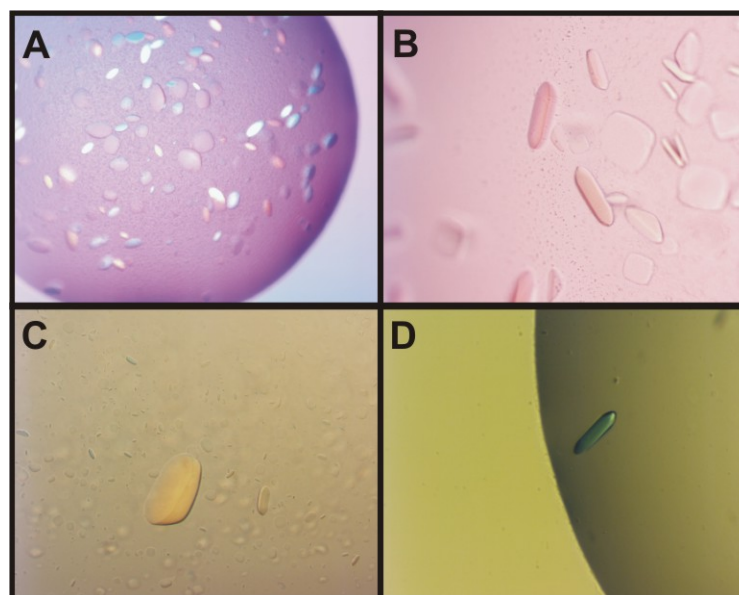
Figure 3.14 **Crystals of HSC under high salt: 3.4M NaCl 100mM Sodium-Succinate pH 5.5 10mM DTE**

To find another crystal form which diffracts X-rays, new crystallization conditions were tested using commercially available screens. HSC-361 was preferred as it lacks the degradation product of SEPT7 (see Figure 3.13 and related text). Initial tiny protein crystals could be obtained using 1.5M Lithium sulphate as a precipitant and 100mM HEPES pH 7.5 (Hampton Crytal screen I No.16) (Figure 3.15 A). The size and nucleation of the crystals were improved by manipulating the crystallization conditions. For example, by changing

the precipitant to ammonium sulphate increased the size and by adding 0.5-1% Dioxane nucleation was decreased (Figure 3.15 B). During crystallization trials we also used the HSC-wt and to our surprise the deletion of 57 amino acids C-terminally in SEPT7 did not make any difference as both the complexes crystallized under same conditions (Figure 3.15 C) and diffracted very similarly to >7Å. Therefore, HSC-wt was used hereafter for further crystallization trials and optimization. To ensure that the complex has similar properties throughout the crystallization trials, several batches of purified complexes were pooled together for final gel filtration. After several optimization procedures like varying the drop sizes, protein:precipitant ratio, pH, buffer and precipitant concentration, using siliconized cover slips and addition of 2.5x excess of GTP prior to gel filtration, the crystals grew large enough to a dimension of 100x100x200μM (Figure 3.15 D). The final optimized crystallization condition was 1.4M ammonium sulphate, 0.1M MES pH 6.5, 0.8% Dioxane.
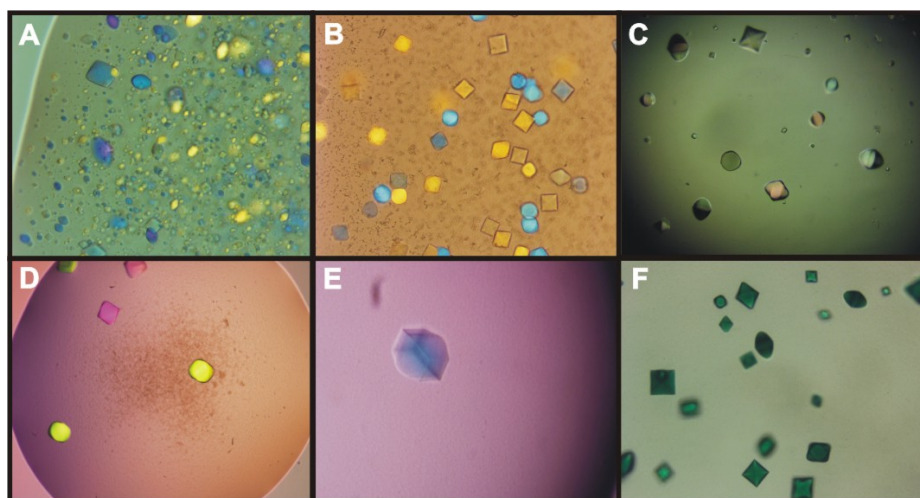
Figure 3.15   **A-D: Optimization of HSC-361 and -wt crystals. E: Selenomethionine crystal. F; Crystals soaked with Ta$_6$Br$_{14}$**

3.5.3   Data collection and heavy atom derivatization

The optimized crystals were harvested and transferred to a cryoprotectant solution containing 20% glycerol along with mother liquor and immediately flash frozen in liquid N$_2$. The frozen crystals were maintained at 100K throughout and tested for diffraction, in an in-house X-ray source. Pre-screened crystals were taken to synchrotron beamline for data collection, a complete dataset up to 6Å for native crystals was colleted at the European Synchrotron Radiation Facility (ESRF), beamline ID14-EH in Grenoble. Clearly the 6Å

data was not sufficient for further crystallographic studies, so further attempts to improve diffraction quality and also heavy atom derivatization was carried for *de novo* phase determination.

Transferring the crystals to higher concentrations of ammonium sulphate did not help, the crystals showed no diffraction, all attempts to shrink the crystals were *in vain*. It was observed that addition of 1-5% glycerol to the crystallization conditions did not affect the crystallization of HSC. In an attempt to reduce the damage induced by the addition of cryoprotectant, the crystals were grown by adding 1% glycerol to the mother liquor. The crystals were transferred to the cryoprotectant solution where the glycerol concentration was gradually increased in small steps to a final 20% glycerol, the diffraction quality of crystals was improved. The crystals diffracted to >4Å at a synchrotron beam line, but exhibited high degree of anisotropy, where in one direction the diffraction was reduced to ~6Å (Figure 3.16). Nevertheless a dataset was collected for the native crystal which was ~100% complete up to 4Å at Swiss Light Source(SLS), beam line X10SA in Villigen, Switzerland. Data collection statistics are summarized in Table 3.4.
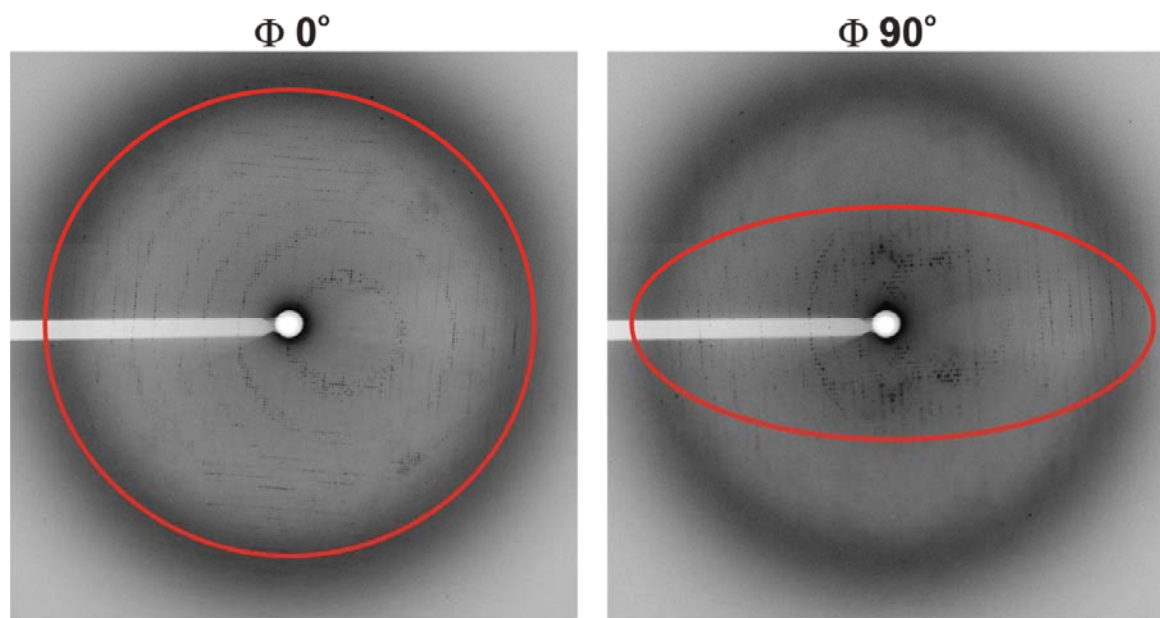

Figure 3.16 **Diffraction images of HSC crystal taken at SLS, Villigen. Right image is when crystal exposed to X-rays at 0°, Left same crystal exposed to X-rays after rotating 90°. Red circles indicate the region of diffraction spots on the image plate.**

Table 3.3 List of Heavy atom compounds used in derivatization.				
Compound	**Concentration**	**Strategy**	**Wavelength**	**Remarks**
$HgCl_2$[†]	1mM	SAD	1.008	See Table 3.4
K_2PtCl_4	2mM	SAD	1.059	,,
Ta_6Br_{14}	1mM	SAD/MAD	1.254	,,
$[Pt(en)I]_2$ (PIP)	1mM	SAD	1.071	,,
$YbCl_3$	2mM	SIR	1.385	1 site found, but not used
$UO_2(OAc)_2$	1mM	SIR	0.979	2 sites found, but not used
Xe*	-	SAD/SIR	1.770	1 site found, but not used
$Hg(OOCCH_3)_2$	1mM	MAD	1.077	No sites found
$K[Au(CN)_2]$	5mM	SAD	1.039	No sites found
$Pt(NH_3)_2Cl_4$	5mM	SAD	1.068	No sites found
$(NH_4)_2[OsBr_6]$	5mM	SAD	1.140	No sites found
$ErCl_3$	2mM	SIR	1.541	No sites found
$EuCl_3$	2mM	SIR	1.541	No sites found
$GdCl_3$	2mM	SAD	1.385	No sites found
$LaCl_3$	2mM	-	-	No data collected
$SmCl_3$	2mM	-	-	No data collected
K_3IrCl_6	2mM	-	-	No data collected
$Pb(NO_3)_2$	2mM	-	-	No data collected
$H_4SiO_4[12WO]$	1mM	-	-	No data collected

† Co-crystallized

*Derivatized   using   Xenon   gas   chamber   available   at   SLS,   Villigen,   Switzerland

Simultaneously while improving the crystals and diffraction quality, crystals were also subjected for heavy atom derivatization using various compounds available in-house. All the heavy atom derivatization was achieved by soaking 1-5mM of the respective heavy atom compounds in the mother liquor over a period of 12-24 hours, except for $HgCl_2$ which was co-crystallized. An example of a tantal cluster (Ta_6Br_{14}) derivatization is shown in Figure 3.15 F. These crystals acquire the green colour, when soaked. The putative derivatives were tested for diffraction in-house, and were taken to SLS, Villigen for data collection. Lists of all the heavy atom compounds tried are given in table 3.3. Several SAD/MAD datasets were collected at different wavelengths (Table 3.3), the data collection statistics for only those which were used in phase determination are summarized in Table 3.4

Apart from classical soaking experiments, the incorporation of selenomethionine, a prudent and most widely used method for obtaining de novo phase information, was also tried with HSC. The selenomethionine incorporated HSC (HSC-SeMet) was purified as described for the native protein with the exception that the cells were grown in minimal media supplemented by selenomethionine (Doublie, 1997). Purification of HSC-SeMet was trivial, whilst the complex did not crystallize under similar conditions as of native. Therefore, crystal seeding was tried where the native crystals were crushed and a series of dilution made using the mother liquor, the dilutions contain small crushed crystals which serve as nucleations. These nucleations were seeded over a freshly prepared crystallization drop, a typical streak seeded drop is shown in Figure 3.17
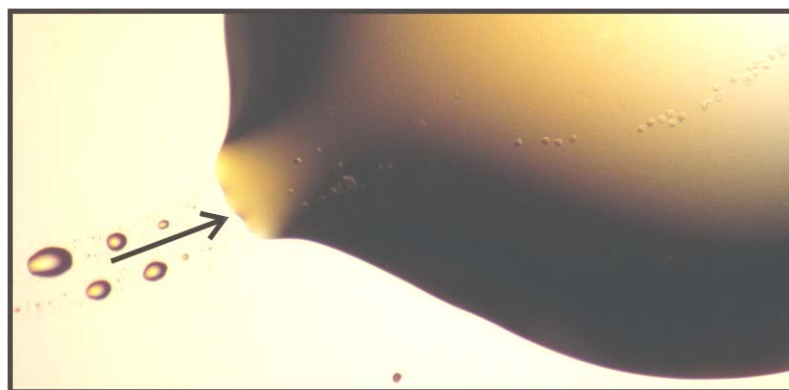

Figure 3.17　　　**Streak seeded crystallization drop; the arrow indicates path of streak which runs diagonal to the box where tiny crystals appeared after 2 days.**

Table 3.4 Data collection and Phasing statistics of HSC crystals

	HSC - Native	HSC - SeMet	HSC - Ta$_6$Br$_{14}$	HSC - HgCl$_2$	HSC - K$_2$PtCl$_4$	HSC - PIP
Data Collection Statistics						
Wavelength (Å)	1.07188	0.97960	1.25447	1.00813	1.0596	1.07188
Space group	P4$_3$22	P4$_3$22	P4$_3$22	P4$_3$22	P4$_3$22	P4$_3$22
Cell Dimensions						
a,b,c (Å)	252.5,252.5,156.4	253.2,253.2,156.3	249.5,249.5,155.7	252.3,252.3,157.8	252.7,252.7,154	251.4,251.4,152.2
α,β,γ (^{o})	90, 90, 90	90, 90, 90	90, 90, 90	90, 90, 90	90, 90, 90	90, 90, 90
Resolution (Å)[*]	50 – 4.0 (4.1-4.0)	20 – 6.0 (6.1-6.0)	15 – 6.0 (6.1-6.0)	15 – 5.0 (5.1-5.0)	50 – 8.0 (8.1-8.0)	50 – 8.0 (8.1-8.0)
Rsym (%)[†*]	22.9 (71.6)	15.7 (63.8)	7.1 (20.2)	21.6 (56.8)	11.4 (39)	10.1 (39.4)
I / σ (I)[*]	11.42 (3.98)	14.69 (4.9)	19.14 (9.39)	7.83 (3.82)	13.49 (5.39)	15.16 (4.98)
Completeness (%)[*]	98.2 (98.9)	99.3 (99)	96.3 (98.4)	97.4 (97.7)	98.4 (97.9)	98.9 (99.5)
Redundancy	16.2	15.6	7.4	7.7	8.5	6.7
Phasing Statistics						
No. of Sites		17	3	1	5	2
FOM	0.54					
FOM (solvent flattened)	0.70					

*Values in parentheses indicate outermost resolution shells

[†] R$_{sym}$ = Σ|**I$_h$** – **<I$_h$>**| / Σ **I$_h$** where **<I$_h$>** is the intensity of the symmetry-equivalent measurements.
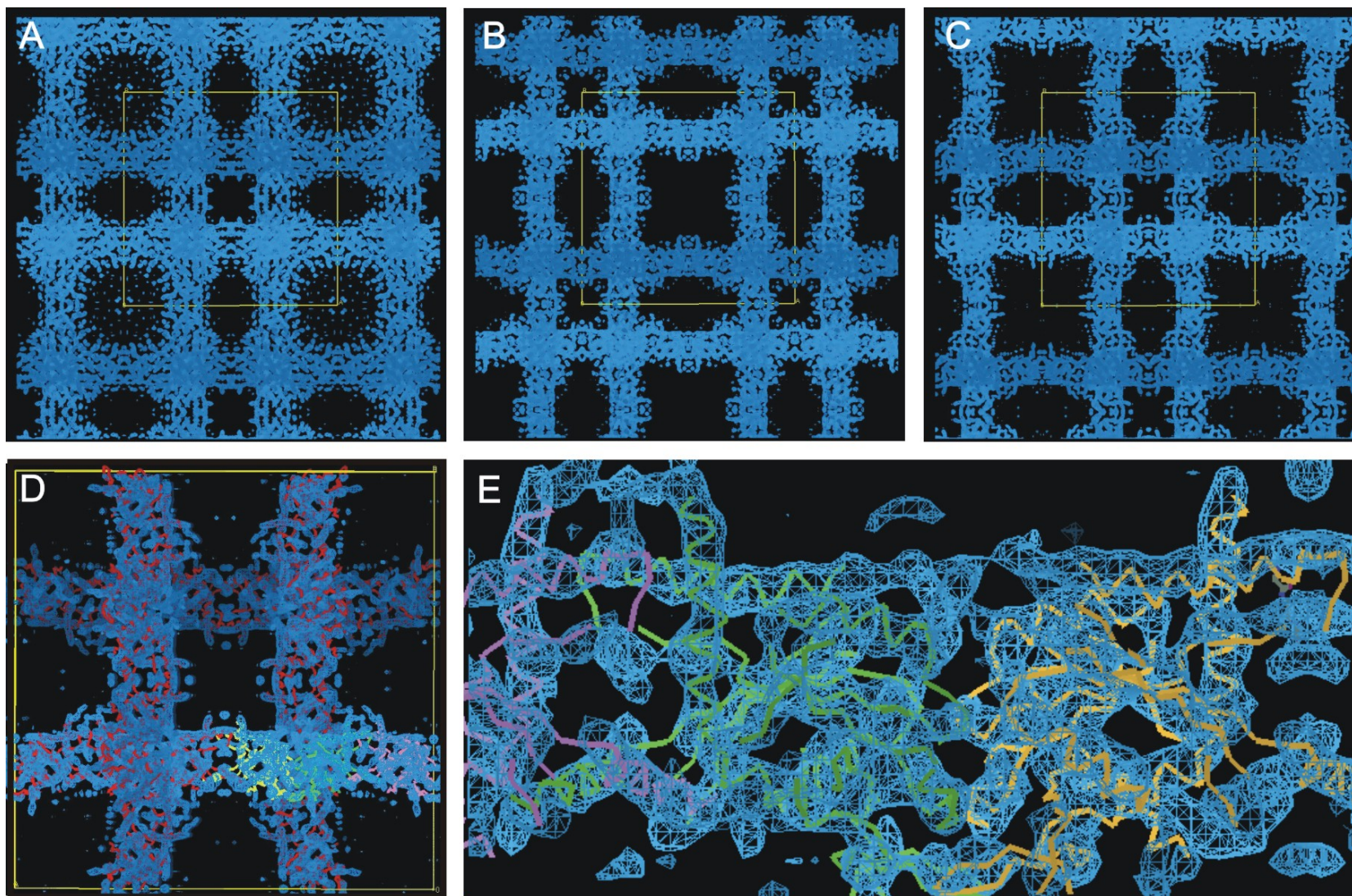
65

Figure 3.18   A-C: Electron density maps from different heavy atoms, yellow box in the centre represent the unit cell. D and E: Superimposition of molecular replacement solution with experimental map, chains in red represent symmetry related molecules.

These tiny crystals were then used for further micro- and macro-seeding, additionally 10mM TCEP was used in the crystallization conditions to prevent oxidation of seleno atoms. The crystal as shown in Figure 3.15 E was used for collecting a SAD data set. Data collection statistics are summarized in Table 3.4

The data sets were processed using the XDS software package (Kabsch, 1993). The crystals belonged to tetragonal space group P4322 with unit cell dimensions a=b=252 Å, c=156 Å, $\alpha=\beta=\gamma=90^{o}$ with a solvent content of 72% and Matthews Coefficient of 4.3 $Å^3$ Da^{-1} (estimated for one hexamer per asymmetric unit).

3.6 Structure solution of HSC

3.6.1 Phase determination

Originally none of the derivatized crystals gave the phase information, except for the HSC-SeMet crystals and crystals soaked with Ta_6Br_{14} cluster. Initial phases were obtained using SOLVE and RESOLVE (Terwilliger, 2003) from selenomethionine sites. The program identified only 16 seleno sites out of 82 (expected for one hexamer) and the resultant electron density looked like a tube mesh (Figure 3.18 A). Similar output was seen for Ta_6Br_{14} crystals with one tantalum cluster per asymmetric unit (Figure 3.18 B). These weak phases were used for cross validation of selenomethionine and Ta_6Br_{14} phases and were also used in calculating anomalous Fourier map using FFT of the CCP4 package (Bailey, 1994) from the SAD datasets collected from various heavy atom derivatives. Only the derivatives which showed anomalous signal above the 5σ cut-off were chosen. The sites were handpicked manually and fed into SOLVE for phase calculation with combined and merged data set of native, SeMet, Ta_6Br_{14}, PIP or $[Pt(en)I]_2$, K_2PtCl_4, $HgCl_2$ which gave good experimental phases up to 5.5 Å. The resultant electron density after RESOLVE showed the secondary structural elements (Figure 3.18 C and D).

Under the assumption that the electron density is a repeating unit of the G domain, molecular replacement was performed with the native data at 4 Å using MOLREP (Bailey, 1994) and a monomeric poly-alanine model of the SEPT2 G domain as a molecular replacement search model. The resultant replacement solution contained 3 monomers. The trimeric model fitted very well with the experimentaly phased electron density (Figure 3.18

D and E) supporting the notion that a trimer and not a hexamer occupies the asymmetric unit. With that information, the crystals turned out to have an unusually high solvent content of ~85.7% and Matthews Coefficient of 8.7 $Å^3 Da^{-1}$

3.6.2 Subunit assignment

Due to high homology between the three septins SEPT2, 6 and, 7 there were no obvious difference in the electron density (Figure 3.18 E). In order to identify the position of each polypeptide, the information provided by the selenomethionine crystals (HSC-SeMet SAD data) was used, as the three septins contain different number of methionines in different positions on the polypeptide chain (see sequence alignment Figure 3.5). The locations of SEPT2, 6 and, 7 could thus be unequivocally identified as seen in Figure 3.19.
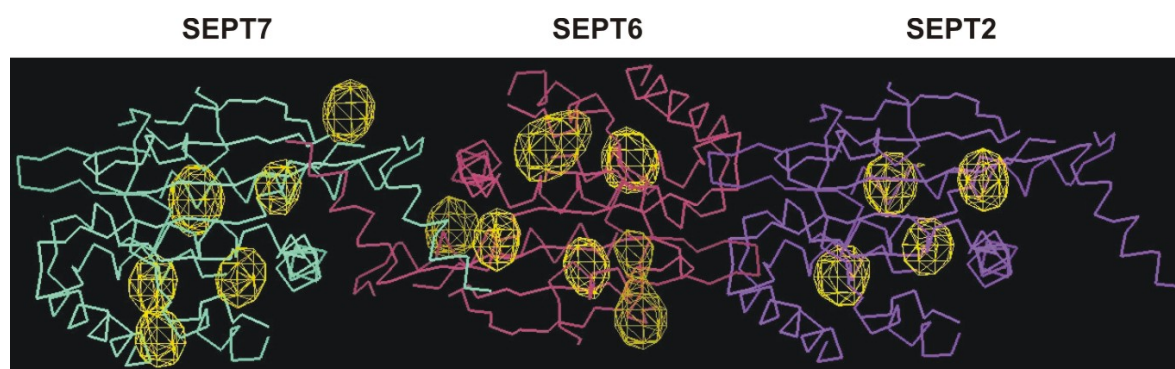

Figure 3.19   **Superimposition of replacement model along with seleno-anomalous map contoured at 5σ**

3.6.3 Phase extension, Model building, and Refinement

The trimeric model (molecular replacement solution) was fitted into experimental phases by using rigid body refinement and by splitting the G domain in to small rigid bodies. The model was then used to generate phases. The model derived phases were combined with experimental phases using SIGMAA (Bailey, 1994) and extended to 4 Å. Further cycles of density modification using DM of the CCP4 package (Bailey, 1994) the electron density was used for model building. Simultaneously CNS composite omit maps were generated to locate missing parts (Brunger et al., 1998). For model building the SEPT2 was taken from SEPT2 G-dimer model and, SEPT6 and SEPT7 were built manually, guided by the molecular replacement model and methionine positions. Side chains were placed

confidently around methionine positions, while the rest was built as poly-alanine polypeptides, as the side chains were not visible.

Initial refinement was done using REFMAC (Murshudov et al., 1997) without adding the nucleotides. Positive densities were observed in the nucleotide binding sites and were attributed to nucleotides. While the densities for SEPT2 and SEPT7 nucleotide binding sites were consistent with GDP, the active site of SEPT6 contains additional density which was tentatively assigned to the γ-phosphate of the GTP. Final refinement was done with the model containing nucleotides. TLS (Translation, Liberation and Screw-rotation displacement) bodies were used as defined in Table 3.5

Table 3.5 List of TLS bodies used in Refinement

	SEPT2	SEPT6	SEPT7
Residue Range	21-34	17-38	29-38
	36-62	40-67	40-65
	78-101	75-101	72-96
	116-139	104-107	103-128
	141-206	109-133	-
	208-214	136-216	130-207
	224-247	222-239	225-237
	253-268	257-262	245-265
	270-304	268-307	260-301

Table 3.6 Refinement statistics of HSC

Resolution (Å)	49.15 – 4
Number of reflections (working / test)	40358 / 2125
R_{work}[a] /R_{free}[b] (%)	37.5 / 39.2
Number of atoms	
Protein	4575
Ligand	87
Number of residues built	706 (out of 1256)
B-factors	
Protein	78.3
Ligand/ion	71.4
R.m.s deviations	
Bond lengths (Å)	0.057
Bond angles (°)	4.7
Ramachandran statistics[c]	
Most favoured regions	86.2%
Additionally allowed regions	13.1%
Generously allowed regions	0.7%

[a] $R_{work} = \Sigma|F_O - F_C| / \Sigma F_O$, where F_O and F_C are the observed and calculated structure factor amplitudes.

[b] R_{free} is calculated similarly to R_{work} using 5% of the test set reflections.

[c] Calculated using PROCHECK (Laskowski et al., 1993)

3.6.4 Trimer Model

The refined trimer model consisting of SEPT2/6/7 as shown in Figure 3.20 consists of an assembly of G domains, which contact each other using the same conserved G- and NC-interfaces as seen in SEPT-315 structure. No density was observed for the coiled-coil regions. To exclude the possibility that the proteins were truncated during crystallization, crystals of the HSC were dissolved and shown to contain full-length protein (Figure 3.21). Dispensability of the coiled-coils is further discussed in EM analysis and Discussion section.
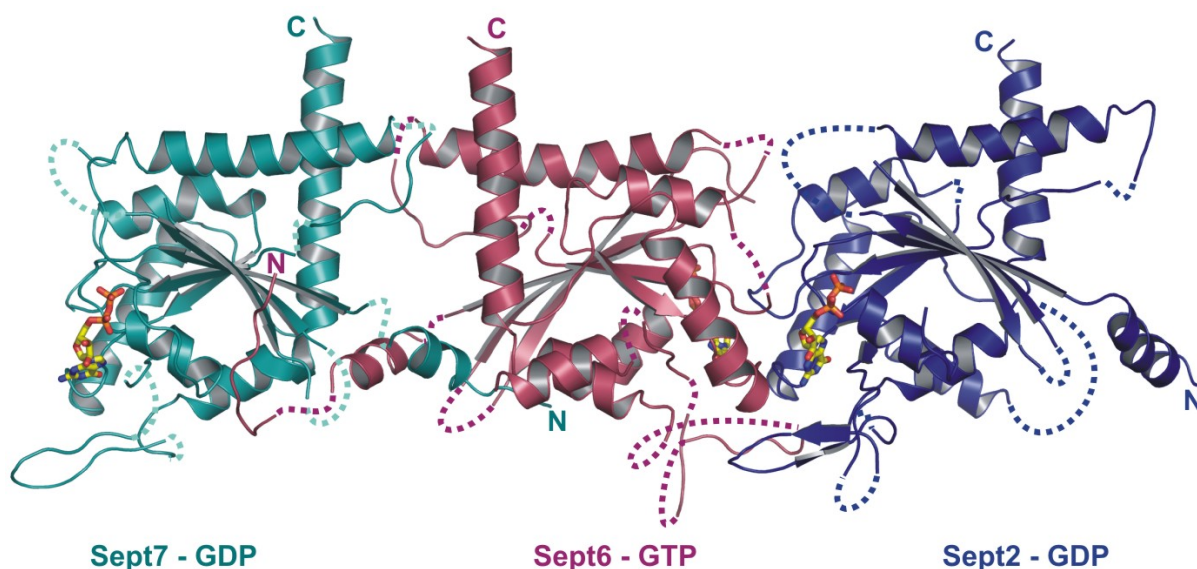

Sept7 - GDP   Sept6 - GTP   Sept2 - GDP

Figure 3.20   **Septin 2/6/7 trimer ribbon model along with nucleotides in ball and stick, the disordered regions are depicted as dotted line.**
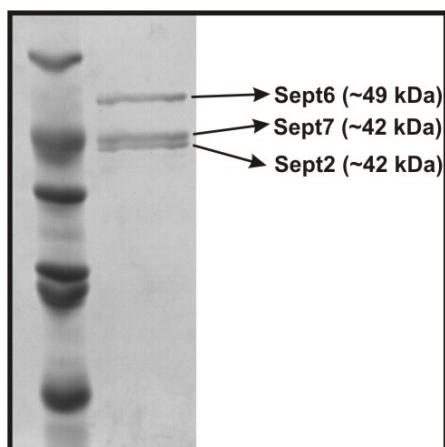

Sept6 (~49 kDa)
Sept7 (~42 kDa)
Sept2 (~42 kDa)

Figure 3.21   **15% SDS gel of crystals of HSC after washing 3 times with mother liquor along with SDS-7 marker.**

3.7 Electron microscopy of human septin complex

From the crystal structure of the human septin complex (SEPT2-SEPT6-SEPT7), a trimer occupies the asymmetric unit, but from the gel filtration the complex elutes as a hexamer. In order to show that the crystal structure also represents the structure in solution electron microscopic studies were done.

Protein samples were prepared in a similar manner as described earlier. The samples were analyzed by Holger Stark and Florian Hauer of Max-Planck-Institute for Biophysical Chemistry, Göttingen. In brief, human septin complex was incubated in high salt buffer (20mM HEPES pH 8.0, 800mM NaCl, 5mM $MgCl_2$ 10mM dithiothreitol) for 30 minutes. Then the samples were applied on a single carbon film on an electron microscopy grid covered with carbon support film (containing 1-4 mm holes) and negatively stained with uranyl formate. Images were taken on a 4k X 4k CCD camera in a Philips CM200 FEG electron microscope. Class averages were calculated from several thousand particles from raw images (Figure 3.23 E) using computer-aided image processing procedures.

Under low salt conditions the heterotrimer forms extended filamentous structures of various length as shown for native and recombinant septin filaments (Field et al., 1996; Farkasovsky et al., 2005; Kinoshita et al., 2002). Under high salt conditions, the long filaments break in to short pieces of uniform length become prevalent. Class averages of human septin complex under high salt conditions shows a linear particle consistent with similar width as observed in the crystal. It consists of six equally sized subunits consistent with an array of G domains (Figure 3.23 A) and also as shown for rat oligomeric septin complex (Hsu et al., 1998).

The length of the particle is twice the size of the asymmetric unit (trimer). Therefore, the particle observed is a dimer of trimer. But it is not possible to deduce from the linear arrangement of subunits in the crystal, the boundaries of the solution particle. In order to identify the dimer of trimer as observed in the electron microscopy, a complex containing maltose binding protein (MBP)-SEPT2 fusion and SEPT6-SEPT7 was analyzed. The MBP fusion complex is an intermediate of the standard purification scheme of the SEPT2-SEPT6-SEPT7 complex. The MBP has almost the same mass as a G domain. If the SEPT2 subunit is located in the middle, an extra mass would appear at the middle part of the

hexamer (Figure 3.22), and similarly if the SEPT2 subunit is located at the end of the hexamer, an extra mass should appear at the ends (Figure 3.22). Single particle analysis showed an extra density located at the centre of the particle (Figure 3.23 C), confirming the arrangement of septins in the order of 7-6-2-2-6-7. The fact that only one extra density is visible instead of two in the class averages might be due to the flexible connection of the tag and/or the arrangement of the particles on the grid. A raw image of a single particle shows both the MBP fusion tags as lateral protrusions highlighted by the arrows (Figure 3.23 D).
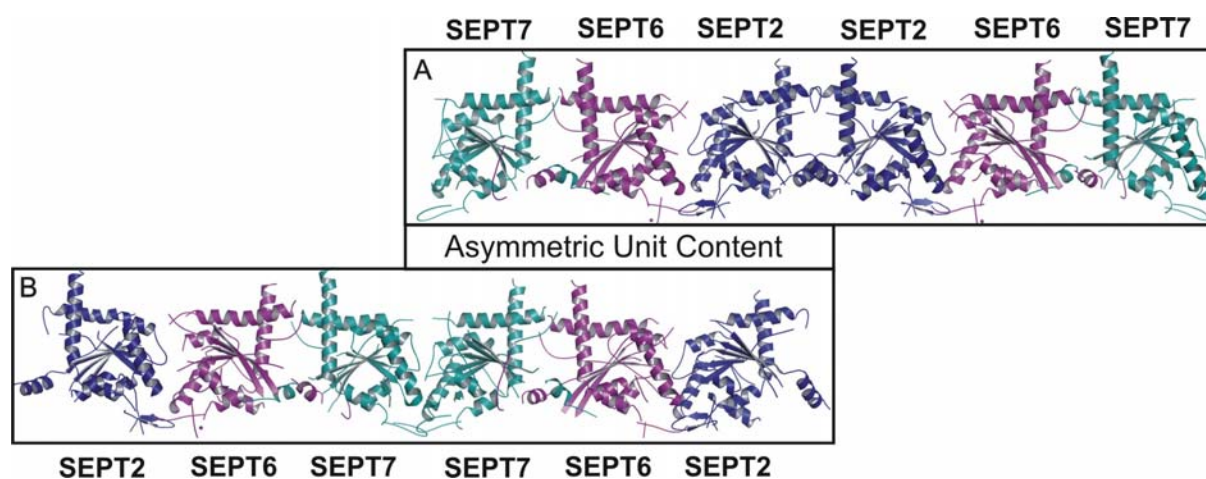

Figure 3.22　　**Possible hexamers, where the asymmetric unit content (trimer) is linearly arranged. A; Possibility one where the hexamer is in 7-6-2-2-6-7 arrangement. B; Possibility two where the hexamer is in 2-6-7-7-6-2 arrangement.**

Similar to the crystal structure, no density corresponding to the C-terminal ends was observed in the electron microscopy images after averaging. To confirm that the C-terminal ends are dispensable for complex formation, the C-terminal ends of the three septins were deleted, SEPT2 (1-308), SEPT6 (1-310), SEPT7 (1-305). The ΔCC complex was isolated using the same purification procedure as wild-type human septin complex. Single-particle analysis did not reveal significant differences compared to the wild-type human septin complex (Figure 3.23 B).
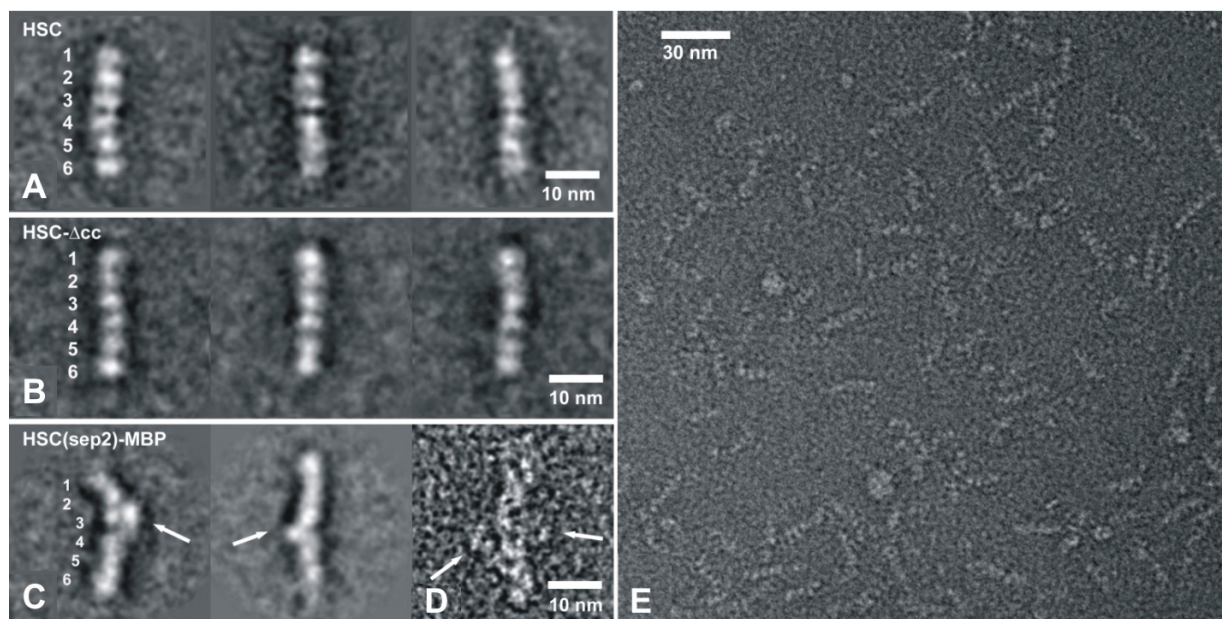
Figure 3.23   **A: Class averages of HSC-wt at high salt concentration obtained after reference-free alignment, MSA and classification. B: Class averages of HSC-Δcc obtained similar to A. C: Class averages of MBP fusion complex. D: A single-particle image of the MBP-fusion complex. E: Raw micrographs recorded for HSC-wt at high salt concentration.**

3.8 Septin – Borg interaction studies

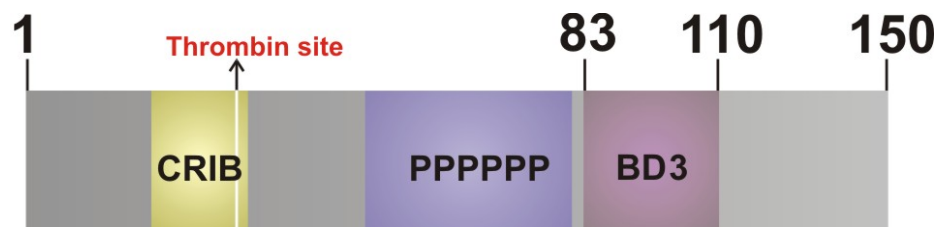### 3.8.1 Purification of Borg3

Figure 3.24   **Domain organization of Borg3, CRIB stand for Cdc42/Rac-interaction binding motif. PPPP stands for poly-proline region. BD3 stands for Borg-homology domain 3.**

According to Macara and co-workers the Borg (Binder of Rho-GTPases) binds to septins and inhibits polymerization. When Cdc42 (a Rho family GTPase) is in its GTP bound form, Borg3 binds to Cdc42 leaving the septins free to polymerize (Joberty et al., 2001). Although the authors show direct binding of Borg3 towards septins, little has been done to show the effect of Borgs on septin polymerization (Sheffield et al., 2003). In order to study whether Borgs play a role in septin filament formation, Borg3 was chosen. Since it was already known to interact with both Cdc42 and septins (Joberty et al., 1999; Joberty et al., 2001).

pGEX6P1 Borg3 (83 – 110) construct was used and purified using GSH columns and eluted using 20mM glutathione, the eluted sample contained GST-tagged Borg3 (83 – 110), hereafter GST-BD3. 50mM TRIS-HCl pH 7.8, 100mM NaCl, 5mM β-mercaptoethanol was used throughout the purification procedure. Similarly pGEX6P1 Borg3 (1 – 110) construct was used to purify Borg3 (1 – 110), hereafter Borg3. The Borg3-GST fusion was cleaved using PreScission protease on the resin, overnight at 4°C. The cleaved protein was eluted with the same above mentioned buffer.

The SDS-gel of GST-BD3 protein, (Figure 3.25 A) the protein band corresponds to a mass of ~30 kDa, which is in line with the calculated mass. The SDS-gel of Borg3 protein, (Figure 3.25 B) the protein band (lane 2) corresponds to a mass of >40 kDa, whilst the calculated mass corresponds to ~12.5 kDa. To check whether the protein is indeed Borg3 and has the predicted mass, MALDI – MS (Matrix Assisted Laser-Desorption Ionization – Mass Spectrometry) analysis and thrombin cleavage was performed. Borg3 has an intrinsic

thrombin cleavage site which is at the end of CRIB motif (Figure 3.24). When the protein was treated with thrombin overnight the protein is cleaved in to two products (Figure 3.25 B; lane 3), but the cleaved products again does not run in the SDS-gel according to their calculated mass. The reason for this might be that the protein is natively unfolded. MALDI mass spectra showed a mass of ~12553.89 Da which is close to the calculated mass 12537.4 Da (Figure 3.26).

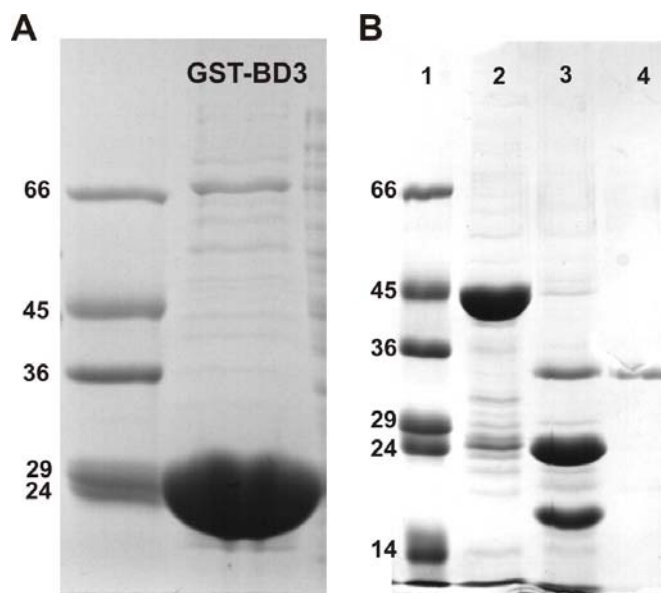

Figure 3.25   **A: 15% SDS-Gel of purified GST-BD3 protein. B: 15% SDS-Gel Borg3 samples, lane1; SDS-marker, lane2; purified Borg3, lane3; Borg3 + Thrombin, lane4; only thrombin.**
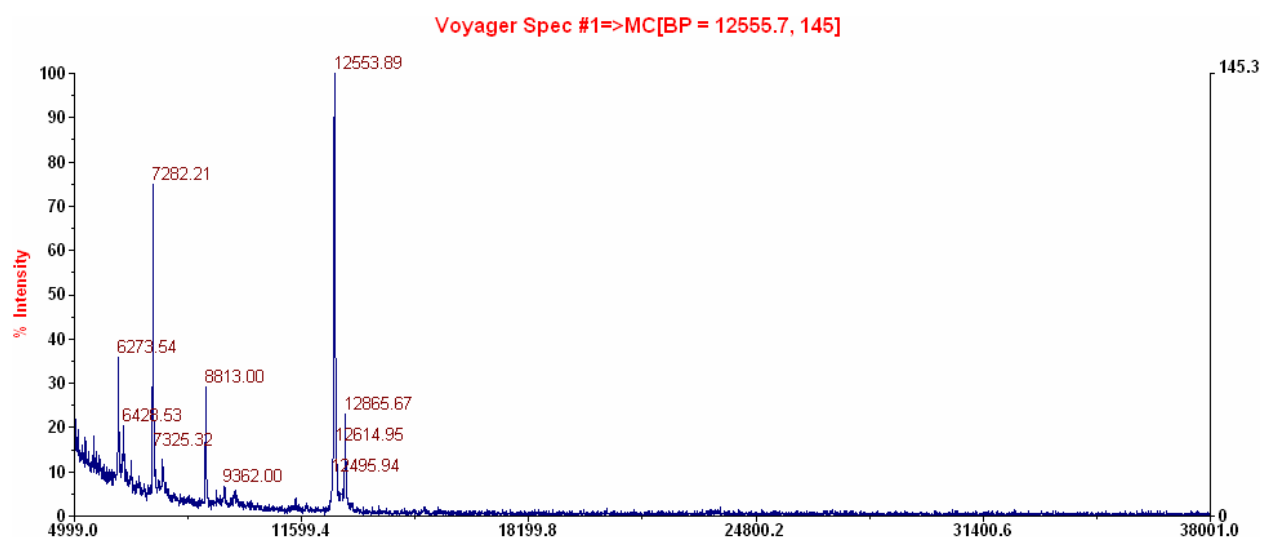

Figure 3.26   **Mass spectra of Borg3 sample.**

3.8.2   Septin and borg complexes

Using Superdex-200 16/60 gel filtration, SEPT2-SEPT6-SEPT7-GST BD3 and SEPT2-SEPT6-SEPT7-Borg3 quaternary complexes were made. 50mM TRIS-HCl pH 7.8, 100mM NaCl, 5mM MgCl$_2$, 5mM DTE was used as gel filtration buffer. Prior to gel filtration both the septin complex and Borg proteins were mixed in 1:5 ratio, and kept in 4°C for 30minutes. Figure 3.27 shows a 15% SDS-gel of quaternary complexes after gel filtration analysis. The gel filtration chromatogram showed no difference between septin complex and septin-Borg complexes. However, no crystals were obtained with either of the complexes and the effect of Borg on septin filament formation is yet to be demonstrated.
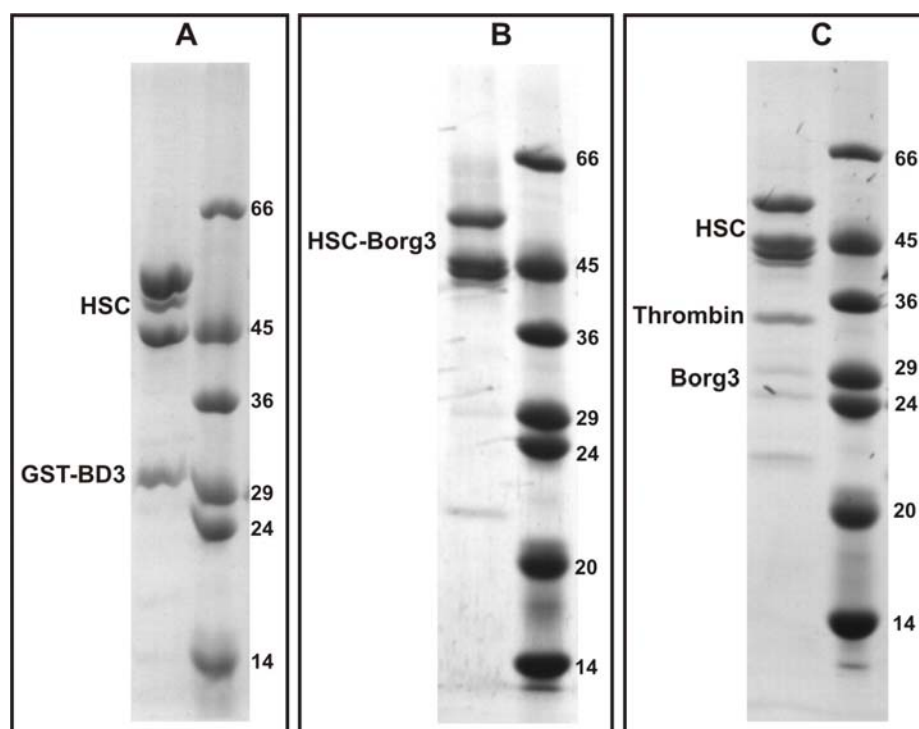

Figure 3.27   **A: 15% SDS-Gel of SEPT2-SEPT6-SEPT7-GST BD3 complex. B: 15% SDS-Gel of SEPT2-SEPT6-SEPT7-Borg3 complex. C: 15% SDS-Gel of SEPT2-SEPT6-SEPT7-GST BD3 complex + Thrombin, to show the Borg protein, which runs at the same place as septins.**

4 Discussion

In this current study, structural analysis of mammalian septins was carried out using X-ray crystallography and electron microscopy. The structure of SEPT2 G domain and septin heterotrimer complex comprising SEPT2-SEPT6-SEPT7 was solved to 3.4Å and 4Å resolution respectively. Using electron microscopy the dispensability of coiled coil domains for the complex formation and the order of septin subunits in the basic hexameric unit was confirmed.

4.1 Dimerization of Septin G domain

The structure of SEPT2 G domain very much resembles Ras and the secondary structural elements were assigned according to Ras G domain nomenclature α1-α5 and β1-β6. Apart from the canonical G domain, septins have additional secondary structural elements. The septin G domain was compared with other GTP binding proteins which form dimers such as TrmE, IIGP1 (Interferon inducible GTPase protein 1), hGBP1 (human guanylate binding protein 1) and dynamin.

The sequence alignment of SEPT2 G domain with Ras, MnME (formerly TrmE), dynamin GTPase domain, IIGP1, and hGBP1shows no obvious sequence similarity among each other except for the G1-G4 nucleotide binding motifs. Topology comparison and superimposition of G domains shows that apart from the canonical G domain none of the extra secondary structural elements or insertions can be compared (Figure 4.1).

SEPT2 G domain elutes as dimer from gel filtration. Crystallographic and biochemical studies showed that SEPT2 G domain dimerizes using its nucleotide binding regions called G interface. Dimerization of the G domain is influenced by the presence of nucleotide but not by nature of the nucleotide. This observation is unique since the G domain of MnME has been shown to dimerize in a GTP dependent manner (Scrima and Wittinghofer, 2006). Similar observations have been seen for hGBP1 (Ghosh et al., 2006) and IIGP1 (Ghosh et al., 2004). In all the cases the switch regions are mainly involved in the dimer formation, except for the SEPT2 G domain, where the switch regions are disordered due to the absence of γ-phosphate.

The reason for the 'nucleotide state' independent dimerization might be due to the additional regions involved in the dimerization, apart from the nucleotide binding regions. Biochemical analysis shows that mutating Trp260 and His270 which are present in the two anti-parallel strands β7 and β8 abolishes dimerization completely. Supporting the argument that G dimer interface is further stabilized by β7 and β8, the residues which were mutated in the G dimer interface does not involve in nucleotide binding directly. However the G dimer mutant proteins are less saturated with nucleotide compared to the wild type and NC dimer mutants. This might be due to the synergistic effect of nucleotide binding and dimerization.

The unique feature of septin G domain is that it dimerizes using two interfaces; G interface and NC interface. Both these interfaces are observed during oligomerization of septin. The NC interface is formed by the extra N and C terminal helices (α0 and α6) and the long α2 helix. The NC interface is most likely not influenced by the presence of nucleotide. Dimerization or oligomerization takes place only through homotypic interfaces such as head-to-head or tail-to-tail (G to G or NC to NC). Since the dimerization is mediated mainly through extra secondary structural elements, the dimerization of septin G domain is different from that of the other GTP binding proteins which form dimers.
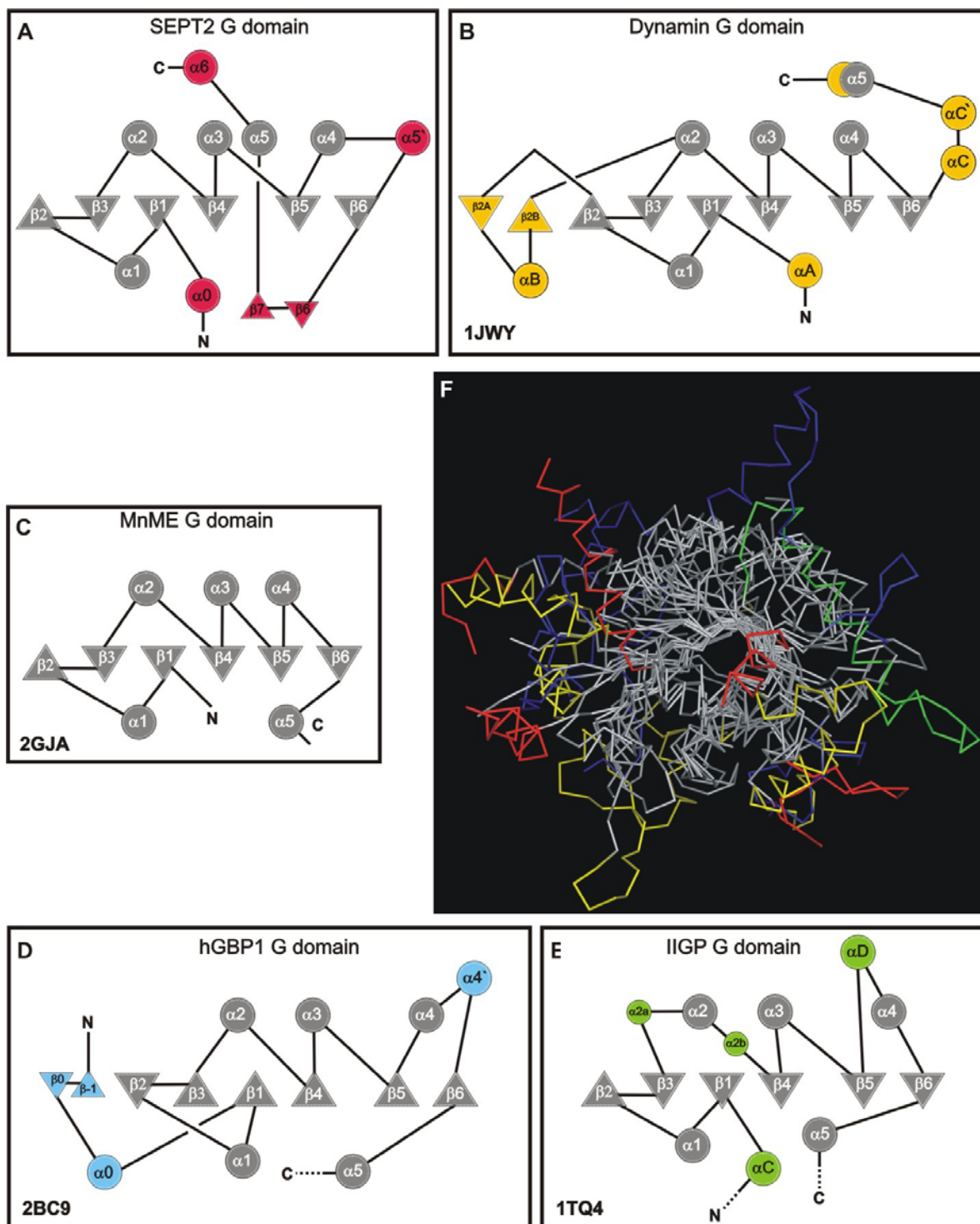
Figure 4.1   **A-E: Topology cartoon of G domains as indicated, the canonical G domain elements are in gray and the extra secondary structural elements or insertions in respective colours. F: Superimposition of different G domains with same colour code as shown in A-E.**

4.2 Human septin complex is a linear hexamer

Combining the X-ray and electron microcopy data, the septin complex was found to be a linear hexamer and the order of septins was confirmed to be SEPT7-SEPT6-SEPT2-SEPT2-SEPT6-SEPT7 (Figure 4.2). The interaction of septin subunits takes place via the same G- and NC-interfaces seen in the crystal of uncomplexed SEPT2.

The SEPT6-SEPT7 interaction is mediated by the NC interface, the longer N-terminus of SEPT6 makes additional contacts with the SEPT7 and may thus be involved in tightening the interaction between the subunits. It has been reported that SEPT6 and SEPT7 are insoluble when they are recombinatly expressed and purified separately. However, the dimeric complex comprising SEPT6-SEPT7 can be purified (Sheffield et al., 2003) leading to the conclusion that both SEPT6 and SEPT7 stabilize each other.

The SEPT6-SEPT2 interaction is via the G interface, similar to that of the SEPT2 G dimer. Notably, the SEPT2-SEPT2 interaction favors the NC interface rather than the G interface found for the isolated SEPT2 in solution supporting the notion that septin interaction appears fairly promiscuous. One particular reason for the difference in the SEPT2-SEPT2 interfaces between the isolated SEPT2 and that of the complex is that the former one might be non-physiological. Due to the absence of partner septin subunit, SEPT2 has no choice but to interact with itself but inside the cell SEPT2 has never been observed or shown to be left alone and interacts with the another septin subunit (SEPT6 in this case). The above mentioned argument is supported by the fact that isolated SEPT2 from insect cells can also form filaments *in vitro* (Huang et al., 2006) where it would use the G and NC interfaces. The other reason which will favor the SEPT2-SEPT6 G interface is the nucleotide bound state of septins which is discussed in detail under section 4.4.
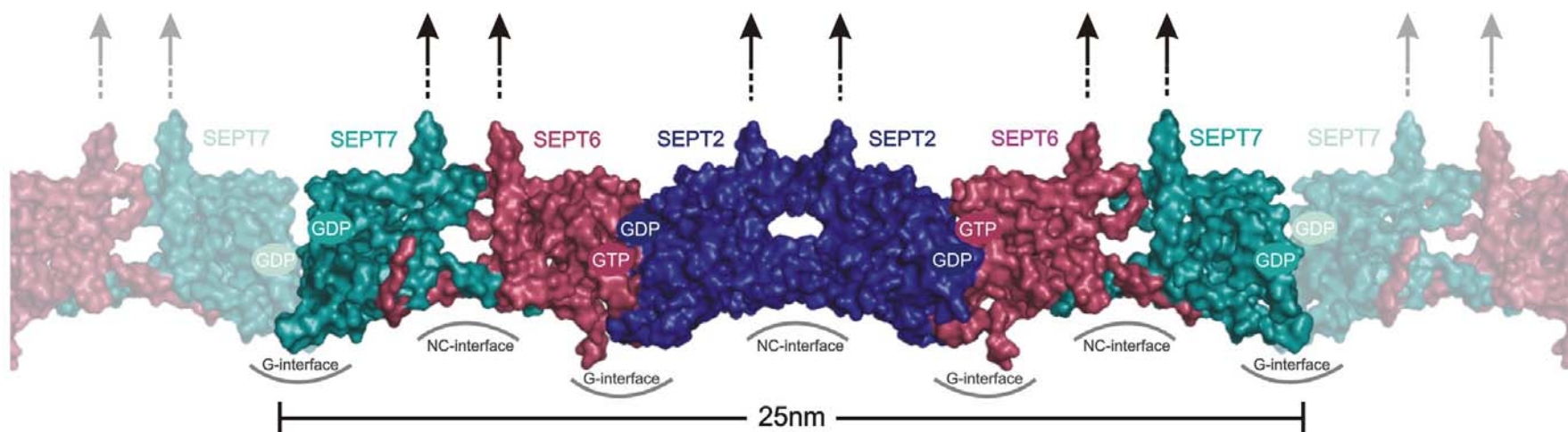
Figure 4.2   **The septin filament. Surface representation of the basic hexameric unit (in dark colours). The neighbouring hexamer makes longitudinal contact using SEPT7 (in faded colours), thereby forming septin filaments. The nature of nucleotides in the subunits is indicated. The presumed orientations of the C-terminal ends predicted to form coiled-coils are shown schematically.**

4.3 Significance of coiled-coil domains

Septins identified so far have a predicted coiled coil domain, except for the members of SEPT3 group of mammalian septins and Cdc10 of budding yeast. The importance of coiled coil domains has been stressed throughout the septin literature, particularly for the interaction of septins between each other during complex and/or filament formation (Versele and Thorner, 2005; Field et al., 1996; Frazier et al., 1998; Nagata et al., 2004; Casamayor and Snyder, 2003; Sheffield et al., 2003). FRET (fluorescence resonance energy transfer) studies using mammalian septins also suggested that the coiled coil domain are important for interaction among septins (Low and Macara, 2006).

Although the resolution of the structure is limited to 4 Å, one would expect to see density for the coiled-coil since the density of the G domain is well defined. Furthermore, no density corresponding to the C-terminal ends was observed in the electron microscopy images after averaging. Thin strands projecting outwards from a rat oligomeric septin complex have been shown before (Hsu et al., 1998) and can also be observed in some of the raw electron microscopic images (figure 3.21 D), but were lost on averaging. Electron microscopic studies also show that the complex and filament formation is not hampered by deleting the coiled coil regions (Figure 3.21 and Figure 4.3). Similarly, recombinant coiled-coil-deleted *Xenopus laevis* Sept2 was shown to form filaments (Mendoza et al., 2002). From this it can be concluded that the coiled coils are not involved in or required for complex and most likely for filament formation.
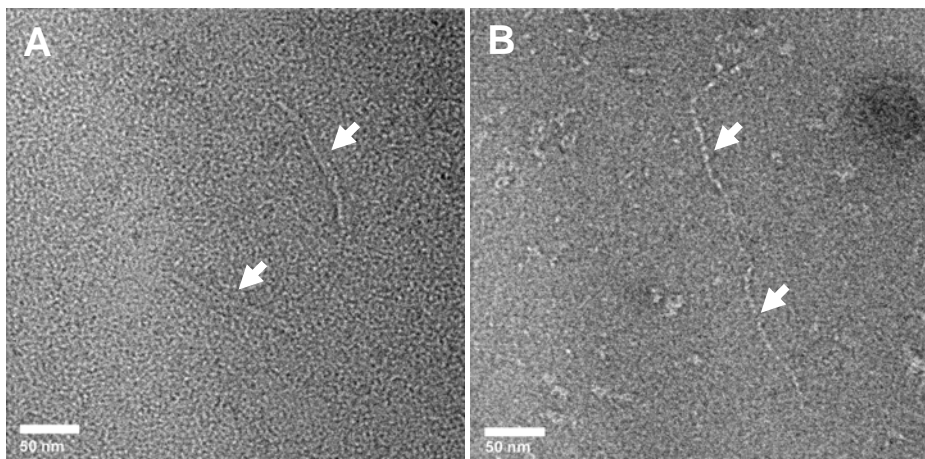

Figure 4.3   **Raw electron micrograph recorded under low salt conditions (50mM NaCl). A: HSC-Wt B: HSC- ΔCC**

This conclusion raises the question about the importance of coiled coil domains, which are present from yeast to human, whether they are apparently dispensable for complex and perhaps also for filament formation. It could be that the septins assemble via the conserved G and NC interfaces leaving the coiled coils to interact with other proteins, as septins are proposed to function as scaffolds (Kinoshita, 2006; Versele and Thorner, 2005). Alternatively the filaments might interact with each other using the coiled coil regions. However, two filaments interacting via their coiled coil domain is yet to be shown.

The reason why the coiled coils are not visible in the crystal structure and electron microscopy images might be that the coiled coil regions are natively unstructured and only adopt structures when they interact with partner proteins. Alternatively, they adopt parallel coiled-coil structures as predicted, but are connected to the α6 of the G domain via a flexible linker. Therefore the C termini might adopt numerous positions relative to the G domain (Figure 4.4). Furthermore, in a recent study using *Caenorhabditis elegans* septins, the authors fused GFP at the C-terminal end and have shown that the coiled-coil domains are flexible (John et al., 2007).


```
hSEPT2:--THMQDLQEVTQDLHYENFRSERLKRGGRKVENEDMNKDQI-------------- : 361
hSEPT7:--THMQDLKDVTNNVHYENYRSRKLAAVTYNGVDNNKNKGQLTKS------------ : 427
hSEPT6:--VNMEDLREQTHTRHYELYRRCKLEEMGFKDTDPDSKPFSLQET----------- : 418
```
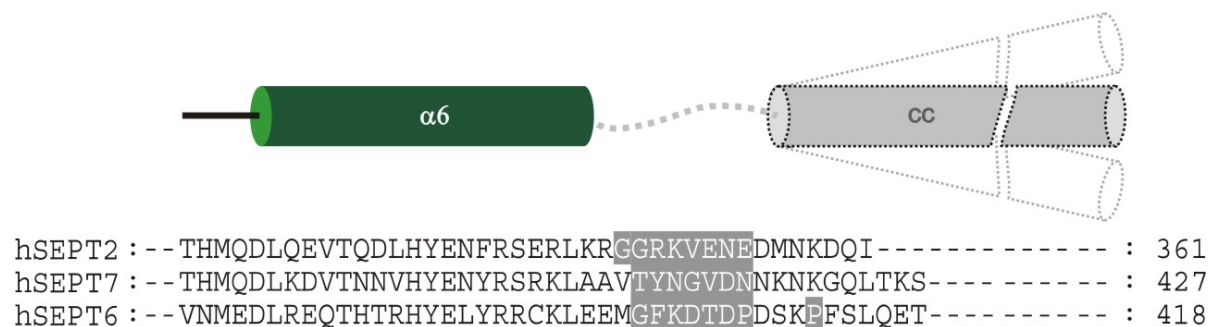
Figure 4.4   **Schematic representation of flexibility of the coiled coil domains. The sequences of the flexible linker region between α6 and CC are highlighted in gray.**

Although the G domain alone is sufficient to mediate complex and filament formation, the close proximity of α6 helices from SEPT6 and SEPT7 indicates that the coiled coils may further stabilize the complex formation as the coiled coils of SEPT6 and SEPT7 have been shown to interact directly with each other (Low and Macara, 2006). However, in the case of SEPT6 and SEPT2 where the α6 helices are far away, the coiled coil regions have been shown to interact with each other. The reason might be that, SEPT2 and SEPT6 indeed interact with each other in the absence of SEPT7, as it is known that heterodimers of SEPT2, SEPT6 and SEPT7 can be made in a combinatorial fashion (Sheffield et al., 2003).

4.4 What does GTP do for septins ?

The nucleotide content of the septin complexes can be compared to α/β tubulin heterodimer, where the α-tubulin has GTP bound in a non-exchangeable site (N-site) and β-tubulin has GDP which can be exchanged (E-site) to GDP/GTP. The difference in the nucleotide states provides stability to the tubulin heterodimer and dynamicity to the microtubules (Nogales, 2001). In the case of septin complexes, the GDP:GTP ratio is >2:1 and found to be conserved from yeast to human. Since the majority of the yeast septin complexes do not exchange nucleotide during one cell cycle period, a structural role for nucleotide was proposed (Vrabioiu et al., 2004).
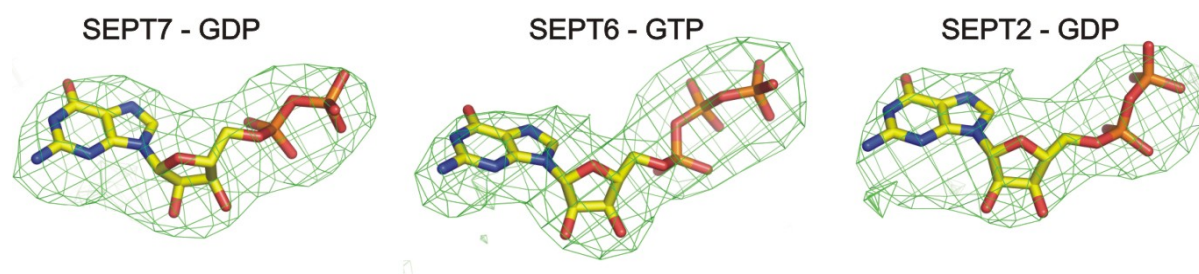

Figure 4.5   **Positive F_o-F_c electron density maps, contoured at 3σ, around the nucleotide-binding sites of the respective septins, and the resulting nucleotide models as indicated.**

In order to identify the septin subunit which is GTP bound, F_o−F_c electron density maps were calculated by omitting the nucleotide of the respective subunit (Figure 4.5). The F_o−F_c electron densities of SEPT2 and SEPT7 are very consistent with a GDP nucleotide, whereas SEPT6 contains additional density that was tentatively assigned to the γ-phosphate of GTP (Figure 4.5). The nucleotide content of the mammalian septin complex present in the crystal is thus consistent with the biochemical findings (Kinoshita, 2003; Field et al., 1996; Farkasovsky et al., 2005).

The reason for the difference in nucleotide states between septin subunits might indicate their different role in stabilizing the complex. From the crystal structure it is clear that the filament forming contact (the longitudinal contact) is formed by the SEPT7 G homodimer (Figure 4.2). This homodimer G interface has GDP bound and electron microscopy studies shows that the filament breaks to a minimal hexameric complex under high salt conditions.

The fact that the SEPT2-SEPT6 G heterodimer is not salt sensitive, might be due to the GTP bound to SEPT6 (Figure 4.2). It seems that the G homodimer is able to hydrolyze GTP, (as seen for SEPT7 in the complex and also for isolated SEPT2) but not the G heterodimer.

The variation in GDP/GTP bound states of septins and the ability to hydrolyse GTP might dictate the rules for septin arrangement. For example in the case of SEPT2-SEPT6-SEPT7 complex analyzed here, where SEPT2 binds to SEPT6, SEPT6 remains GTP bound and thus locks SEPT2 into the complex. For SEPT7-SEPT6, the long N-terminus of SEPT6 favours and/or stabilizes the NC interaction and the C-terminal coiled coils might additionally stabilize further. The trimer which has SEPT7 G interface and SEPT2 NC interface can interact only with their respective similar interfaces since the septin interaction takes place only via head-to-head or tail-to-tail (NC to NC or G to G).

Although the nucleotide states of different septin subunits can be determined easily, it is still not clear why only SEPT6-GTP is not hydrolysed as the resolution of the trimeric complex is limited to 4Å resolution. From the SEPT2 G domain structure, His158 can be seen near the phosphates of guanine nucleotide (Figure 4.6 A). This His158 could in principle be the catalytic residue which positions the attacking water molecule to cleave the γ-phosphate as shown for EF-Tu (Cool and Parmeggiani, 1991). The His158 is totally invariant in human and in other organisms except in yeast Cdc10 septin (Figure 4.6 B). Further studies to elucidate the GTPase reaction mechanism in septins are underway.

Since it has been shown by FRAP (Fluorescence recovery after photo-bleaching) experiments (Dobbelaere et al., 2003) and polarized fluorescence microscopy (Vrabioiu and Mitchison, 2006) that septin organization is highly dynamic *in vivo* during certain stages of cell cycle. From the above proposed role for nucleotide, it is tempting to propose that the dynamics of septins might also be governed by the nucleotide state.

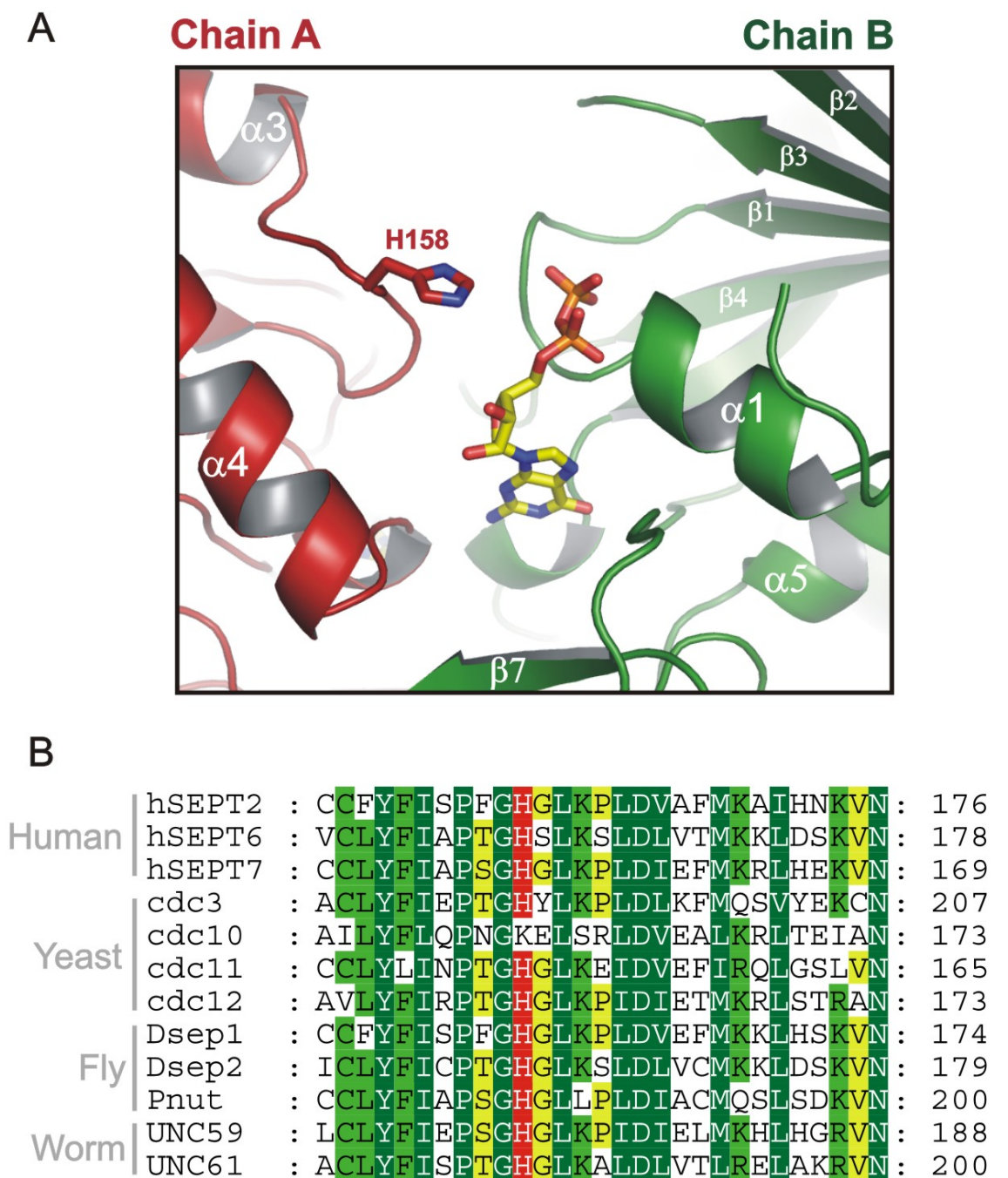**Figure 4.6**   **A: Guanine nucleotide binding region of SEPT2 with the proposed catalytic residue His158 from Trans. B: Sequence alignment of septins (of the loop between α4 and α3) from different organism, the conserved His is shown in red.**

4.5 Architecture of septin filament

The hexamer particle observed in electron microscopy under high salt conditions can be called the basic functional unit or the building block of septin filament for the SEPT2-SEPT6-SEPT7 combination of subunits. The structure of septin complex was obtained in a polymerized form. Therefore it was easy to get the information on the filament forming contacts (longitudinal contacts) from the crystal structure. This situation can be compared to tubulin where the structure was solved in polymerized form (protofilaments) using electron crystallography. The longitudinal contacts in the septin filaments are made of SEPT7 and SEPT7 G interface. These interactions are very similar to what was observed in the hexamer and also SEPT2 G dimer crystals. The asymmetric heterotrimers associate head-to-head using SEPT2 NC interface to form hexameric unit and then these hexamers associate tail-to-tail using SEPT7 G interface to form septin filament. The hexameric unit is non-polarized along the filament axis but is rotationally asymmetrical (Figure 4.2).
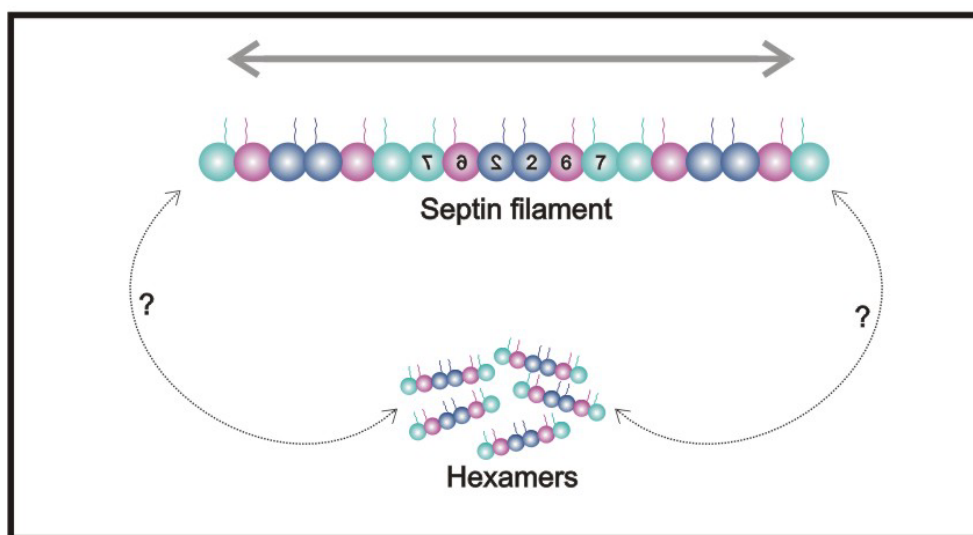
Figure 4.7   **Septin complex are bipolar, which assemble head-to-head forming a non-polar filament.**

Since septins can polymerize and form filaments, they can be classified as cytoskeletal structures. It would be interesting to compare septin filaments with other well characterized cytoskeletal structures like filamentous actin (F-actin) and microtubules. The septin filament shows no structural polarity when compared to F-actin and tubulin protofilaments. It is not clear that whether septin have a growing and shrinking end like the F-actin (Figure

4.7). Septin filaments are similar to intermediate filaments which also lacks structural polarity. Furthermore the dynamicity of both septin and intermediate filaments are controlled by phoshorylation of protein subunits. But unlike intermediate filament proteins, septins are nucleotide binding proteins whose assembly does not depend on coiled coil domains. However, the role of nucleotide in dynamic behaviour of septin organization is still a subject of debate.

4.6 Universality of septin filament

We now know that a mammalian septin complex (a three component system) forms hexamers where the G domain is arranged in a linear fashion. In order to show that this is a common design principle, the recombinant yeast septin complex (a four component system) consisting of Cdc3-Cdc10-Cdc11-Cdc12 was analysed using electron microscopy. Single particle analysis shows a particle of 32 nm length and similar width, which is clearly composed of eight subunits (Figure 4.8), as predicted from previous biochemical analysis (Farkasovsky et al., 2005; Frazier et al., 1998). Similarly in a recent study using *Caenorhabditis elegans* septin complex (a two component system) it was shown that they also form a linear tetramer which are 17-19 nm in length (John et al., 2007). Furthermore, the linear arrangement of UNC-59 and UNC-61 was shown using C-terminal GFP fusion and antibodies. In the case of yeast septin complex, the arrangement of subunits is still ambiguous and clearly more structural studies are required. However, in all the cases the C-terminal coiled coil domains are not visible suggesting that the septins assemble using their G domains via the G and NC interfaces. Therefore the assembly principle of septins seems to be universal and conserved in all organisms.
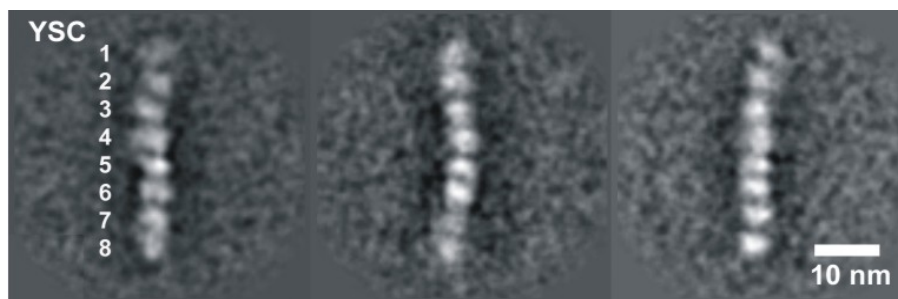
Figure 4.8   **Class averages of the Cdc3-Cdc10-Cdc11-Cdc12 yeast septin complex (YSC), the YSC forms a linear octameric complex.**

The width of filaments observed in both the crystal structure and electron microscopy is not more than 5nm, for both mammalian and yeast septin complex. In the case of *Caenorhabditis elegans* septin complex it was reported as 5-7 nm (John et al., 2007). In any case the width is not 7-9 nm as reported in a number of studies (Field et al., 1996; Frazier et al., 1998; Versele et al., 2004). The difference might arise as the electron microscopic images were recorded under low salt conditions, where septin might form higher order structures. A tightly packed paired filament of 8-9 nm width was shown recently by dialysing *Caenorhabditis elegans* septin complex to low salt (John et al., 2007). Similar higher order structures can be seen for mammalian septin under low salt conditions (Figure 4.3). However, how septin filaments assemble in to a paired filament or bundles is still not clear.

5 Summary

Septins form a family of GTP-binding proteins which are conserved from yeast to man. A typical septin primary structure consists of conserved G domain flanked by variable N-terminus and a C-terminus predicted as coiled-coils of variable length. Septin subunits assemble into homo- and hetero-oligomers, filaments and ring like structures. Deletion and mutation studies in yeast septins show incomplete cell division, suggesting an important role for septins in cytokinesis. Septins were proposed to form scaffold like structures at the cell division site and in budding yeast septin rings function as a diffusion barrier along the mother and daughter cell. Although they have key roles in cytokinesis, little is known concerning the structure of septin subunits or the organization and polarity of septin filaments. In this study structural characterization of mammalian septins was carried out, as an approach to better understand the complexity involved in septin filament formation. The structure of SEPT2 G domain and the heterotrimeric human SEPT2-SEPT6-SEPT7 complex were determined using X-ray crystallography to a resolution of 3.4 Å and 4 Å respectively.

The structure of SEPT2 G domain very much resembles the canonical G domain such that of Ras, with four additional secondary structural elements. These extra secondary structural elements are involved in dimerization or oligomerization of septins. A dimer was observed in the asymmetric unit of the SEPT2 G domain crystal, which is consistent with the gel filtration experiments. Due to the crystal lattice, SEPT2 was found to dimerize using two interfaces. Interface 1 is along the nucleotide binding site, which was termed as G interface. Interface 2 is on the opposite site and mediated by the extra N-and C-terminal helices, therefore called NC interface. Biochemical studies show that SEPT2 G domain dimerizes using its G interface. Dimerization is influenced by the presence of nucleotide, but not by the nature of nucleotide. The observation that GDP itself can influence dimerization is unique among the GTP binding proteins of TRAFAC class.

The structure of heterotrimeric SEPT2-SEPT6-SEPT7 complex shows that these subunits use the same G and NC interface to interact with each other. Crystallographic studies also show that different septin subunits contain different nucleotides bound to it. SEPT2 and

SEPT7 were found to contain GDP in the nucleotide binding site, whereas SEPT6 contains GTP. Although the crystal contains full length protein, no density corresponding to the C-terminal coiled coils was observed. Electron microscopy studies were done to further confirm the basic repeating unit which forms filaments and the dispensability of coiled coil domains for the complex formation. Surprisingly, the coiled coil deleted complex showed no difference in electron microscopy images as compared to wild type. Therefore, the G domain alone is sufficient to mediate complex formation

Crystallography and electron microscopy studies reveal that the septin complex is a linear hexamer where the subunits are arranged in the order of SEPT7-SEPT6-SEPT2-SEPT2-SEPT6-SEPT7. The SEPT6-SEPT7 interaction takes place by means of the NC interface. The SEPT6-SEPT2 interaction is via the G interface, similar to that of the SEPT2 G dimer. Notably, the SEPT2-SEPT2 interaction favors the NC interface rather than the G interface found for the isolated SEPT2 in solution supporting the notion that septin interaction appears fairly promiscuous. The structure of septin complex was obtained in a polymerized form. Therefore it was easy to get the information on the filament forming contacts (longitudinal contacts) from the crystal structure. The longitudinal contacts in the septin filaments are made of SEPT7-SEPT7 G interface.

Although the hexameric unit shows rotational asymmetry it has no structural polarity along the filament. Therefore, the architecture of septin filaments differs fundamentally from that of other cytoskeletal structures.

6 Zusammenfassung

Septine bilden eine Familie GTP bindender Proteine, die von Hefe bis Mensch stark konserviert sind. Der typische Aufbau von Septinen beinhaltet die konservierte G Domäne, flankiert von einem variablen N-Terminus und einer Coiled-coil Region variabler Länge am C-Terminus. Septine sind in der Lage sowohl homo- als auch hetero-Oligomere zu bilden, die Filamente und Ring-ähnliche Strukturen ausbilden können. Deletions- und Mutationsstudien von Septinen aus Hefe zeigen, dass sie eine wichtige Rolle in der Zytokinese übernehmen, da sie zu unvollständiger Zellteilung führen. Es wird angenommen, dass Septine während der Zellteilung Gerüst-ähnliche Strukturen an der Teilungsstelle ausbilden, die als Diffusionsbarriere zwischen Mutter- und Tochter-Zelle fungieren. Obwohl Septine eine wichtige Rolle übernehmen, ist wenig über ihre Struktur, ihre Organisation oder Polarität bekannt. Um die Komplexität der Septin-Filament-Ausbildung zu untersuchen, sollten diese Proteine sowohl strukturell als auch funktionell charakterisiert werden. Hierzu wurden die Struktur der SEPT2 G Domäne und des heterotrimeren SEPT2-SEPT6-SEPT7 Komplex mittels Röntgenstrukturanalyse bis zu einer Auflösung von 3.4 Å, bzw. 4 Å gelöst.

Die Struktur der SEPT2 G Domäne entspricht der typischen G-Domäne von Ras. Vier zusätzliche, bisher nicht gefundene, Strukturelemente sind verantwortlich für die Dimerisierung und Oligomerisierung der Septine. Demzufolge wurde in der asymmetrischen Einheit des SEPT2 Kristalls ein Dimer gefunden, welches über Gelfiltrationsexperimente bestätigt werden konnte. Aufgrund von Kristallkontakten konnten zwei verschiedene, für die Dimerisierung verantwortliche, Kontaktflächen identifiziert werden. Kontaktfläche 1 (sog. "G Kontaktfläche") verläuft entlang der Nukleotidbindungsstelle. Bindungsstelle 2 (sog. "NC Kontaktfläche") befindet sich auf der gegenüberliegenden Seite und wird über N- und C-terminale Helices vermittelt. Biochemische Studien zeigen, dass die G Domäne von SEPT2 über die "G Kontaktfläche" dimerisiert. Dies ist abhängig von der Anwesenheit von Nukleotiden, nicht jedoch von der Art des Nukleotids. Die Beobachtung, dass allein GDP die Dimerisierung von G Proteinen auslöst ist einzigartig für GTP bindende Proteine der TRAFAC-Klasse.

Die Struktur des heterotrimeren SEPT2-SEPT6-SEPT7 Komplexes zeigt, dass die einzelnen Monomere die gleichen Kontaktflächen, sowohl die "G Kontaktfläche" als auch die "NC Kontaktfläche", benutzen um miteinander zu interagieren. Kristallografische Studien zeigen zudem, dass die verschiedenen Septin-Untereinheiten verschiedene Nukleotide gebunden haben. SEPT2 und SEPT7 binden demnach GDP, während SEPT6 GTP enthält. Obwohl vollständige Proteine kristallisiert wurden, konnte keine Dichte für die C-terminalen Coiled-coil Regionen gefunden werden. Weiterhin wurden EM-Studien durchgeführt, um sowohl die kleinste Einheit, die Filamente ausbilden kann, zu identifizieren, als auch um die Entbehrlichkeit der Coiled-coil Domänen zu bestätigen. Überraschenderweise weisen Konstrukte ohne Coiled-coil-Regionen im EM keinen Unterschied zu den Wildtyp-Proteinen auf. Folglich ist einzig die G Domäne ausreichend, um Filamente auszubilden

Die kristallografischen- und EM-Studien zeigen, dass der Septin Komplex ein lineares Hexamer bildet, in dem die Untereinheiten wie folgt aneinander gereiht sind: SEPT7-SEPT6-SEPT2-SEPT2-SEPT6-SEPT7. Während die SEPT6-SEPT7 Interaktion, wie im SEPT2 G Domänen-Dimer, über die "G Kontaktfläche" verläuft, befindet sich im SEPT2-Dimer des Hexamers die "NC Kontaktfläche". Dies unterstützt die Annahme, dass Septine promiskuitiv miteinander interagieren und beide Kontaktflächen nutzen können. Die Struktur des Septin Komplexes wurde in polymerisierter Form erhalten. Demzufolge konnten Informationen über die Filament-vermittelnden Kontakte (longitudinale Kontakte) direkt aus der Kristallstruktur übernommen werden: Die longitudinalen Kontakte der Septin Filamente werden über die SEPT7-SEPT7 "G Kontaktfläche vermittelt.

Obwohl die hexamere Einheit Rotationsasymmetrie aufweist, besitzt sie keine strukturelle Polarität entlang der Filament-Achse. Demzufolge unterscheidet sich der Aufbau der Septin Filamente drastisch von anderen zytoskelettalen Strukturen.

7 References

Adams,A.E. and Pringle,J.R. (1984). Relationship of actin and tubulin distribution to bud growth in wild- type and morphogenetic-mutant Saccharomyces cerevisiae. J. Cell Biol. *98*, 934-945.

Bailey,S. (1994). The Ccp4 Suite - Programs for Protein Crystallography. Acta Crystallographica Section D-Biological Crystallography *50*, 760-763.

Barral,Y., Mermall,V., Mooseker,M.S., and Snyder,M. (2000). Compartmentalization of the cell cortex by septins is required for maintenance of cell polarity in yeast. Molecular Cell *5*, 841-851.

Beites,C.L., Xie,H., Bowser,R., and Trimble,W.S. (1999). The septin CDCrel-1 binds syntaxin and inhibits exocytosis. Nat Neurosci *2*, 434-439.

Bourne,H.R., Sanders,D.A., and McCormick,F. (1991). The Gtpase Superfamily - Conserved Structure and Molecular Mechanism. Nature *349*, 117-127.

Brown,J.L., Jaquenoud,M., Gulli,M.P., Chant,J., and Peter,M. (1997). Novel Cdc42-binding proteins Gic1 and Gic2 control cell polarity in yeast. Genes Dev. *11*, 2972-2982.

Brunger,A.T. (1992). Free R-Value - A Novel Statistical Quantity for Assessing the Accuracy of Crystal-Structures. Nature *355*, 472-475.

Brunger,A.T. (1997). Free R value: Cross-validation in crystallography. Macromolecular Crystallography, Pt B *277*, 366-396.

Brunger,A.T., Adams,P.D., Clore,G.M., Delano,W.L., Gros,P., Grosse-Kunstleve,R.W., Jiang,J.S., Kuszewski,J., Nilges,M., Pannu,N.S., Read,R.J., Rice,L.M., Simonson,T., and Warren,G.L. (1998). Crystallography & NMR system: A new software suite for macromolecular structure determination. Acta Crystallographica Section D-Biological Crystallography *54*, 905-921.

Byers,B. and Goetsch,L. (1976a). A highly ordered ring of membrane-associated filaments in budding yeast. J. Cell Biol. *69*, 717-721.

Byers,B. and Goetsch,L. (1976b). Loss of Filamentous Ring in Cytokinesis-Defective Mutants of Budding Yeast. Journal of Cell Biology *70*, A35.

Casamayor,A. and Snyder,M. (2003). Molecular Dissection of a Yeast Septin: Distinct Domains Are Required for Septin Interaction, Localization, and Function. Mol. Cell. Biol. *23*, 2762-2777.

Chen,G.C., Kim,Y.J., and Chan,C.S. (1997). The Cdc42 GTPase-associated proteins Gic1 and Gic2 are required for polarized cell growth in Saccharomyces cerevisiae. Genes Dev. *11*, 2958-2971.

Cool,R.H. and Parmeggiani,A. (1991). Substitution of Histidine-84 and the Gtpase Mechanism of Elongation Factor-Tu. Biochemistry *30*, 362-366.

Cowtan,K.D. and Zhang,K.Y.J. (1999). Density modification for macromolecular phase improvement. Progress in Biophysics and Molecular Biology *72*, 245-270.

Didomenico,B.J., Brown,N.H., Lupisella,J., Greene,J.R., Yanko,M., and Koltin,Y. (1994). Homologs of the Yeast Neck Filament-Associated Genes - Isolation and Sequence-Analysis of Candida-Albicans Cdc3 and Cdc10. Molecular & General Genetics *242*, 689-698.

Dobbelaere,J., Gentry,M.S., Hallberg,R.L., and Barral,Y. (2003). Phosphorylation-Dependent Regulation of Septin Dynamics during the Cell Cycle. Developmental Cell *4*, 345-357.

Doublie,S. (1997). [29] Preparation of selenomethionyl proteins for phase determination. In Methods in Enzymology
Macromolecular Crystallography Part A, W.C.Charles, ed. Academic Press), pp. 523-530.

Drenth,J. (1999). Principles of Protein X-ray Crystallography. Springer Verlag, Berlin).

Emsley,P. and Cowtan,K. (2004). Coot: model-building tools for molecular graphics. Acta Crystallographica Section D-Biological Crystallography *60*, 2126-2132.

Farkasovsky,M., Herter,P., Voss,B., and Wittinghofer,A. (2005). Nucleotide binding and filament assembly of recombinant yeast septin complexes. Biological Chemistry *386*, 643-656.

Farkasovsky,M. and Wittinghofer,A. (2003). GTPase activity and filament assembly of yeast septins. Yeast *20*, S66.

Field,C.M., al Awar,O., Rosenblatt,J., Wong,M.L., Alberts,B., and Mitchison,T.J. (1996). A purified Drosophila septin complex forms filaments and exhibits GTPase activity. J. Cell Biol. *133*, 605-616.

Field,C.M. and Kellogg,D. (1999). Septins: cytoskeletal polymers or signalling GTPases? Trends in Cell Biology *9*, 387-394.

Frazier,J.A., Wong,M.L., Longtine,M.S., Pringle,J.R., Mann,M., Mitchison,T.J., and Field,C. (1998). Polymerization of Purified Yeast Septins: Evidence That Organized Filament Arrays May Not Be Required for Septin Function. J. Cell Biol. *143*, 737-749.

Garcia-Ranea,J.A. and Valencia,A. (1998). Distribution and functional diversification of the ras superfamily in Saccharomyces cerevisiae. FEBS Lett. *434*, 219-225.

Ghosh,A., Praefcke,G.J.K., Renault,L., Wittinghofer,A., and Herrmann,C. (2006). How guanylate-binding proteins achieve assembly-stimulated processive cleavage of GTP to GMP. Nature *440*, 101-104.

Ghosh,A., Uthaiah,R., Howard,J., Herrmann,C., and Wolf,E. (2004). Crystal structure of IIGP1: A paradigm for interferon-inducible p47 resistance GTPases. Molecular Cell *15*, 727-739.

Gladfelter,A.S., Pringle,J.R., and Lew,D.J. (2001). The septin cortex at the yeast mother-bud neck. Current Opinion in Microbiology *4*, 681-689.

Haarer,B.K. and Pringle,J.R. (1987). Immunofluorescence Localization of the Saccharomyces-Cerevisiae Cdc12 Gene-Product to the Vicinity of the 10-Nm Filaments in the Mother-Bud Neck. Mol. Cell. Biol. *7*, 3678-3687.

Hall,P.A., Jung,K., Hillan,K.J., and Russell,S.E.H. (2005). Expression profiling the human septin gene family. Journal of Pathology *206*, 269-278.

Hall,P.A. and Russell,S.E.H. (2004). The pathobiology of the septin gene family. Journal of Pathology *204*, 489-505.

Hartwell,L.H. (1971). Genetic control of the cell division cycle in yeast : IV. Genes controlling bud emergence and cytokinesis. Experimental Cell Research *69*, 265-276.

Hsu,S.C., Hazuka,C.D., Roth,R., Foletti,D.L., Heuser,J., and Scheller,R.H. (1998). Subunit composition, protein interactions, and structures of the mammalian brain sec6/8 complex and septin filaments. Neuron *20*, 1111-1122.

Huang,Y.W., Surka,M.C., Reynaud,D., Pace-Asciak,C., and Trimble,W.S. (2006). GTP binding and hydrolysis kinetics of human septin 2. FEBS Journal *273*, 3248-3260.

Ihara,M., Tomimoto,H., Kitayama,H., Morioka,Y., Akiguchi,I., Shibasaki,H., Noda,M., and Kinoshita,M. (2003). Association of the Cytoskeletal GTP-binding Protein Sept4/H5 with Cytoplasmic Inclusions Found in Parkinson's Disease and Other Synucleinopathies. J. Biol. Chem. *278*, 24095-24102.

Ito,H., Iwamoto,I., Morishita,R., Nozawa,Y., Narumiya,S., Asano,T., and Nagata,K.i. (2005). Possible role of Rho//Rhotekin signaling in mammalian septin organization. Oncogene *24*, 7064-7072.

Iwase,M. and Toh-e,A. (2004). Ybr267w is a new cytoplasmic protein belonging to the mitotic signaling network of Saccharomyces cerevisiae. Cell Structure and Function *29*, 1-15.

Jensen,S., Geymonat,M., Johnson,A.L., Segal,M., and Johnston,L.H. (2002). Spatial regulation of the guanine nucleotide exchange factor Lte1 in Saccharomyces cerevisiae. J Cell Sci *115*, 4977-4991.

Joberty,G., Perlungher,R.R., and Macara,I.G. (1999). The Borgs, a new family of Cdc42 and TC10 GTPase-interacting proteins. Mol. Cell. Biol. *19*, 6585-6597.

Joberty,G., Perlungher,R.R., Sheffield,P.J., Kinoshita,M., Noda,M., Haystead,T., and Macara,I.G. (2001). Borg proteins control septin organization and are negatively regulated by Cdc42. Nat Cell Biol *3*, 861-866.

John,C.M., Hite,R.K., Weirich,C.S., Fitzgerald,D.J., Jawhari,H., Faty,M., Schlapfer,D., Kroschewski,R., Winkler,F.K., Walz,T., Barral,Y., and Steinmetz,M.O. (2007). The Caenorhabditis elegans septin complex is nonpolar. EMBO J *26*, 3296-3307.

Johnson,E.S. and Blobel,G. (1999). Cell cycle-regulated attachment of the ubiquitin-related protein SUMO to the yeast septins. Journal of Cell Biology *147*, 981-993.

Johnson,E.S. and Gupta,A.A. (2001). An E3-like Factor that Promotes SUMO Conjugation to the Yeast Septins. Cell *106*, 735-744.

Johnstone,B.H., Handler,A.A., Chao,D.K., Nguyen,V., Smith,M., Ryu,S.Y., Simons,E.L., Anderson,P.E., and Simons,R.W. (1999). The widely conserved Era G-protein contains an RNA-binding domain required for Era function in vivo. Molecular Microbiology *33*, 1118-1131.

Jordan,M.A. and Wilson,L. (2004). Microtubules as a target for anticancer drugs. Nature Reviews Cancer *4*, 253-265.

Kabsch,W. (1993). Automatic Processing of Rotation Diffraction Data from Crystals of Initially Unknown Symmetry and Cell Constants. Journal of Applied Crystallography *26*, 795-800.

Kartmann,B. and Roth,D. (2001). Novel roles for mammalian septins: from vesicle trafficking to oncogenesis. J Cell Sci *114*, 839-844.

Kim,H.B., Haarer,B.K., and Pringle,J.R. (1991). Cellular Morphogenesis in the Saccharomyces-Cerevisiae Cell-Cycle - Localization of the Cdc3 Gene-Product and the Timing of Events at the Budding Site. Journal of Cell Biology *112*, 535-544.

Kinoshita,A., Kinoshita,M., Akiyama,H., Tomimoto,H., Akiguchi,I., Kumar,S., Noda,M., and Kimura,J. (1998). Identification of septins in neurofibrillary tangles in Alzheimer's disease. American Journal of Pathology *153*, 1551-1560.

Kinoshita,A., Noda,M., and Kinoshita,M. (2000). Differential localization of septins in the mouse brain. Journal of Comparative Neurology *428*, 223-239.

Kinoshita,M., Kumar,S., Mizoguchi,A., Ide,C., Kinoshita,A., Haraguchi,T., Hiraoka,Y., and Noda,M. (1997). Nedd5, a mammalian septin, is a novel cytoskeletal component interacting with actin-based structures. Genes & Development *11*, 1535-1547.

Kinoshita,M. (2003). Assembly of Mammalian Septins. J Biochem (Tokyo) *134*, 491-496.

Kinoshita,M. (2006). Diversity of septin scaffolds. Current Opinion in Cell Biology *18*, 54-60.

Kinoshita,M., Field,C.M., Coughlin,M.L., Straight,A.F., and Mitchison,T.J. (2002). Self- and Actin-Templated Assembly of Mammalian Septins. Developmental Cell *3*, 791-802.

Kleywegt, G. J. Moleman - Uppsala University, Uppsala, Sweden. 1-1-2004.
Ref Type: Unpublished Work

Kozubowski,L., Larson,J.R., and Tatchell,K. (2005). Role of the Septin Ring in the Asymmetric Localization of Proteins at the Mother-Bud Neck in Saccharomyces cerevisiae. Mol. Biol. Cell *16*, 3455-3466.

Kuhlenbaumer,G., Hannibal,M.C., Nelis,E., Schirmacher,A., Verpoorten,N., Meuleman,J., Watts,G.D.J., Vriendt,E.D., Young,P., Stogbauer,F., Halfter,H., Irobi,J., Goossens,D., Del Favero,J., Betz,B.G., Hor,H., Kurlemann,G., Bird,T.D., Airaksinen,E., Mononen,T., Serradell,A.P., Prats,J.M., Broeckhoven,C.V., Jonghe,P.D., Timmerman,V., Ringelstein,E.B., and Chance,P.F. (2005). Mutations in SEPT9 cause hereditary neuralgic amyotrophy. Nat Genet *37*, 1044-1046.

Laskowski,R.A., MacArthur,M.W., Moss,D.S., and Thornton,J.M. (1993). Procheck - A Program to Check the Stereochemical Quality of Protein Structures. Journal of Applied Crystallography *26*, 283-291.

Leipe,D.D., Wolf,Y.I., Koonin,E.V., and Aravind,L. (2002). Classification and evolution of P-loop GTPases and related ATPases. Journal of Molecular Biology *317*, 41-72.

Longtine,M.S. and Bi,E. (2003). Regulation of septin organization and function in yeast. Trends in Cell Biology *13*, 403-409.

Longtine,M.S., DeMarini,D.J., Valencik,M.L., Al Awar,O.S., Fares,H., De Virgilio,C., and Pringle,J.R. (1996). The septins: roles in cytokinesis and other processes. Current Opinion in Cell Biology *8*, 106-119.

Low,C. and Macara,I.G. (2006). Structural Analysis of Septin 2, 6, and 7 Complexes. J. Biol. Chem. *281*, 30697-30706.

Macara,I.G., Baldarelli,R., Field,C.M., Glotzer,M., Hayashi,Y., Hsu,S.C., Kennedy,M.B., Kinoshita,M., Longtine,M., Low,C., Maltais,L.J., McKenzie,L., Mitchison,T.J.,

Nishikawa,T., Noda,M., Petty,E.M., Peifer,M., Pringle,J.R., Robinson,P.J., Roth,D., Russell,S.E.H., Stuhlmann,H., Tanaka,M., Tanaka,T., Trimble,W.S., Ware,J., Zeleznik-Le,N.J., and Zieger,B. (2002). Mammalian Septins Nomenclature. Mol. Biol. Cell *13*, 4111-4113.

Mahamadou,F., Michel,F., and Yves,B. (2002). Septins: a ring to part mother and daughter. Current Genetics *41*, 123-131.

Matthews,B.W. (1968). Solvent content of protein crystals. Journal of Molecular Biology *33*, 491-497.

Mcdade,S.S., Hall,P.A., and Russell,S.E.H. (2007). Translational control of SEPT9 isoforms is perturbed in disease. Human Molecular Genetics *16*, 742-752.

Mehr,I.J., Long,C.D., Serkin,C.D., and Seifert,H.S. (2000). A homologue of the recombination-dependent growth gene, rdgC, is involved in gonococcal pilin antigenic variation. Genetics *154*, 523-532.

Meier,T.I., Peery,R.B., McAllister,K.A., and Zhao,G. (2000). Era GTPase of Escherichia coli: binding to 16S rRNA and modulation of GTPase activity by RNA and carbohydrates. Microbiology-Sgm *146*, 1071-1083.

Mendoza,M., Hyman,A.A., and Glotzer,M. (2002). GTP Binding Induces Filament Assembly of a Recombinant Septin. Current Biology *12*, 1858-1863.

Mitchison,T.J. and Field,C.M. (2002). Cytoskeleton: What Does GTP Do for Septins? Current Biology *12*, R788-R790.

Murshudov,G.N., Vagin,A.A., and Dodson,E.J. (1997). Refinement of macromolecular structures by the maximum-likelihood method. Acta Crystallographica Section D-Biological Crystallography *53*, 240-255.

Nagata,K.I. and Inagaki,M. (2005). Cytoskeletal modification of Rho guanine nucleotide exchange factor activity: identification of a Rho guanine nucleotide exchange factor as a binding partner for Sept9b, a mammalian septin. Oncogene *24*, 65-76.

Nagata,K.i., Asano,T., Nozawa,Y., and Inagaki,M. (2004). Biochemical and Cell Biological Analyses of a Mammalian Septin Complex, Sept7/9b/11. J. Biol. Chem. *279*, 55895-55904.

Neufeld,T.P. and Rubin,G.M. (1994). The Drosophila peanut gene is required for cytokinesis and encodes a protein similar to yeast putative bud neck filament proteins. Cell *77*, 371-379.

Nogales,E. (2001). Structural insights into microtubule function. Annual Review of Biophysics and Biomolecular Structure *30*, 397-420.

Oegema,K., Savoian,M.S., Mitchison,T.J., and Field,C.M. (2000). Functional analysis of a human homologue of the Drosophila actin binding protein anillin suggests a role in cytokinesis. Journal of Cell Biology *150*, 539-551.

Pan,F., Malmberg,R., and Momany,M. (2007). Analysis of septins across kingdoms reveals orthology and new motifs. BMC Evolutionary Biology *7*, 103.

Peng,X.R., Jia,Z., Zhang,Y., Ware,J., and Trimble,W.S. (2002). The Septin CDCrel-1 Is Dispensable for Normal Development and Neurotransmitter Release. Mol. Cell. Biol. *22*, 378-387.

Perutz,M. (1956). Isomorphous replacement and phase determination in non-centrosymmetric space groups. Acta Crystallographica *9*, 867-873.

Petsko,G.A. (1975). Protein crystallography at sub-zero temperatures: Cryo-protective mother liquors for protein crystals. Journal of Molecular Biology *96*, 381-388.

Praefcke,G.J.K. and McMahon,H.T. (2004). The dynamin superfamily: Universal membrane tubulation and fission molecules? Nature Reviews Molecular Cell Biology *5*, 133-147.

Prakash,B., Praefcke,G.J., Renault,L., Wittinghofer,A., and Herrmann,C. (2000). Structure of human guanylate-binding protein 1 representing a unique class of GTP-binding proteins. Nature *403*, 567-571.

Rhodes,G. (2000). Crytallography made crystal clear. Academic Press).

Rossmann,M. and Blow,D.M. (1962). Detection of subunits within the crystallogrpahic asymmetric unit. Acta Crystallographica *15*, 24-31.

Russell,S.E.H. and Hall,P.A. (2005). Do septins have a role in cancer? British Journal of Cancer *93*, 499-503.

Sambrook,J.F.E.F.M.T. (1989). Molecular Cloning. A Laboratory Manual. Cold Spring Harbor Laboratory Press).

Saraste,M., Sibbald,P.R., and Wittinghofer,A. (1990). The P-Loop - A Common Motif in Atp-Binding and Gtp-Binding Proteins. Trends in Biochemical Sciences *15*, 430-434.

Schmidt,K. and Nichols,B.J. (2004). A barrier to lateral diffusion in the cleavage furrow of dividing mammalian cells. Current Biology *14*, 1002-1006.

Schneider,T.R. and Sheldrick,G.M. (2002). Substructure solution with SHELXD. Acta Crystallographica Section D-Biological Crystallography *58*, 1772-1779.

Scott,M., McCluggage,W.G., Hillan,K.J., Hall,P.A., and Russell,S.E.H. (2006). Altered patterns of transcription of the septin gene, SEPT9, in ovarian tumorigenesis. International Journal of Cancer *118*, 1325-1329.

Scott,M., Russell,S.E.H., and Hall,P.A. (2005). Over-expression of the human septin SEPT9 in borderline and malignant ovarian epithelial tumours. Laboratory Investigation *85*, 204A.

Scrima,A., Vetter,I.R., Armengod,M.E., and Wittinghofer,A. (2005). The structure of the TrmE GTP-binding protein and its implications for tRNA modification. Embo Journal *24*, 23-33.

Scrima,A. and Wittinghofer,A. (2006). Dimerisation-dependent GTPase reaction of MnmE: how potassium acts as GTPase-activating element. Embo Journal *25*, 2940-2951.

Sheffield,P.J., Oliver,C.J., Kremer,B.E., Sheng,S., Shao,Z., and Macara,I.G. (2003). Borg/Septin Interactions and the Assembly of Mammalian Septin Heterodimers, Trimers, and Filaments. J. Biol. Chem. *278*, 3483-3488.

Spiliotis,E.T. and Nelson,W.J. (2006). Here come the septins: novel polymers that coordinate intracellular functions and organization. J Cell Sci *119*, 4-10.

Takai,Y., Sasaki,T., and Matozaki,T. (2001). Small GTP-binding proteins. Physiol Rev. *81*, 153-208.

Takizawa,P.A., Derisi,J.L., Wilhelm,J.E., and Vale,R.D. (2000). Plasma membrane compartmentalization in yeast by messenger RNA transport and a septin diffusion barrier. Science *290*, 341-344.

Taylor,G. (2003). The phase problem. Acta Crystallographica Section D-Biological Crystallography *59*, 1881-1890.

Terwilliger,T.C. (2003). SOLVE and RESOLVE: Automated Structure Solution and Density Modification. In Methods in Enzymology
Macromolecular Crystallography, Part D, W.C.Charles, ed. Academic Press), pp. 22-37.

Urrutia,R., Henley,J.R., Cook,T., and McNiven,M.A. (1997). The dynamins: redundant or distinct functions for an expanding family of related GTPases? Proc. Natl. Acad. Sci. U. S. A *94*, 377-384.

Versele,M., Gullbrand,B., Shulewitz,M.J., Cid,V.J., Bahmanyar,S., Chen,R.E., Barth,P., Alber,T., and Thorner,J. (2004). Protein-Protein Interactions Governing Septin Heteropentamer Assembly and Septin Filament Organization in Saccharomyces cerevisiae. Mol. Biol. Cell *15*, 4568-4583.

Versele,M. and Thorner,J. (2004). Septin collar formation in budding yeast requires GTP binding and direct phosphorylation by the PAK, Cla4. J. Cell Biol. *164*, 701-715.

Versele,M. and Thorner,J. (2005). Some assembly required: yeast septins provide the instruction manual. Trends in Cell Biology *15*, 414-424.

Vetter,I.R. and Wittinghofer,A. (2001). Signal transduction - The guanine nucleotide-binding switch in three dimensions. Science *294*, 1299-1304.

Vrabioiu,A.M., Gerber,S.A., Gygi,S.P., Field,C.M., and Mitchison,T.J. (2004). The Majority of the Saccharomyces cerevisiae Septin Complexes Do Not Exchange Guanine Nucleotides. J. Biol. Chem. *279*, 3111-3118.

Vrabioiu,A.M. and Mitchison,T.J. (2006). Structural insights into yeast septin organization from polarized fluorescence microscopy. Nature *443*, 466-469.

Wang,B.C. (1985). Resolution of phase ambiguity in macromolecular crystallography. Methods Enzymology *115*, 90-112.

Ware,J., Peng,X.R., Dent,J., Kato,K., Martinez,C., Christel,P., Nurden,P., Nurden,A., and Trimble,W. (2001). A prototypic platelet septin, CDCrel-1, and its participation in platelet secretion. Blood *98*, 702A.

Wu,J.Q., Kuhn,J.R., Kovar,D.R., and Pollard,T.D. (2003). Spatial and temporal pathway for assembly and constriction of the contractile ring in fission yeast cytokinesis. Developmental Cell *5*, 723-734.

Zhang,J.S., Kong,C., Xie,H., McPherson,P.S., Grinstein,S., and Trimble,W.S. (1999). Phosphatidyl inositol polyphosphate binding to the mammalian septin H5 is modulated by GTP. Current Biology *9*, 1458-1467.

Acknowledgements

I sincerely thank Prof. Dr. Alfred Wittinghofer for giving me an opportunity to work on an exciting topic. His profound insight and passion for science is a tremendous source of encouragement.

I am very grateful to Prof. Dr. Herbert Waldmann for agreeing to be the co-referent for my thesis and for wonderful discussion.

I thank Prof. Dr. Rolf Kinne, Prof. Dr. Martin Engelhard and International Max Planck Research School for support and inspiration. I thank Dr. Jutta Rötter for many helps especially during the initial days and wonderful IMPRS retreats.

I thank Marian for introducing me to the world of septins and many tips and tricks. I thank Michael Weyand for teaching me crystallography and several discussions.

I thank Dr. Holger Stark and Florian Hauer for the collaboration and for kindly providing the electron microscopy images.

Many thanks to the Ilme, Wulf, Eckhard, Toni, Nils, Lena, Rolf and other members of MPI-Dortmund/Heidelberg X-ray community for collecting several datasets and crystallographic advice. I would like to thank Ingrid for giving 'septins' the highest priority during SLS trips and several helps in computing. I thank Georg for providing us an ever running generator.

Doro for many constructs and clones, Caro for many useful tips and tricks, members of A2.12 and Beate for pleasant lab atmosphere.

I would like to thank Christoph, Andrea, Raphael and Lothar for several helps, suggestions and enlightening discussions. I thank Shehab for reading my thesis. I thank Delia, Katja, Simon, Micahel, Stephan, Antje and other members of Abteilung Structurelle Biologie for lovely working atmosphere and nice Pottenstein and Ringberg times. I am also grateful to Rita for her bureaucratic assistance.

I thank the past members of the department, Toshi, Oli Daumke, Dennis and Reza for valuable advices and encouragements.

I personally thank Sudiptha, Partha, Neelakshi, Bala, Harkal and Anchal for their support and good time. Special thanks to Agni and Revathy for their help, stimulating discussions and optimistic encouragements.

My very special thanks are addressed to my parents and friends whose care, help and moral support made this work possible.

Erklärung

Ich versichere hiermit, dass ich die vorliegende Arbeit selbständig und ohne fremde Hilfe, nur unter Verwendung der angegebenen Hilfsmittel, angefertigt habe.

Dortmund,

Minhajuddin Sirajuddin

Publication and Database submissions

1. **Sirajuddin,M**., Farkasovsky,M., Hauer,F., Kuhlmann,D., Macara,I.G., Weyand,M., Stark,H., and Wittinghofer,A. (2007). Structural insight into filament formation by mammalian septins. Nature. 2007 Sep 20; 449 (7160):311-5. Epub 2007 Jul 18.

2. Crystal structure of Sept2 G-domain : PDB ID **2QA5**

3. Crystal structure of human septin trimer 2/6/7 : PDB ID **2QAG**

Lebenslauf

Persönliche Daten:	Minhajuddin Sirajuddin
	Grotenbachstr. 65, 44225 Dortmund
	geb. am 31.08.1980 in Ranipet, Indien
	Staatsangehörigkeit: Indisch (Indian)
	Familienstatus: ledig
1995 – 1997	Government Higher Secondary School, Ranipet, India
	Abschluss: Higher secondary (10 + 2)
1997 – 2000	C. Abdul Hakeem College, University of Madras, India
	Abschluss: B. Sc (Bio-Chemistry)
2000 – 2002	University of Madras, Guindy Campus, Chennai, India
	Abschluss: M. Sc (Bio-Chemistry)
2002 – 2003	Project Assistant
	Molecular Biophysics Unit, Indian Institute of Science, Bangalore, India
2003 – 2007	Promotionsarbeit am Max-Planck-Institut für molekulare Physiologie, Dortmund, Germany